Triple Oxygen Isotopes in Evolving Continental Crust, Granites, and Clastic Sediments

Ilya N. Bindeman

Department of Earth Sciences University of Oregon Eugene OR 97403-1272 USA

bindeman@uoregon.edu

INTRODUCTION

This Chapter considers triple oxygen isotope variations and their 4 Gyr temporal evolution in bulk siliciclastic sedimentary rocks and in granites. The $\delta^{18}O$ and $\Delta'^{17}O$ values provide new insights into weathering in the modern and ancient hydrosphere and coeval crustal petrogenesis. We make use of the known geological events and processes that affect the rock cycle: supercontinent assembly and breakup that influence continent-scale and global climate, the fraction of the exposed crust undergoing weathering, and isotopic values of precipitation.

New data from a 5000 m Texas drillhole into the Oligocene Frio Formation demonstrate minimal isotopic shifts from mudrocks to shales during diagenesis, mostly related to expulsion of water from smectite-rich loosely cemented sediment and its conversion to illite-rich shale. Inversion of triple oxygen isotope fractionations return isotopic values and temperatures along the hole depth that are more consistent with weathering conditions in the Oligocene and modern North America ($\delta^{18}O = -7$ to -15%, and T of +15 to +45 °C) rather than $\delta^{18}O$ from 8 to 10% diagenetic water in the drill hole at 175-195 °C. More precise T and $\delta^{18}O_{\rm water}$ are obtained where the chemical index of alteration (CIA) based detrital contribution is subtracted from these sediments. Triple oxygen isotopes from suspended sediments in major world rivers record conditions (T and $\delta^{18}O_{\rm w}$) of their watersheds, and not the composition of bedrock because weathering is water-dominated.

In parallel, the Chapter presents new analyses of 100 granites, orthogneisses, migmatites, tonalite-trondhjemite-granodiorite (TTG), and large-volume ignimbrites from around the world that range in age from 4Ga to modern. Most studied granites are orogenic and anatectic in origin and represent large volume remelting/assimilation of shales and other metasediments; the most crustal and high- δ^{18} O of these are thus reflect and record the average composition of evolving continental crust. Granites also develop a significant progressive increase in δ^{18} O values from 6–7% (4–2.5 Ga) to 10–13% (~1.8–1.2 Ga) after which δ^{18} O stays constant or even decreases. More importantly, we observe a moderate -0.03% step-wise decrease in $\Delta'^{17}O$ between 2.1 and 2.5 Ga, which is about half of the step-wise decrease observed in shales over this time interval. We suggest that granites, as well as shales, record the significant advent and greater volumetric appearance of low- Δ'^{17} O, high- δ^{18} O weathering products (shales) altered by meteoric waters upon rapid emergence of large land masses at ~2.4 Ga, although consider alternative interpretations. These weathering products were incorporated into abundant 2.0-1.8 Ga orogens around the world, where upon remelting, they passed their isotopic signature to the granites. We further observe the dichotomy of high- $\Delta'^{17}O$ Archean shales, and unusually low- $\Delta'^{17}O$ Archean granites. We attribute this to greater contribution from shallow crustal hydrothermal contribution to shales in greenstone belts, while granites in the earliest 3.0-4.0 Ga crust and TTGs require involvement of hydrothermal products with lower- Δ'^{17} O signatures at moderately high- δ^{18} O, which we attribute to secondary silicification of their protoliths before partial melting.

The Chapter further discusses evolution of the shale record through geologic history and discusses the step-wise change in $\delta^{18}O$ and $\Delta'^{17}O$ values at Archean–Proterozoic transition. Denser coverage for shales in the past 1 billion years permits investigation of the rocks and their weathering in the last supercontinent cycle, with observed lighter $\delta^{18}O$ values, characteristic for the mid-Phanerozoic at the initiation of Gondwana breakup. The continuing increase in $\delta^{18}O$ values of the shales since $4\,Ga$ is interpreted to reflect accumulation of weathering products via shale accretion to continents, as low-density and buoyant shales tend to not subduct back into the mantle.

The rock cycle passes triple oxygen isotopic signatures from precipitation to sedimentary, metasedimentary, and finally to anatectic igneous rocks. Continental crust became progressively heavier in $\delta^{18}O$, lighter in $\Delta^{\prime\,17}O$ due to incremental accumulation of high- $\delta^{18}O$ sediments in accretionary wedges. Second-order trends in $\delta^{18}O$ and $\Delta^{\prime\,17}O$ are due to supercontinent cycles and glacial episodes.

The evolution of continental crust since its formation in the early Archean has been a major theme of petrologic investigation for many decades (Goldschmidt 1933; Taylor and MacLennan 1995; Wedepohl 1995; Rudnick and Gao 2003; Greber et al. 2017; Spencer et al. 2017; Bucholz et al. 2018). The appearance of each new chemical analytical method or a new isotopic system, as well as improving geological and geochronologic investigation and recognition of ancient geologic formations adds greater understanding of Earth and the early processes of its evolution. It is reasonable to assume that weathering conditions on Earth have evolved as conditions (such as solar luminosity and CO₂ and O₂ concentrations) changed, and thus both uniformitarian and non-uniformitarian approaches can apply, especially to the Archean. As the Archean and Proterozoic eons capture ~88% of Earth's history, most events occurring in Earth's crust are rooted there: the timing and rate of plate tectonics, the appearance of first continents, their composition (mafic vs. silicic); their emergence from water as subaerial land masses, the evolution of the atmosphere and the causes of the Great Oxidation Event at 2.3 Ga, Snowball Earth glaciations in early and late Proterozoic, and the appearance of microbial and multicellular life (Holland 1984; Buick et al. 1998; Bekker and Holland 2012; Hoffman 2013).

Shales, what do they reflect?

Mudrocks constitute 50 to 80% of total sedimentary rock mass (Pettijohn 1957, Ronov and Yaroshevsky 1969), and shales have been traditionally used to deduce the role of continental weathering and sediment recycling through geologic time, and to constrain the average chemical composition of the exposed and eroding continental crust (Goldschmidt 1933; Wedepohl 1995; Rudnick and Gao 2003). Their chemical and isotopic compositions have been used since the early days of geochemistry to address weathering conditions and sediment provenance, and address fundamental questions of elemental and isotopic fluxes from and into the mantle and the hydrosphere, and element and isotope recycling in the framework of plate tectonics, after the acceptance of that theory (Holland 1984). Unmetamorphosed clay-rich shales are known to exist since 3.4–3.5 Ga, and they are relevant to the study of conditions under which organic matter becomes incorporated into weathering products throughout geologic history (Buick et al. 1998; Hayes et al. 1999; Retallack 2001; Sageman and Lyons 2004; Kump 2014).

Like many other sedimentary rocks, shales and mudrocks represent a mixture of detrital and authigenic (equilibrated with weathering fluid at a specific temperature and water, and less pronounced exchange during transport and post-depositional diagenesis) components (Sageman and Lyons 2004). The authigenic component is important for recording environmental factors. Silverman (1951), Savin and Epstein (1970a,b) and Bindeman et al. (2019) demonstrated that oxygen isotopic values of recent sediments and authigenic shale samples reflect exclusively isotopic values of meteoric water at respective values of temperature, since weathering proceeds with a great excess of water over rocks.

Other isotopic systems in sediments such as Sr, Nd, Hf, Mg, Li, Ti, and Si, whose dissolved concentration in weathering water is low, reflect provenance (exposed bedrock) of the crust undergoing weathering (Goldstein and Jacobsen 1988; Bayon et al. 2015, 2018, 2020; Li et al. 2016; Dellinger et al. 2017; Greber et al. 2017). Therefore shales and their constituent detrital and secondary minerals are a valuable resource for the investigation of the detrital portion of crustal maturation. In their oxygen and hydrogen isotopes they additionally record evolving weathering conditions: δ^{18} O and temperature on the Earth's surface (Fig. 1), which themselves are related to watershed latitude, and global climate as well as the concurrent (and hotly debated!) δ^{18} O value of seawater. This complexity creates both significant opportunities and challenges in the application of isotope geochemistry to sedimentary environments. Shales remained the "most studied but poorly understood rock" (Shaw and Weather 1965), but recent advances in isotopic analysis of multiple elements in shales and sediments will solve many of the puzzles stored in shales.

Prior efforts to characterize stable isotopes in shales, mudrocks, soil weathering profiles, and marine sediments date back to the early 1970s (Savin and Epstein 1970a,b) using conventional methods and relying on 30 mg of material. The $\delta^{18}O$ and δD isotopic investigation of shales and the details of their partitioning among their constituent minerals (clay minerals and secondary quartz) has been performed in the past in great detail by Taylor and Epstein (1962), Savin and Epstein (1970a,b), Yeh and Savin (1976), Yeh and Epstein (1978), and others (Churchman et al. 1976; Savin and Lee 1988; Sheppard and Gilg 1996). Their results showed that: 1) The clay and quartz components in shales are isotopically heavy, and $\delta^{18}O$ is shifted during weathering by a few to +25% with respect to the the mantle or the igneous protolith, with meteoric waters diverse in $\delta^{18}O$, and at different temperatures. 2) Upon formation of secondary minerals and their accumulation in sedimentary basins, rates of isotope exchange with ambient water are slow, and thus shales show little isotope exchange with lacustrine or sea waters after deposition (Land and Lynch 1996). 3) Diagenesis occurs in a narrow temperature window of 80 to 120 °C (Eberl 1993) and leads to a profound change in clay mineralogy and morphology (e.g., smectite and kaolinite are transformed into illite

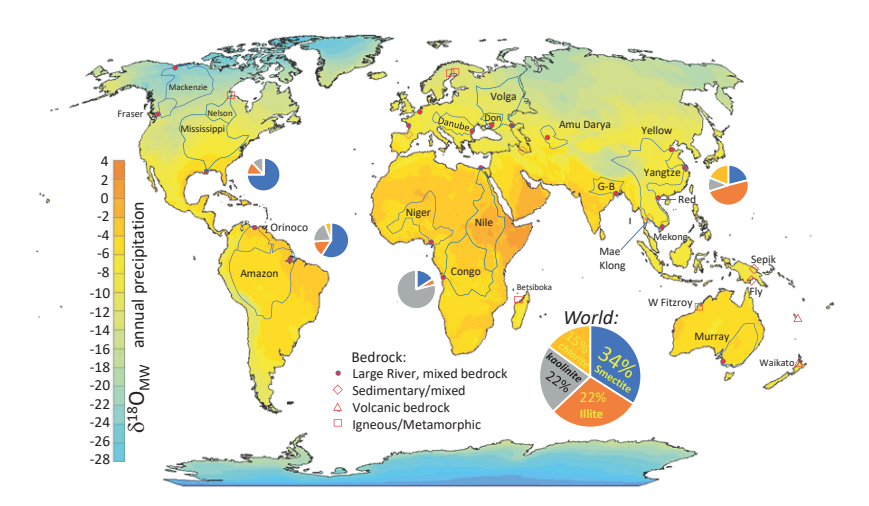


Figure 1. The isotopic composition of precipitation in the modern world, and river basins that were sampled for triple oxygen isotope analysis of suspended sediments. The sampled river basins cover most of the modern environments of weathering from tropical to Arctic, and from wet to arid. XRD-determined clay proportions for selected rivers and global average are shown. Predominant watershed bedrock types are also shown, but isotopic values of clays are not influenced by the bedrock, and reflect predominantly the temperature of weathering and $\delta^{18}O_{MW}$. [Used by permission of Elsevier, from Bindeman et al. (2019), EPSL, Vol. 528:115851, Fig. 1]

and chlorite, developing shistosity (Fig. 2). However, these changes may cause only 1-2 permil $\delta^{18}O$ increases due to loss of porewaters (Wilkinson et al. 1992), and they do not erase the multi-permil isotopic differences between shales formed in diverse environments. 4) Low post-diagenetic Darcy permeability of fine-grained shales leads to the preservation of both O and H isotopic signatures in the geologic record, far better than in cherts or carbonates (Land and Lynch 1996; Sheppard and Gilg 1996). 5) After diagenetic reactions are complete, fine-grained shales become virtually impermeable to secondary waters (Fig. 2, Pettijohn 1957).

Of the many chemical and isotopic proxies targeting these diagenetic processes, oxygen isotopes serve as the boundary between evolving lithosphere and hydrosphere, as oxygen makes up 49–53 wt% of rocks and 89 wt% of waters. Upon weathering, oxygen (and hydrogen) isotopic values of weathering products reflect that of the water, due to the great quantitative excess of water over rock (Silverman 1951; Savin and Epstein 1970a,b). Likewise, chemical precipitates from sea or meteoric water reflect the oxygen isotopic value of that water. If unaltered by subsequent isotopically different waters, these chemical sediments (carbonates, cherts, phosphates, etc.) should reflect the original oxygen isotopic values. It is also important to stress that shales record $\delta^{18}{\rm O}$ and $\delta^{17}{\rm O}$ values of *precipitated* water, while cherts, carbonates and phosphates for the most part provide a record of seawater.

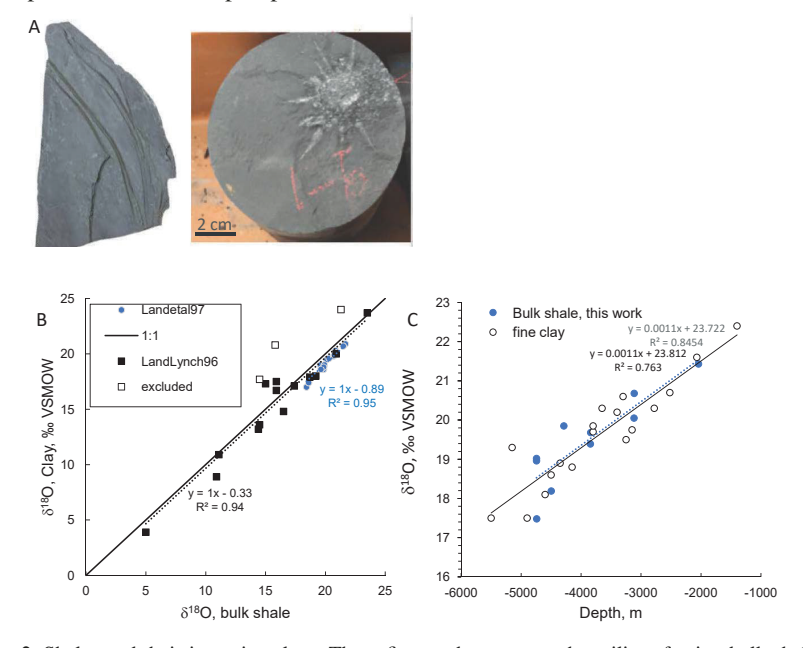


Figure 2. Shales and their isotopic values. These figures demonstrate the utility of using bulk shale as a proxy for weathering conditions, and that more tedious analysis of fine clay fractions shows equal scatter in the results. A) An unaltered shale with fine-grained texture, and a shale core sample that underwent secondary alteration, visible in disruption of thinly laminated schistosity, and recrystallization into coarser texture. Wells 6 and 1 Pleasant Bayou, Brazoria County Texas. B) Comparison of bulk shale analysis with that of the fine clay <0.1 μm fraction showing offset linear relationships. Plotted data for Phanerozoic shales are from Land and Lynch (1996) showing whole rock (WR) analyses offset by 0.33‰, and data from Land et al. (1997) sampling the Oligocene Frio Formation (Brazoria county, coastal Texas) offset by 0.89‰ because the quartz fraction in shale is a few per mil heavier than the bulk clay by mass balance. There is an overlap within the field of bulk shale and fine clay data, taken from Land et al. (1997) sampling the Frio Formation, and the shallower Miocene formation. C) Comparison of bulk shale analysis herein (Table 1) with isotope analyses for fine <0.05 μm clay from Yeh end Savin (1977) and <0.1 μm clay from Morton and Land (1985) from the same depths of the Frio Formation. Notice close overlap justifying the use of bulk shale measurements. The scatter is likely due to inherent depositional heterogeneity of the deposits or perhaps may indicate the additional presence of high-δ¹8O (amorphous?) quartz in fine-clay fraction.

14010 11 0	my gen n	sotope unary	oo or r reasur	ne Buyou I B	Turbottu Court	ity, restas arm note smale samples.
Depth, m	$T^{\circ}\mathbf{C}$	δ'^{17} O, ‰	δ'^{18} O, %o	$\Delta^{\prime17}\mathbf{O}_{0.5305}$	$\Delta^{\prime 17}\mathbf{O}_{0.528}$	
0	21	9.142	17.545	-0.166	-0.122	surface sediment
-1326 ^a	62	10.154	19.41	-0.143	-0.094	loose smectite-rich shale, Miocene
-1326 ^b	62	10.139	19.409	-0.158	-0.109	"
-2042	85	11.059	21.204	-0.19	-0.137	"
-3114	119	10.707	20.469	-0.152	-0.101	denser shale, Frio Fm Oligocene
-3117	120	10.398	19.852	-0.133	-0.083	"
-3840	143	10.219	19.489	-0.12	-0.071	laminated illite-rich shale Frio Fm Oligocene
-3845	143	10.038	19.204	-0.15	-0.102	"
-4287	157	10.268	19.656	-0.159	-0.11	II .
-4498	164	9.397	18.027	-0.166	-0.121	II .
-4740	171	9.066	17.329	-0.127	-0.084	п
-4743a	171	9.86	18.841	-0.135	-0.088	п
-4743 ^b	171	9.804	18.782	-0.16	-0.113	"
-4743°	171	11.127	21.267	-0.155	-0.101	quartz
-4743°	171	8.107	15.500	-0.116	-0.077	clay

Table 1. Oxygen isotope analyses of Pleasant Bayou #1 Brazoria county, Texas drill hole shale samples.

Note: Temperature is estimated using Dutton et al. (2015). $\delta^{\prime 17}$ O has $\pm 0.01\%$ average (1s) error based on five 8-cycles analysis (40 sample-standard repetitions). $\delta^{\prime 18}$ O has error of 0.1% based on standards; a,b means different areas of the same core sample. c refers to minerals (bulk Qz and bulk clay) extracted from this sample, computed liambda of quartz-clay triple oxygen isotope fractionation is 0.5239 at this temperature,

In the Figure 3 we plot concurrent records for carbonates, cherts, and shales. All of these show a general temporal increase of δ^{18} O, but with a different pattern. Note for example the decrease in δ^{18} O_{shale} values in the Permo–Triassic (~0.25 Ga), and lack of a similar signal in carbonates and cherts. There has been a bitter and contentious debate regarding these records in the past 50 years: either they record the result of decreasing δ^{18} O value of seawater and higher temperatures in the Archean and the Precambrian, or they record the result of alteration by meteoric waters (Muehlenbachs and Clayton 1976; Perry et al. 1978; Holland 1984; Gregory et al. 1991; Muehlenbachs 1998; Wallmann 2001, 2004; Veizer et al. 2002; Kasting et al. 2006; Sengupta and Pack 2018; Kanzaki 2020a). This Chapter will touch upon these lines of discussion by employing triple oxygen isotope values.

Mineralogically, shales contain two primary components: 60–70% clays, e.g., kaolinite, chlorite, illite, and smectites, and 20–30% quartz, with only minor amounts of other constituents e.g., feldspars, zircon, rutiles, etc. This mineralogical constancy characterizes shales of different ages (Shaw and Weaver 1965). Therefore, the oxygen isotope composition of mineralogically similar bulk shales through time, provides a consistent record of the weathering of terrestrial surfaces exposed to atmosphere and hydrosphere.

No systematic triple oxygen investigation of shales and sediments has been performed to our knowledge except for our recent efforts (Bindeman et al. 2018, 2019), although related low-temperature rock types such as cherts, low-T silica, and clays have been targeted both historically and recently (Fig. 3, Knauth and Lowe 2003; Levin et al. 2014; Hayles et al. 2017; Sharp et al. 2016; Liljestrand et al. 2020). The advent of Secondary Ion Mass Spectrometry (SIMS) in the past decade has resulted in tens of thousands of zircon detrital and igneous

analyses that permit linking their O and Hf isotopic values to U–Pb age (Valley et al. 2005; Dhuime et al. 2015; Hawkesworth et al. 2017; Spencer et al. 2017, 2019). Zircons preserve δ^{18} O values well even when there is no host rock available (especially for the oldest Hadean earth, 4.4–4.0 Ga, Wilde et al. 2001; Valley et al. 2002; Cavosie et al. 2018), this record however is "twice removed" from surficial environments as it reflects magmatic and metamorphic crystallization temperatures. However, these efforts by different methods and research groups may nicely complement each other by providing cross-checks

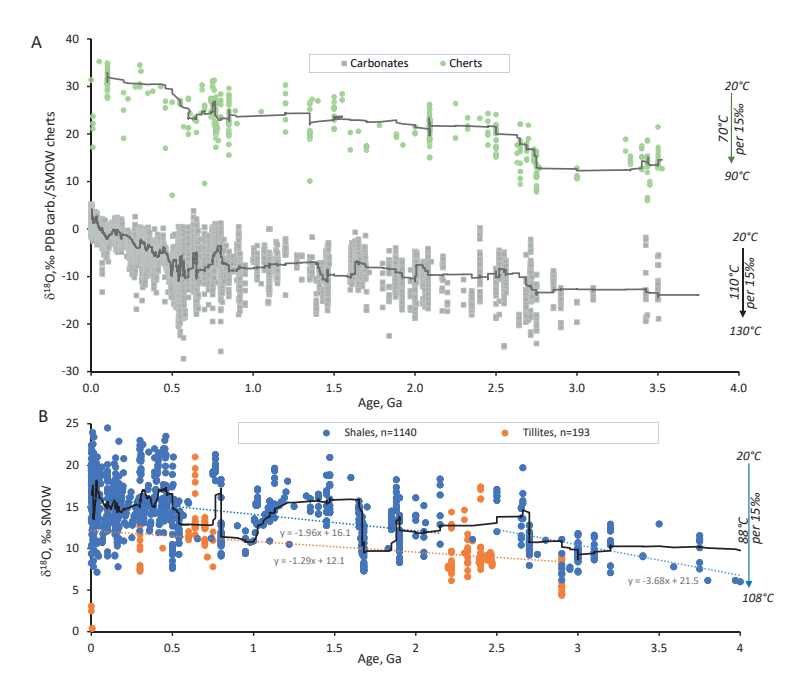


Figure 3. Comparison of $\delta^{18}O$ values of carbonates and cherts (A) with those for bulk shales and tillites (B). Data in this figure are from Bindeman et al. (2016) compilation with addition of data from Payne et al. (2015, shales and pelites only) and Gaschnig et al. (2016, tillites). Shales and tillites both indicate temporal $\delta^{18}O$ increase with an offset. These three sedimentary archives all show temporal increase but exhibits significant differences in the shape of the trends. In particular, the Phanerozoic record for shales exhibit a U-shaped trend, while the other proxies show an overall increase with time. **Arrows** indicate required temperature range and bounds to maintain $\delta^{18}O$ ocean at modern $\sim 0\%_0$ values, or a required $\delta^{18}O$ change of ocean to keep the temperature constant. Each arrow is pegged to specific $\delta^{18}O$ values on the y-axis corresponding to indicated temperatures at $0\%_0$ seawater.

Shales, granites and continental crust growth

Continental erosion generates fine-grained weathering products, which accumulate in depositional basins, river deltas, and are less dense (2 g/cc) than the bulk of the continental crust (2.7 g/cc). Even upon diagenesis and porosity reduction, shales and sediments remain much less dense and thus *largely* do not subduct into the mantle but instead accumulate in accretionary sedimentary prisms during plate collisions (Lackey et al. 2008, 2012). The rock cycle turns them into metamorphic, anatectic, and then igneous rocks (Fig. 4), commonly forming granitic stocks and batholiths. These high-grade crystalline rocks eventually become part of consolidated cratons. The mantle-derived juvenile magmas and their differentiates often provide heat and mass for crustal remelting and assimilation. In other cases however, relamination of silicic crust in subduction zones (e.g., Hacker et al. 2011)

accretes metamorphosed accretionary (and high- $\delta^{18}O$) sediments to the arc margins. Shallow subduction and trench migration also aid in the re-accretion of sediments, and slab brake-off lead to granite and ignimbrite flare ups (Chapman et al. 2013), remelting these sediments, such as in wide areas of western N America and Mexico (Watts et al. 2011; Ducea and Chapman 2018). Older metavolcanics, sandstones, carbonates, and greywackes constitute other components of arc rocks in creating the new crust, however siliciclastic sediments and shales constitute the majority of sedimentary rocks (Wedepohl 1995; Simon and Lecuyer 2005). Their subsequent weathering again into shale, passes their isotopic and chemical signatures to the second generation of shale. This rock cycle serves as an interesting topic to balance and reconcile multitude of elemental and isotopic fluxes and cycling and continental crust growth and evolution, multiple research groups around the world are engaged into this effort using their elements or isotopes of expertise.

Here I stress and demonstrate that transformation of sediments into metamorphic rock, then migmatite, and then anatectic granite (e.g., Fig. 4), inherit the absolute majority of oxygen originally derived from the hydrosphere via weathering. Bucholz and Spencer (2019) recently presented a nice overview of strongly peraluminous granites in the Precambrian, as these granites most closely reflect bulk sediment melt (cf Fig. 4). It is thus somewhat paradoxical that even the anatectic granite contains most of the oxygen that is ultimately derived from ancient rain water! The evolution of the continental crust, from the oxygen isotope perspective, thus includes continuous build-up of weathering-derived oxygen with its triple oxygen signatures (high- δ^{18} O, low- Δ'^{17} O), into the crust. A good analogy is our prior effort in studying low- δ^{18} O magmas worldwide (Bindeman 2008) showing that magmatic rocks with δ^{18} O values less than the mantle value of 5.7% are derived from re-melted hydrothermally altered rocks, and thus surface-derived oxygen (e.g., Friedman et al. 1974). A good example is the Yellowstone hotspot interacting with continental crust, and driving widespread hydrothermal alteration which gives the crust low- δ^{18} O values (e.g., Colón et al. 2019). Then, multiple overlapping calderas bury, remelt, and recycle this low- δ^{18} O hydrothermally altered surface of volcanic and plutonic rocks (Watts et al. 2011). These 1-2 Ma caldera cycles at hot-spot volcanoes represent an analogy for the entire crust evolution on perhaps 1–2 Ga timescales.

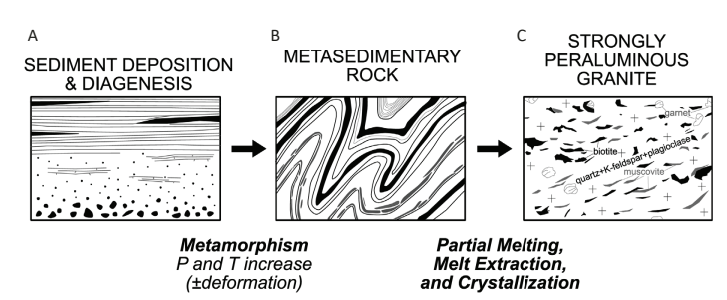


Figure 4. Rock cycle and largely isochemical and iso-isotopic transformation of shales into granite [Used by permission of Oxford Journals from Bucholz and Spencer (2019), Journal of Petrology, Vol. 60, p. 1299–1348, Fig. 1].

Here we extend this statement by suggesting that oxygen in most recycled continental crust reflects inheritance and cumulative build-up of oxygen inherited via exchange reaction from the hydrosphere. The hydrospheric effect on rocks largely excludes mantle and mantlederived igneous rocks, because while slabs with diverse $\delta^{18}O$ have been subducted at least since mid-early Archean (Condie et al. 2013; Brenner et al. 2020), their mass is negligible to that of the mantle, and thus the shift in mantle $\delta^{18}O$ is also negligible, but still is occasionally recognizable (Turner et al. 2007).

Investigation of triple oxygen isotopes in high-grade metamorphic, in anatectic rocks, and in granites provide a needed complementary view into the evolution of the continental crust in each time interval. Many orogenic granites represent the result of direct anatectic melting, or a large-degree assimilation of metasedimentary crust. Thus they average its composition and serve as a "time interval" average of hydrosphere conditions acquired during previous rock and attendant supercontinent cycles. The increasing δ^{18} O values of shales (Fig. 3, and decreasing Δ'^{17} O values) and granites (figures below) are considered to be correlated; they both indicate the inheritance of heavy oxygen from surface weathering reactions, and their time-integrated addition of hydrosphere-cycled oxygen into the silicate earth.

PART I: TRIPLE OXYGEN ISOTOPES IN WEATHERING PRODUCTS FROM MODERN AND RECENT ENVIRONMENTS

Weathering reactions and stable isotopic parameters

Continental weathering of silicate rocks proceeds with depletion of alkaline elements and calcium, followed by silica removal, leading to overall enrichment in Al in secondary neo-formed clays (Retallack 2001). As a consequence, Al-based indices of alteration, such as the Chemical Index of Alteration (CIA= Al₂O₃/(Al₂O₃+CaO+Na₂O+K₂O)_{mol}; Nesbitt and Young 1982), make use of Al/Si ratios, or other proposed chemical parameters, and typically serve as a measure of weathering intensity. To illustrate, a weathering reaction for anorthite proceeds as follows:

$$CaAl_2Si_2O_8 + H_2O + 2H^+ + CO_3^{2-} = Al_2Si_2O_5(OH)_4 + CaCO_3$$
Feldspar Kaolinite Calcite
$$CIA=50$$

$$CIA=100$$
(1)

As oxygen is exchanged in these reactions, the products carry a time-integrated isotopic record of weathering waters $\delta^{18,17}O_{WW}$, and temperatures:

$$\delta'^{18,17}O_{\text{weathering product}} = \Delta'^{18,17}O_{\text{mineral-MW}}^{f(T)} + (\delta'^{18,17}O_{\text{WW}}^{f(T)} + \Delta'^{18,17}_{\text{MW-WW}})$$
(2)

Similarly,

$$\Delta'^{17}O_{\text{weathering product}} = \Delta\Delta'^{17}O_{\text{mineral-MW}}f^{(T)} + (\Delta'^{17}O_{\text{WW}}f^{(T)} + \Delta'^{17}O_{\text{MW-WW}})$$
(3)

where for both meteoric waters (MW) and weathering waters (WW), fractionation factors are functions of temperature, and Δ_{MW-WW} is a potential offset between meteoric and weathering waters (e.g., due to evaporation in soils and watersheds and other effects).

Here and below, we use linearized definitions of $\delta^{18,17}O = (\delta^{18}O/1000+1)\cdot 1000$ (Miller 2002; Miller and Pack 2021, this volume), see Miller and Pack (2021, this volume) for definitions, and $\Delta'^{17}O$ is defined using a "rock" scale slope of 0.5305, but data is also presented in Tables and some figures with respect to the common scale with the slope of 0.528. In linearized coordinates these relationships are strict and fully interchangeable: $\delta'^{18,17}O_{min} - \delta'^{18,17}O_{water} = \Delta'_{mineral-MW} = 1000 \ln \alpha_{mineral-MW}$. Data presented in this work is normalized to VSMOW scale using $\delta^{18,17}O$ values of standards obtained at the University of Oregon: SCO=5.24% $\Delta'^{17}O$ =-0.05%; UWG2 garnet $\Delta'^{17}O$ =-0.06%; SKFS chert ($\Delta'^{17}O$ =-0.14%) and others; see Miller et al. (2020), Miller and Pack (2021, this volume), and Sharp and Wostbrock (2021, this volume).

Globally, isotopic values $\delta'^{18,17}O$ and δD in precipitation are strong functions of mean annual temperature (MAT) (e.g., Fig. 1; Dansgaard 1964; Rozanski et al. 1993;

Surma et al. 2021, this volume), a relationship that has been utilized widely to target paleoclimate based on isotopic values of surface mineral proxies. Furthermore, since the mass-dependence global waters varies along the widely utilized meteoric water line: $\delta D = 8 \cdot \delta^{18}O + 10$ (Dansgaard 1964). A multitude of studies since have demonstrated better applicability of local meteoric water lines, which are different from global by slope and intercept. For D/H ratio, the offset, or d-excess, is typically related to humidity of the boundary layer undergoing evaporation, and to a lesser extent, to the amount of precipitation (Criss 1999; Surma et al. 2020).

For triple oxygen isotopes, Luz and Barkan (2010) have proposed the widely utilized global triple oxygen meteoric water line:

$$\delta'^{17}O = 0.528 \cdot \delta'^{18}O + 0.033 \tag{4}$$

where the 0.528 slope of mass dependent oxygen fractionation is largely adhered to in most subsequent studies. Likewise, the 0.033 intercept value which we below call Y, or "Excess_ $\Delta^{17}O_{MW}$ " is related to humidity and precipitation effects, affecting offsets in triple oxygen isotope plots (e.g., Δ_{MW-WW}). Investigation of triple oxygen isotope effects in precipitation is a topic of current research represented by Passey and Levin (2021, this volume) and Surma et al. (2021, this volume).

Unlike bio(chemo)genic water precipitates for which water isotopic compositions are better known, each clay mineral during formation and transport interacts with a variety of waters: mean annual precipitation (MAP), evaporated soil waters, higher-altitude waters, diagenetic waters, and finally river water, and at different environmental temperatures including mean daily and seasonal climatic variations. Furthermore, some clays such as illite and chlorite may be derived from recycling of older sedimentary rocks, having experienced repeated weathering cycles that can reset initial O isotopic values. However, due to the large excess of meteoric water involved in weathering, we argue and test below that MAT and MAP can be used as first order proxies for world clay δ'^{18} O and Δ'^{17} O_{MW} signatures, and using the simplest global relationships such as Equation (4) (with and without intercept) is the most parsimonious approach to weathering, and that meteoric water serves as the average weathering water (Bindeman et al. 2019, Fig. 1).

Using triple oxygen isotopes in weathering products to estimate T and $\delta'^{18}O_w$ values

Before we enroll into a process and algorithm to deconvolute and interpret paleoclimate signatures of mudrocks and shales—the dominant but mixed sedimentary rock throughout the Earth's history—the reader may ask the question: why simply not use bio(chemo)genic proxies such as cherts and carbonates that directly precipitate from waters (e.g., Fig. 3)? There are two main answers. First, having an independent proxy using the most abundant sedimentary rock type can provide most robust constraints into evolution of weathering through time, as we think the uniformitarian nature of isotopic fractionation and equations that govern evaporation, water cycling and isotope fractionations holds through time. Second, carbonates and especially cherts have been plagued by the evidence of their post-depositional alteration (McKenzie 2005; Ryb and Eiler 2018; Liljestrand et al. 2020), which can be avoided by considering petrographically intact shales, e.g., those without any recrystallization and coarsening features (Fig. 2b). Additionally, Precambrian carbonates and especially cherts are polygenic (high-*T* hydrothermal and low-*T* chemogenic, Marin et al. 2010; Zakharov et al. 2021, this volume), and commonly represent mixed sources and processes.

Sedimentary proxies involving only δ^{18} O has always suffered from resolving effects of temperature or the starting δ^{18} O_w value. It plagues discussion of their relative effects and interpretation of isotopic records such as shown on Figure 3, as due to higher temperatures or lower δ^{18} O value of the hydrosphere in the Precambrian (Muehlenbachs and Clayton 1976; Veizer et al. 1999; Knauth and Lowe 2003). Triple oxygen isotope geochemistry is called

to resolve these question as there is an additional independent fractionation equation for δ^{17} O. Likewise, when hydrogen isotopes are deemed primary for hydrous phases, such as opal, smectites and kaolinites, for which both D/H and δ^{18} O fractionations factors are known (Savin and Lee 1988; Sheppard and Gilg 1996), it is possible to independently determine three unknowns: T, δ^{18} O and δ D (Capuano 1992; Delgado and Reyes 1996; Mix and Chamberlain 2014). This involves solving two fractionation equations for δ^{18} O and δ D in combination with a δ D – δ^{18} O meteoric water line equation, e.g., δ D = $8 \cdot \delta^{18}$ O + 10 of Dansgaard (1964). Hydrogen isotopes are however not part of the same isotopic system and easily modified by secondary processes in ancient weathering products and thus emphasis here on triple oxygen isotope geochemistry is warranted.

The triple oxygen isotope value of a particular phase of the weathering product or, by extension, a chemogenic precipitate (e.g., chert and carbonate) will reflect three parameters: i) the isotope fractionation relative to the parental water (Eqns. 2–3: $\Delta'^{18}O_{mineral-MW} = \delta'^{18}O_M - \delta'^{18}O_W$), ii) the mean annual temperature of weathering, iii) the $\delta^{18}O$ and $\delta^{17}O$ values of parental meteoric water that participated in weathering reactions, or an assumption about their relationship, through for example a global or local MWL (e.g., Eqn. 4).

The appearance of the first independently determined <u>triple</u> oxygen fractionation equation for quartz (Pack and Herwartz 2014; Sharp et al. 2016) and analogous efforts for other minerals (Chapters by Wostbrock and Sharp 2021; Passey and Levin 2021, both this volume), added another equation, yielding three equations ($\Delta^{17}O_{mineral-water}$ fractionation, $\delta^{18}O_{mineral-water}$ fractionation, and meteoric water line) for three unknowns ($\delta^{18}O_W$, $\delta^{17}O_W$, T).

For example, we proposed these two equations for bulk shale—water fractionation (e.g., Bindeman et al. 2018, 2019):

$$10^{3} \ln \left({^{18}R_{\text{shale}}} \right)_{^{18}R_{\text{water}}} = \frac{3.97 \cdot 10^{6}}{T^{2}} - \frac{4.9 \cdot 10^{3}}{T}$$
 (5)

$$\Delta'^{17}O_{\text{shale-water}} = \left(\frac{3.97 \cdot 10^6}{T^2} - \frac{4.9 \cdot 10^3}{T}\right) \left(0.5305 - \frac{2.05}{T} - \lambda\right)$$
(6)

Here, to characterize the triple oxygen composition of a sample, the Δ'^{17} O value is used to show the amount of 17 O excess relative to a reference line $\lambda = 0.528$ per Equation (4).

Bindeman et al. (2019) numerically solved the Equations (4–6) to obtain the temperature of weathering and $\delta'^{17}O$ and $\delta'^{18}O$ values of meteoric waters in equilibrium with modern suspended sediments in modern river watersheds, for which these parameters are independently known (MAT and $\delta'^{18}O$ for river or watershed waters). They further explored parameter space: changes in the slope of the Equation (4) and ^{17}O excess parameters (Fig. 5a). This Chapter additionally presents computed meteoric waters in equilibrium with river clays (Fig. 5b). These authors observed an overall match of observed modern river sediments and weathering products, and computed parameters based on them. They suggested a slope of 0.528 and an intercept *Y* that ranges from 0.033 to 0. Furthermore, Equations (5) and (6) can be linearly combined with the quartz–water fractionation equations of Sharp et al. (2016) to derive fractionation for any shale with a known wt% of authigenic quartz.

Comparison of waters involved in weathering at each well-studied watershed is a worthy task (see Fig. 5b and chapters by Passey and Levin 2021; Herwartz 2021, both this volume). Special environments, such as extremely dry regions in Africa, have high δ^{18} O values and local MWL with 17 O excess parameter in Equation (4) of 0 or even less than 0 for lake waters (Passey and Ji 2019). A study of triple oxygen variations of soil water, river water, and mean annual precipitation is thus urgently needed for different regions around the world.

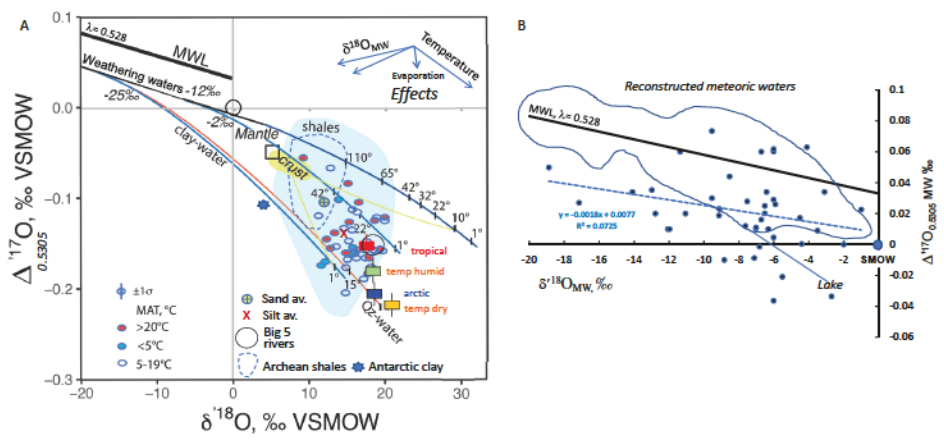


Figure 5. A) Triple-oxygen isotopes for the <4 \mu m fraction suspended sediment load from world rivers (Fig. 1), plotted for mean annual temperature (MAT) of weathering conditions in their respective watersheds. Clay-water fractionation lines emanate from the parental weathering waters. Note the significant overlap of clay triple-oxygen isotopic values from different climates, broadly explained by counterbalancing relationships of isotopic fractionation and MAT-δ18O_{MW} values. Clays from the modern world overlap the field of post-Archean shales, and this advocates for a comparable range of $\delta^{18}O_{MW}$ and surface temperatures, and overall hydrologic conditions of weathering since the post-Archean (inset showing Effects). The concave up yellow curves denote the mixing of weathering products with their detrital crustal material (see Fig. 4); the proportion of detritus is greater in global silt and sand. Two water lines are shown, the MWL of Luz and Barkan (2010), and the WW, "weathering water" line explained by the extent of the evaporation of water participating in weathering in soils (small vector under Effects). [Used by permission of Elsevier, from Bindeman et al. (2019), EPSL, Vol. 528:115851, Fig. 7]. B) Meteoric water line reconstructed using triple oxygen isotopic values of clays in rivers and temperature (MAT) and δ18O_{MW} values of their watersheds using formula 8 in text and data in Bindeman et al. (2019). Note that inverted this way waters are shifted downward, towards evaporated waters. Field and a line to the lake shows data from Passey and Levin (2021, this volume).

Bindeman et al. (2019) compiled δ^{18} O data from IAEA online resources and observed that river water and mean annual precipitation in their watershed basins for most rivers and precipitation around the world broadly agree (within $\sim 1\%$). We thus assume that weathering can be approximated, at least for now, by the values of precipitation, and use global MWL Equation (4).

To illustrate the above procedures, Figure 6 plots triple oxygen isotope values of a hypothetic weathering product in $\delta'^{18}O$ and $\Delta'^{17}O$ space, and explains the equation-solving approach. A system of three Equations (4–6) has three unknowns: temperature, $\delta'^{18}O$ and $\delta'^{17}O$ of parental meteoric water. We can thus solve them analytically, given an extra fractionation equation provided by $\delta'^{17}O$.

The above $\Delta^{'17}\text{O}-\delta^{'18}\text{O}$ reference framework is that which we will employ in the rest of this Chapter, and can also be conveniently thought in terms of previously used slopes of $\delta^{'17}\text{O}$ vs. $\delta^{'18}\text{O}$. Slopes of the fractionation lines in terrestrial environments range between <0.516 and 0.5305 and are specific to temperature, process, and the compositions of substances. Highest temperature equilibrium between silicates in igneous rocks show a slope close to 0.53, horizontal line in Figure 6 (Herwartz and Pack 2014; Pack et al. 2016). In this Chapter, we adopt the "rock" 0.5305 reference line, in which the $\delta^{'17}\text{O}$ deviation from this reference fractionation line is always negative and expressed as $\Delta^{'17}\text{O} = \delta^{'17}\text{O} = 0.5305 \cdot \delta^{'18}\text{O}$. We also report $\Delta^{'17}\text{O}$ values in Tables relative to a reference line with a slope of 0.528 and zero intercept, most commonly used in low-*T* and hydrologic communities. In particular this slope is characteristic for VSMOW-SLAP (Surma et al. 2021, this volume). For minerals that formed at lower temperature in equilibrium with water, such as amorphous silica, clays, quartz, and calcite, fractionation between water

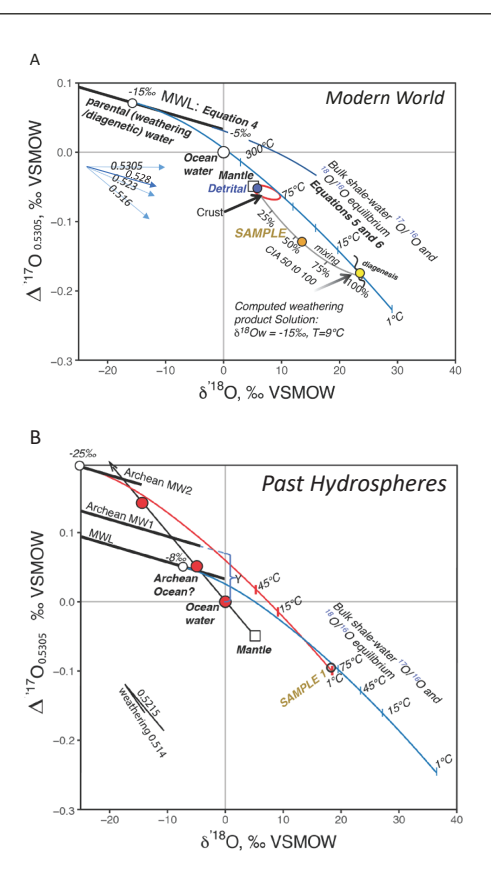


Figure 6. A) An example of the application of bulk shale—water triple oxygen isotopic values to resolve the isotopic values of weathering waters and the temperature of weathering. This involves solving a system of 3 unknowns: temperature, Δ'^{17} O, and δ'^{18} O, of parental weathering waters using a system of three Equations (4–6) in text. Concave down fractionation lines are for bulk shale emanating from δ'^{18} O_w=-5%c, and -15%c parental waters. Also shown is the concave up mixing curve between weathering product and the detrital component of shales. Weathering product is computed via a mass balance equation using independent chemical information for sample in this case the Chemical Index of Alteration (CIA). Diagenesis (see text) is mostly rock-dominated and is conservative of the weathering-related Δ'^{17} O and δ'^{18} O values, but leads to scatter in the data for each formation. **B)** Effect of changing δ'^{18} O values of the ocean on its Δ'^{17} O. Sample 1 can be solved for temperature and δ'^{18} O_w = -25%c, and using the modern MWL gives +76 °C and -8%c δ'^{18} O_w. **Red dots** along the line denote hypothetical ancient ocean water, each with a corresponding MWL. The shift likely proceeds along a line connecting the mantle and the modern ocean water as it predominantly involves high-*T* interaction of seawater at mid ocean ridges (Sengupta and Pack, 2018), and weathering with the comparable slopes shown from Bindeman et al. (2019). *Y* is an excess Δ'^{17} O as per Equations. (4) and (8).

and minerals results in a smaller slope value within the 0.525–0.524 range (Cao and Liu 2011; Bao et al. 2016; Sharp et al. 2016). Some lower T kinetic processes involving water and gases fractionate isotopes yielding an even lower exponent of 0.516 (Young et al. 2002; Pack 2021, this volume) or even 0.500 for gases in vacuum (Clayton and Mayeda 2009). These smaller slopes lead to strongly negative Δ'^{17} O values at the same δ'^{18} O values (Fig. 6). For example, below we explore formation of secondary quartz under low-T conditions (silicification) as the mechanism to explain strongly negative Δ'^{17} O values in some shales.

Computing the weathering product

Shales and recent sediments represent a mixture of solely physically weathered to strongly chemically weathered materials (Shaw and Weather 1965). The contribution of unweathered detrital (feldspars, amphiboles, etc) and previously weathered detrital (muscovites, illites) products needs to be evaluated to estimate $\delta'^{18}O$ and $\Delta'^{17}O$ isotopic values of the weathering product, by for example, using XRD. Figure 6 explores this. The proportions of detrital contribution to weathering products can also be evaluated based on a chemical analysis of a rock, and by using the simplest of weathering proxies, the CIA parameter defined by Nesbitt and Young (1982). CIA essentially measures the degree of feldspar conversion to clay minerals; a value of 45–50 signifies the absence of chemical weathering and the average composition of continental crust from Rudnick and Gao (2003) yields values between 45–50. Values between ~85 for K-Na bearing clays, and 100 for Ca-Na-K free kaolinite and chlorite, denote a rock that had undergone nearly complete chemical weathering, and thus likely oxygen isotope exchange with weathering waters. Since the CIA parameter does not include silica, addition of detrital quartz would not affect the CIA value. We note however that the detrital/ authigenic proportions of quartz very likely proportional to that of clays during weathering and sediment transport in silt- and smaller-size particles (Pettijohn 1957). For example, windblown and water-transported silt-size and smaller quartz was considered entirely authigenic as demonstrated by its high δ^{18} O values of +19.1 ± 1.4% worldwide (Churchman et al. 1976).

Figure 6 illustrates a graphical way of derivation of a weathering product, which algebraically involves a solution of a simple linear relationship $\delta^{1x}O_{\text{shale}} = \delta^{1x}O_{\text{weathering product}}$ $X + \delta^{1x}O_{\text{detrital}}$ (1-X), where X are normalized CIA values (CIA = 50 corresponds to X=0, and CIA = 100 corresponds to X=1) and solve it for $\delta^{1x}O_{\text{weathering product}}$ since the concentration of oxygen is the same in detrital and weathered materials. One needs to know or assume $\delta^{18}O_{\text{detrital}}$ and $\delta^{17}O_{\text{detrital}}$ values, note the unprimed delta values needed for mass balance calculations. Bindeman et al. (2019) computed a global average silicate surface undergoing weathering as +11.5% and -0.105% respectively. Different watershed areas in the modern world, especially for any sizable rivers that sample a variety of bedrock types are shown to be close to these values, as 60–70% of all silicate surface is represented by well mixed sedimentary rocks.

The sensitivity analysis shows that variation of CIA within ± 10 units results in $\pm 1\%$ change in the final output, computed $\delta^{\prime 18}O_w$, and ± 8 °C in computed temperature (Bindeman et al. 2018). Such uncertainties are comparable to other sedimentary proxies, such as cherts and carbonates. Evidence for this is that a typical CIA index for shales is 75 and does not vary much across their geologic history (Bindeman et al. 2016, 2018; Gaschnig et al. 2016). Thus, any procedure of correction for detrital contribution, likely offsets detrital estimates by a comparable constant, on average. Given this, one can simply compare measured values for shales as proxies for the environments, without computing absolute temperature and isotopic values of weathering waters involved. Such apple-to-apple comparisons permits broad statements regarding the change of the weathering conditions on earth through time. If no CIA correction is applied to measured $\delta^{\prime 18}$ O and $\Delta^{\prime 17}$ O values of modern river sediments, and thus effectively assuming that they are entirely composed of the weathering product, the computed $\delta^{'18}O$ of the water shows the comparable range, but the T of weathering is increased by ~10 °C and the resulting values are more scattered (Bindeman et al. 2019). These results are easily understood considering that the mixing lines are sub-parallel to the fractionation lines in Figure 6, where an increase in detrital proportion corresponds mostly to an increase in temperature with less effect on $\delta'^{18}O_w$.

Weathering in different climate regions

Studies of $\delta^{18}O$ and δD in monomineralic clays are used historically to reconstruct paleoclimate (Savin and Epstein 1970a,b; Capuano et al. 1996; Sheppard and Gilg 1996; Bauer and Vennemann 2014; Mix and Chamberlain 2014). Monomineralic clays such as smectite and

kaolinite do exhibit scattered correlation with temperatures below ~15 °C (Sheppard and Gilg 1996; Savin and Hsieh 1998) and overlap at higher temperatures. Bulk clays and weathering products are typically a mixture of common clay types: smectite, kaolinite, illites, and chlorite, with secondary quartz and albite, and proportions of these depends on the climate (e.g., Fig. 1, Newman 1987). It is difficult to nearly impossible to separate individual clays from a mixture and when handling common sediments derived by weathering, and so bulk analysis is sometimes the only option available (Gilg 2004).

Increasing Mean Annual Temparature (MAT) causes a decrease in clay–water isotope fractionation, thus $\delta^{18}O_w$ of meteoric waters decrease with decreasing MAT (Dansgaard 1964; Rozanski et al. 1993).

$$\delta^{18}O_{MW} = 0.69 \cdot MAT - 13.6 \tag{7}$$

As a result of opposing effects of temperature on clay–water fractionation (Eqn. 5) and this hydrologic relationship (Eqn. 7) between temperature and $\delta^{18}O_{MW}$, bulk clays from different climatic regions do not vary much isotopically (Bindeman et al. 2019; Fig. 5a). Only subarctic clays formed from very low- $\delta^{18}O$ waters display low- $\delta^{18}O$ values, there is little difference among different climate zones. Although this is discouraging news for paleoclimatology involving isotopic values of bulk clays, this effort captures the global climate conditions in the modern world with its temperature, hydrologic cycle, and weathering conditions.

Furthermore, measured $\delta'^{18}O$ and $\delta'^{17}O$ of clay samples from the river basins modern world (Fig. 1) with broadly known MAT of their watersheds and $\delta'^{18}O_w$ values of precipitation constitute a "natural experiment" of weathering. It enables solution of fractionation Equations (6) and (7), to solve the MWL Equation (4) for the intercept *Y*. The inverted equation for this purpose is:

$$Y = \delta'^{17}O_S - 0.528 \cdot \delta'^{18}O_S - (\delta'^{18}O_S - \delta'^{18}O_{MW}) \cdot (0.5305 - 2.05/T)$$
(8)

where Y is $\Delta'^{17}O$ —Excess as per Equation (4) (e.g., 0.033), T is MAT for each river basin, and $\delta'^{18}O_{MW}$ is compiled water data, subscript "S" refers to measured sample data.

Data for $\delta'^{17}O_S$, $\delta'^{18}O_{SN}$, $\delta'^{18}O_{SM}$ and MAT are substituted to this equation to compute the *Y* parameter, and results of inversion are presented on Figure 5b. One can see that the computed MWL, using this procedure plots subparallel to the global MWL (Eqn. 4), with smaller *Y*. This likely reflects more evaporated waters in soils involved in weathering and production of clays, than in precipitation (Passey and Ji 2019: Passey and Levin 2021, this volume). This was also suggested in Bindeman et al. (2019) by comparing computed vs. compiled MAT and $\delta'^{18}O_{MW}$. The Equation (8) enables further and more detailed analysis and quantification of the weathering products found in a particular water basin. This equation should be further improved by experimental determination of the clay—water $\delta^{17}O$ fractionation equation, as was done for quartz and carbonates (Wostbrock and Sharp 2021, this volume). This may result in revision of the 1.85 or 2.05 fit parameter in the last terms of Equations (6) and (8).

Bindeman et al. (2019) presented triple-oxygen isotope analyses of clay- and silt-size sediments from 45 rivers worldwide (Figs. 1, 5), which together cover about 25% of Earth's continental area, extending from the tropics to polar regions. They found that a majority of the studied clays closely approximate weathering products, always having high- δ^{18} O signatures regardless of the bedrock type, and in equilibrium with local meteoric waters at the respective MAT. Globally averaged, sediment-flux weighted suspended river sediment δ^{18} O and Δ^{17} O values are +14.8% and -0.16%, respectively. These values are significantly skewed toward O isotope signatures for the southeast Asia and western Pacific regions, characterized by very high sediment fluxes to the ocean (Milliman and Farnsworth 2011). Using both clay-and silt-size fractions, the total flux-weighted silicate weathering δ^{18} O signature exported to the world's ocean is -2.59%, almost 50% higher than the previous estimate, underscoring

greater proportional effect of modern weathering on global hydrospheric fluxes. This is also yielding an ice-free world hydrosphere estimate of -0.78%, very close to estimates provide by Sengupta and Pack (2018) and -1% value of Shackleton and Kennett (1975). Overall, the modern river clays represent a snapshot of modern weathering conditions on continents, and associated first-order climatic signatures related to MAT and δ^{18} O of the hydrosphere.

Effects of diagenesis on δ^{18} O and Δ'^{17} O in shales

Sediments weathered by low- $\delta^{18}O$ meteoric waters most commonly accumulate in marine environments, forming kilometer-thick sedimentary sequences. Yeh and Savin (1976) demonstrated with marine sediments that clay residence times of up to 10^6 – 10^7 yr in cold ~0 to -1% seawater does not affect their O and H isotopic values acquired during weathering. Yeh and Esslinger (1986) demonstrated no $\delta^{18}O$ modification of original detrital clays in Mississippi River delta or DSDP site 323 upon burial to depths as deep as 600 m.

It is indeed important to relate isotopic values of weathering products to those of consolidated shales that went through diagenesis. For weathering products, these values reflect surface weathering conditions $(T, \delta^{18}O, \delta^{17}O)$, with consolidated sedimentary rocks, and it is thus essential to establish the offset (if any) diagenesis induces in the original products. The latter is important to our ability to read the climate signature in sedimentary rocks.

The most important reaction of siliciclastic sediment diagenesis is the smectite to illite transition, that occurs between ~70 and 130 °C (Eberl 1993). This process leads to strong reduction of porosity from >20% to commonly <5%. This topic has been visited previously using δ^{18} O of bulk sediments, clays and quartz, carbonate cement, and pore fluids (Hower et al. 1976; Wilkinson et al. 1992; Land et al. 1997; Lynch et al. 1997). An excellent locale to test this question is in the thick piles of Oligocene–Miocene sediments along the Texas coast, where many wells up to 5000 m in depth fully span the smectite/illite transition (Fig. 7)

Our recent measurements of $\Delta'^{17}O$ and $\delta^{18}O$ (Fig. 7) were matched with samples from the same Pleasant Bayou and General Crude drill holes, according to depth, from Lynch et al. (1997), Land et al. (1997), clay and fine quartz analyses of Yeh and Savin (1977), where XRD-determined mineralogy is presented from these studies. Furthermore, $\delta^{18}O$ of diagenetic pore waters has also been analyzed in this Texas drillcore, as well as in DSDP, other Texas drill holes, and the Bengal fan in India (Lawrence et al. 1979; Land et al. 1992; Wilkinson et al. 1992). Collectively, they demonstrate a trend from ~-1% for ice-free seawater to "shifted" $\delta^{18}O$ values of +8–10% at the greatest depths of 4–5 km, and within the illite stability field. Significant scatter of analyzed $\delta^{18}O$ waters with depth (Fig. 7) permit different statistical fits, from linear to parabolic. This scatter is likely not analytical, but reflects different, and not-linear, progress of illitization reactions, and perhaps lateral dewatering via permeable sandstone layers at different depths. Isotopically negative water in shallow depth of Mississippi delta for example (Fig. 7) reflect volcanic glass alteration and carbonate precipitation from pore water in limited pore space (Lawrence and Taylor 1972).

The main observation of our new and previous analyses is that the δ^{18} O value of bulk sediment undergoing transformation to illite is shifted by 1-2% to slightly lighter values, in agreement with Lynch et al. (1997). Equilibrium smectite and illite-water fractionation factors as a function of temperature, and partial expulsion of water, are sufficient to explain the trends on Fig. 7 (Suchecki and Land 1983; Wilkinson et al. 1992). We here observe a minimal effect on Δ'^{17} O (Fig. 7), showing perhaps a slightly positive trend with depth. Water is lost during diagenesis from the smectite to illite transition. We suggest that isotope shifts related to progressive diagenetic water loss likely work in the same direction, favoring heavier δ^{18} O_w with decreasing total water with depth as is observed in Figure 7. No Δ'^{17} O analyses of basinal water is available to our knowledge; we thus concentrate on δ^{18} O values assuming that Δ'^{17} O will follow similar trends, by relating shales with basinal water on Figure 8. Fractionation lines are concave up with slopes of 0.525~0.528, mixing curves are concave up with slopes of ~0.51, and

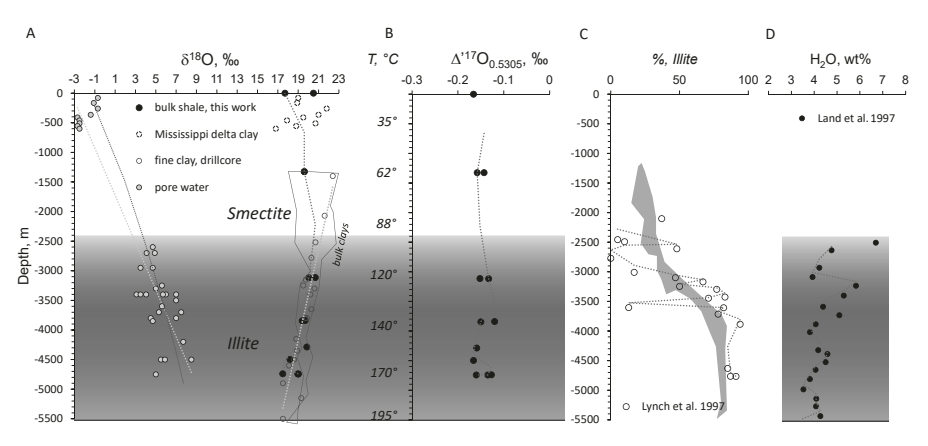


Figure 7. Triple oxygen isotopes in the deep Texas drillhole crossing the Oligocene Frio Formation, and Miocene and younger sediments in coastal Texas (**A–B**). Also shown are the diagenetic transformation of smectite into illite, which is accompanied by dehydration. A field for <0.01 and 0.05 μm bulk clays in **A** is from Yeh and Savin (1977), and the Mississippi River delta data are for <0.3 μm clay, and the water and are from the hole DSDP 323 (Yeh and Eslinger, 1986). Deeper water analyses from the same Texas drillhole are from Willkinson et al. (1992). Dutton et al. (2012) estimated a 24 °C/km geothermal gradient, and aging of sediment at 25 Myr per 100 °C increase, suggesting that the studied section represents ~45 Ma worth of sediment accumulation and burial diagenesis. These sediments sample Mississippi watershed, with relatively constant sediment input flux since the Oligocene (Galloway et al. 2011). There is little isotopic change with depth, with an ~2% decrease in δ^{18} O, and no resolvable trend in Δ^{17} O, despite the pronounced transformation from smectite-rich unconsolidated sediment, to illite-bearing laminated shale (Fig. 2a). Some variation in O isotopic composition is likely due slight variations in sediment composition.

the linear "diagenetic water line" on Figure 8 has an intermediate slope around ~0.52. Upon transition to illite, the micas, quartz, water, and pore water-precipitated cements are broadly in internal equilibrium with each other (Yeh and Savin 1986). Milliken et al. (1981) and Land et al. (1997) reported stages of mineral cement evolution in the Frio Formation drillhole involving dissolution of detrital K-feldspar and quartz and precipitation of secondary quartz and mica. We verified this result by plotting δ^{18} O values of the <2 μ m fraction quartz reported in Land et al. (1997), and observed (Fig. 8) adherence to quartz–bulk shale fractionation using the quartz–water fractionations of Sharp et al. (2016) for any quartz formed below smectite–illite transition where the temperature >120 °C. Using the 0.1–0.5 μ m quartz fraction from Yeh and Savin (1977), quartz–water equilibrium is achieved at 85 °C, in broad agreement with Milliken et al. (1981) on growth of authigenic quartz in pore spaces. This result is a test for internal equilibrium in shale upon precipitation of secondary silica during transition of smectite into illite.

When plotted on a Δ'^{17} O vs. δ^{18} O diagram, there is a significant overlap of samples from different depths. When data points are compared to empirically calibrated bulk-shale—water curves (Fig. 9) our new triple oxygen isotope analyses are scattered, but cluster around δ^{18} O values of –5 to –15% equilibrium for parental water, and at T of +10 and +40 °C. The average δ^{18} O and Δ'^{17} O shale of the Frio Formation belongs to 15 °C and δ^{18} O of –11.5% parental water. Although the bulk-shale—water fractionation are semi-empirically calibrated by Bindeman et al. (2018) using the quartz—water fractionation of Sharp et al. (2016), datapoints are positioned much lower in δ^{18} O and Δ'^{17} O than would be required for shales in the borehole temperature range of 85–170 °C and pore waters with +10% δ^{18} O. This indicates that shales provide a record of *weathering* conditions, rather than diagenetic transformations. Furthermore, if corrected for detrital contribution (as per Fig. 6, using CIA = 70 in these rocks), the computed

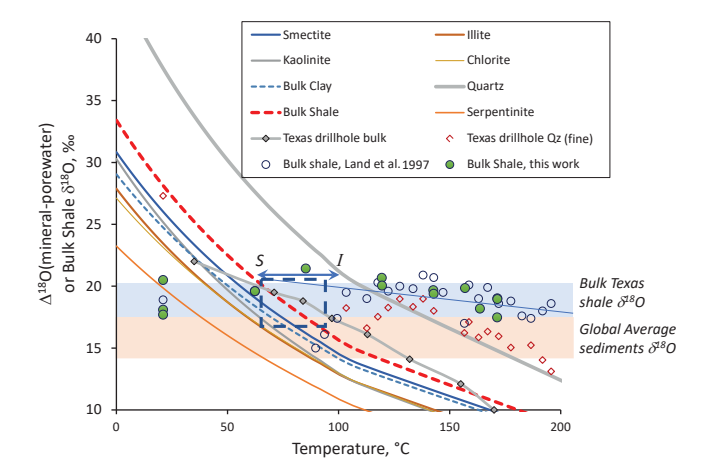


Figure 8 Δ^{18} O (bulk shale–porewater) and Δ^{18} O (quartz–porewater) values vs. temperature in the Texas drillhole (Fig. 7), is compared to experimentally determined isotopic fractionation factors (Savin and Lee 1988; Sheppard and Gilg 1996; Sharp et al. 2016). Porewater δ¹⁸O values are linearly approximated from Fig. 7 to compute the Δ^{18} O(shale–porewater) values shown. Notice that shale quartz with T > 122 °C is in equilibrium with pore waters, while fine <0.5 µm quartz from Yeh and Savin (1977) is in equilibrium at ~80 °C. The Texas drillhole bulk shales (grey diamonds and lines) hover around the red dashed line representing computed bulk shale-water equilibrium fractionation. Superimposed on this graph using the same vertical axis are bulk shale $\delta^{18}O$ data from Fig. 7 plotted against drillhole temperature. Shale $\delta^{18}O$ values can also be read as Δ^{18} O(shale-0\% seawater) fractionation. Note that in the smectite (S) to illite (I) transition temperature window (dashed box with arrows), computed bulk-shale-0% seawater fractionation is equivalent to the original bulk shale δ^{18} O value, yielding no net flux of oxygen isotopes at these temperatures for the Texas drillhole samples. For modern average global sediments (e.g., Fig. 5a), the crossover temperature is ~30 °C higher. At T higher than the indicated crossovers, bulk shales will be shifted down due to diagenesis, and waters are shifted up as is observed in Fig. 7. For lower in δ^{18} O global average shale, this shift is likely to be less, and only for deeper diagenetic conditions shown. Notice that plotted shale bulk δ^{18} O values do not follow the bulk shale—water **dashed red curve**, and thus retain their original δ^{18} O values because the shale–porewater system is a rock-dominated.

weathering product corresponding to the Frio Formation will shift further down and to the right, and will overlap the composition of weathering products in equilibrium with either the modern Mississippi River watershed, or those slightly higher δ^{18} O weathering products in equilibrium with Oligocene waters.

We further observe no definite relationship between borehole T and the measured isotopic values. While some variation is due to analytical error ($\pm 0.2\%$ $\delta^{18}O$ and 0.01% $\Delta'^{17}O$, 1σ), other variation may reflect slight variation in provenance of sediments. In either case the data does not show any systematic trend with temperature of diagenesis or transition of smectite to illite. Frio Fm changes $\delta^{18}O$ from ~21% at smectite-rich top and T from 25 to 35 °C to +18.5% at depth. However, variations in modern Mississippi river muds show a similar range, suggesting that observed vertical isotopic trends in the Frio Formation may be partly reflecting temporal depositional variations. Hower et al. (1976) interpreted mineralogical and chemical changes as the response of the shale to burial metamorphism and concluded that the shale was a closed system for all components except H_2O , CaO, Na_2O , and CO_2 . This isochemical nature was challenged somewhat by Land et al. (1997) who observed minor uptake of K_2O with depth related to illitization. These authors suggested that 0.2–0.3 wt% extra K_2O was derived from KFsp dissolution from adjacent silt and sandstone layers. Given that oxygen is a major element, its isotopes should be predominantly conserved.

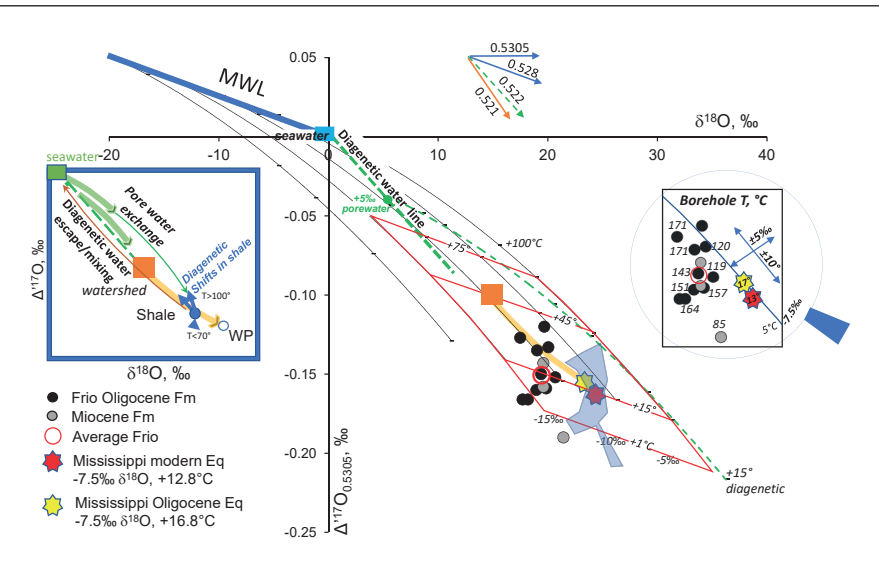


Figure 9. A triple oxygen diagram for samples from a Pleasant Bayou Texas drillhole (Fig. 7–8) superimposed on a grid of calculated values for bulk-shale-meteoric water fractionation lines, each emanating from a point on the meteoric water line. The evaporated meteoric water line with a slope of 0.528 and intercept Y=0, is shown in blue as in Figure 5a, and a hypotherical diagenetic water line connecting 0% seawater with bulk shales is shown in green. Concave up shale-diagenetic water equilibrium fractionation lines are also shown in green and are emanating from the diagenetic water (dashed) line in main figure and square inset. These may denote evolution of triple oxygen isotopes in pore waters and in shales experiencing diagenetic shifts. Pre-diagenetic pore waters likely evolve along the straight line resulting from a combination of concave up mixing and concave down fractionation lines. The approximate directions for low and high-T diagenetic shifts is shown in the square inset. The **brown box** denotes the likely detrital composition of the Mississippi watershed, taken as the average of modern Earth's surface triple oxygen isotopic values. A concave up yellow line connects this box with the average value of the Frio Formation shale to compute its weathering product based on whole-rock chemical analysis (e.g., Fig. 6a); the blue angular polygonal field represents computed weathering products for the Oligocene Frio and Miocene formations. Shale samples scatter around +15 to +45 °C and -5 to -15% δ^{18} O parental meteoric water values, weathering products are shifted to lower T and higher δ^{18} O, and overlap with equilibrium weathering product estimated values for both modern and Oligocene-Miocene weathering conditions. The scatter in data reflect the some depositional isotopic diversity, and minor effects related to diagenesis as is explained in the square inset and Figure 7. The circular inset shows the portion of the diagram with borehole temperatures included for each sample. Notice that there is no correlation between the borehole temperatures and their isotopic temperatures that are computed based on shale-meteoric water isotope fractionation. This is due to the fact that diagenesis is a strongly rock-dominated process and is largely isochemical, and thus preserving the weathering conditions.

The *average* composition of the Frio Formation plots much closer to the temperature and $\delta^{18}O$ of precipitation in the Mississippi River Basin. Global temperatures that were involved in generating weathering products at the Oligocene–Miocene boundary were 5–6 °C higher than today's 12.8 °C, thus around ~+17 °C (Retallack 2007). Given comparable to modern orography and latitudes of N America then, $\delta^{18}O$ of precipitation was likely comparable in $\delta^{18}O$ to that of modern Mississippi River draining wide swaths of the N. American continent, by analogy with a relationship between average precipitation and river water (Galloway et al. 2011). In the warmer periods of the Oligocene and Miocene, $\delta^{18}O$ values of precipitation may have been 1% heavier given the global $\delta^{18}O$ –T relationship (Eqn. 7), but Antarctica was just in the beginning of its ~34Ma glaciation, and thus the oceans were ~1% lighter than today (Shackleton et al. 1975). For example, Zanazzi et al. (2015) found no variation in $\delta^{18}O$ of precipitation in northern part of North America based on *Perissodactyl* mammal tooth enamel. The Mississippi River, and this Texas drillcore thus represent a good insight into average Earth surface conditions in Late Cenozoic.

The paragraphs below provide further insight into diagenetic processes and their effects on isotopic values of shales. The Frio Formation was deposited in $-1\% \delta^{18}$ O Oligocene seawater, and the exchange reactions were inhibited for tens of millions of years (Savin and Epstein 1972b). Burial to several kilometer depth and geothermal T increase, perhaps approaching that of the smectite/illite transition of ~70–120 °C, (Figs. 7, 9) initiated chemical solution-reprecipitation and thus isotopic exchange reactions (Hower et al. 1976; Eberl 1993). At this stage, the mildly shifted $\delta^{18}O = 0\%$ seawater, filling the remaining ~10–15% porespace, begins reacting and exchanging oxygen with the surrounding silicates. The important observation on Figure 8, is that the sense of isotopic fractionation is such that the original bulk δ^{18} O of +18% of surface sediment has zero $permil\ \Delta^{18}O_{shale-water}\ (=\delta^{18}O_{shale}-\delta^{18}O_{porewaters})\ fractionation\ at\ 85\ ^{\circ}C.\ For\ a\ world\ average\ surface$ sediment of 14.1% (Bindeman et al. 2019), the temperature of the inversion is higher at ~100 °C. Thus, the initial transition of smectite to illite is accompanied by zero isotopic shifts in marine porewater, and expelled porewater may be in equilibrium with silicate. If ancient seawater were -10% as is commonly proposed, then the corresponding meteoric water evaporating from that ocean, and weathering products would have also have shifted to lower values, and the logic on minimal diagenetic transformation holds for ancient times.

Subsequent burial, heating, and exchange leads to dissolution of smectite and formation of illite and appearance of diagenetic quartz, (Hower et al. 1976; Land et al. 1997), that is a predominantly isochemical reaction. The precipitating quartz fills the porespace, and precipitating K-mica from dissolution of detrital K-feldspar (Land et al. 1997) further reduces porosity. We plotted $\delta^{18}O$ analyses of <2 μ m quartz presented in Land et al. (1997) along the Texas drillcore (Fig. 8) and observe that quartz is in ($\delta^{18}O_{Qz} - \delta^{18}O_{porewaters}$) equilibrium starting at 122 °C, and fine <0.5 μ m quartz from Yeh and Savin (1977) is already in equilibrium at ~80 °C. Data for porewaters at respective depths are approximated from data in Figure 7, and are chiefly derived from Land (1992) and Wilkinson et al. (1992).

Subsequent diagenesis in a rock-dominated system proceeds with slightly decreasing $\delta^{18}O$ values for shale, and an increase in porewater $\delta^{18}O$ (Fig. 7), as is observed in the highest temperatures at 5 km in the Texas drillcores. Upon temperature decrease, due to for example a hypothetical closed system retrogression of Frio formation as a result of the uplift, shale would regain its original $\delta^{18}O$ value due to retrograde reaction with porewater. Such retrograde reactions would likely close to isotopic exchange at temperatures not that different than the illite-smectite transition, and yield zero overall isotopic effects. The reasoning above depends of course on the quite important diagenetic smectite–illite transition. However, many shales worldwide do not reach 5 km depths nor the temperature of 200 °C as in deepest holes of the Frio Fm, and thus hover around illite–smectite boundary, and so they maintain the original $\delta^{18}O$ value characteristic of deposition. Longstaffe (1983) reviewed several such examples.

I thus conclude that a typical shale retains isotopic values of the original sediment. Diagenesis shifts its $\delta^{18}O$ value to within ~1‰, as is observed in our dataset (Figs. 7–9). We also believe that $\delta^{18}O$ (and $\Delta'^{17}O$) values in shales are preserved in geologic record. Consolidated shale (Fig. 2), due to its very small crystal size, has negligible filtration porosity and permeability to secondary fluids with different in $\delta^{18}O$ (Land and Lynch 1997). If secondary interaction with such water occurs, it will result in petrographic evidence such as crystal size coarsening, recrystallization, and chemical alteration that are possible to recognize petrographically, in XRD and thin sections (Fig. 2) and to be avoided during sampling and analysis.

We draw attention here that this Chapter reviews only shales and not sandstones, which commonly undergo a complex recrystallization history by low- δ^{18} O artesian waters generating overgrowths with secondary δ^{18} O values recognizable by SIMS (Longstaffe 1983; Pollington et al. 2011). Likewise, lacustrine, periglacial, and syn-snowball earth low- δ^{18} O, high- Δ'^{17} O waters and depositional environments, will undoubtedly have an alternate scenario to marine

deposition, and leading to generation of the low- $\delta^{18}O$ shales. This is observed for shales and tillites formed at the 2.2–2.4 Ga Huronian and 0.5–0.6 Ga Cryogenian age, when shales presumably formed from ultra-low-synglacial waters (Fig. 9, Bindeman et al. 2016), and is also observed for the Pliocene Antarctic claystone analyzed by us in Figure 5a, and perhaps lower overall $\delta^{18}O$ values of tillites as compared to shales (Fig. 3). Land and Lynch (1996), who compared lacustrine and ocean-deposited shales for non-glacial time intervals argued that these are lower by only 1–2‰ $\delta^{18}O$, again emphasizing expulsion of porewater as the dominant mechanism of diagenesis. Further work needs to be done on the particular synglacial formations and their diagenetic history.

Effects of metamorphism and anatexis on δ^{18} O and Δ'^{17} O

It is important to discuss what happens to triple oxygen isotopes during further transformation of shales into schists, gneiss, and later anatectic granites (e.g., Fig. 4). The Texas drillhole with its illite-dominated mineralogy and ~190 °C bottom temperature can be viewed as lowermost greenschist metamorphic facies (Fig. 7). Illite-dominated Frio Formation shale has 4.1 ± 0.8 wt% H_2O stored in clays and 7.7 ± 1.4 wt% carbonate cement (3.2 wt% CO₂) in pore space (Land et al. 1997). Carbonate cement has the average $\delta^{18}O$ value of $+24.7\pm0.7\%$ SMOW (Land et al. 1997), largely in equilibrium with +6% pore waters and bulk silicate shale at these depths at the drillhole temperatures (Land et al. 1992, 1997). To estimate overall $\delta^{18}O$ fractionation shifts related to hypothetical transformation of this shale into a crystalline schist, and further into amphibole gneiss, we choose the illite starting composition of Frio Formation. Using temperature-dependent fractionation factors for illite– H_2O and quartz– CO_2 (Zheng et al. 1993) enable computation of overall $\delta^{18}O$ effects related to loss of H_2O and CO_2 in either Rayleigh or a batch process.

The $\Delta^{18}O(\text{shale-CO}_2)$ fractionation stays negative over a 200–750 °C temperature range, and a complete loss of 3 wt% CO₂ at 450 °C will result in –0.2‰ depletion of the remaining rock. The $\Delta^{18}O(\text{shale-water})$ is initially positive (+0.2‰ at 200 °C, thus initially compensating for the negative isotopic effect of CO₂ loss, but crosses over to negligibly negative –0.05‰ values at temperatures higher than ~425 °C. The overall effect upon $\delta^{18}O$ of losing both 3 wt% of clay-held water, and carbonate-hosted CO₂ is thus close to zero to perhaps –0.2‰ for a shale containing 3.2 wt% initial CO₂ (7–8% initial carbonate). The calculations and conclusion are in agreement with earlier work of Valley (1986) on decarbonation reactions of limestones and calcareous sediments and their limited extent on changing bulk rock $\delta^{18}O$ values. Details of devolatilization, whether continuous or punctuated, have little effect.

Thus, at post-diagenetic temperatures higher than 200 °C, there are minimal isotopic effects on $\Delta'^{17}{\rm O}$ as in Figures 5–6. This observation when coupled with a small $\delta^{18}{\rm O}$ effects of devolatilization and metamorphism of shale into schist, suggests preservation of diagenetic $\delta^{18}{\rm O}$ and $\Delta'^{17}{\rm O}$ values essentially unchanged well into the metamorphic and igneous realms. It also adds to the credence of using metamorphic schists as recorder of environmental surface conditions, provided that these rocks have not been modified by secondary fluids with different oxygen isotopic values. Moreover, if zircons crystallized within these schists and gneisses, these zircons should reflect and preserve triple oxygen isotopic values of the host rock. Thus, *if* zircons formed in this way and are found as detrital grains in sediments, especially where the original host rock is now absent, especially for the oldest zircons (Valley et al. 2002; Hawkesworth et al. 2015; Spencer et al. 2019), these indeed provide a distant glimpse into surface weathering conditions that existed before crystallization of zircons as metamorphic mineral grains. I propose to couple the triple oxygen investigation of zircons with their chemical and isotopic features that proves their supracrustal origin.

PART II: SHALES ACROSS THE GEOLOGIC HISTORY

Overview of temporal trend of δ^{18} O and Δ'^{17} O and Archean vs. post Archean shales

The earliest observation that early Precambrian shales have lower $\delta^{18}O$ than modern shales belongs to Silverman (1951). Longstaffe and Schwatrz (1977) and Land and Lynch (1997) presented early data of temporal evolution of $\delta^{18}O$ in clastic sedimentary rocks and shales. Subsequent work incrementally added to the temporal records. Figure 10 shows a temporal increase in shale $\delta^{18}O$ values with variation modulated by the supercontient cycle. Valley et al. (2005), Dhuime et al. (2015) and others observed temporal increases in zircon $\delta^{18}O$ values (Fig. 10). However, zircons record a history of high-temperature igneous and metamorphic crystallization and recrystallization reactions in maturing metasedimentary crust, but diluted by a normal- $\delta^{18}O$, mantle-derived component, with constant $\delta^{18}O$ value across the geologic history. The reason for the zircon $\delta^{18}O$ increase, like the record of granites that we present below, is rooted in evolution of shales.

The reason for a δ^{18} O temporal increase is unlikely to be related to a dramatic change in the crustal compostion from mafic to silicic. Taylor and McLennan (1993), Rudnick and Gao (2003), Gashnig et al. (2016) provided a detailed discussion of chemical composition of shales and tillites through time, suggesting that exposed areas of the crust undergoing weathering retained approximately similar proportions of crustal and mantle derived compositions, on average dioritic through time; an exception noted is of greater proportions of komatiites in the Archean (yielding high Ni, Cr, V concentrations in shales, Li et al. 2016). The δ^{49} Ti measurements for the same shale suite studied by us for oxygen isotopes in Figure 10, demonstrated that proportions of silicic to mafic rocks undergoing weathering has also remained approximately constant since at least 3.5 Ga (Greber et al. 2017). Furthermore, Ptáček et al. (2020) used an inversion of elemental composition in fine terrigenous sediments and demonstrated a that a continuous >50% felsic contribution is required starting from 3.5 billion years ago. This finding is consistent with an early onset of plate tectonics. We demonstrate above that the composition of the crust, whether slightly more mafic or more granitic, plays only a small role in the current $\delta^{18}O$ (and $\Delta^{\prime 17}O$) values of weathering products; these are determined primarily by temperature and δ^{18} O of the weathering waters.

Bindeman et al. (2018) presented triple oxygen data for shales across geologic history (Fig. 10b), and I add here new data covering the Phanerozoic. There is a stepwise shift to more negative and more diverse Δ'^{17} O values during and after the Archean-Proterozoic transition. The extended dataset presented here (Table 2) supports this observation, and the granites discussed below also show this step-wise change at ~2.1–2.4 Ga. Shales older than 2.5 Ga, yield an average $\Delta^{\prime 17}O = 0.047 \pm 0.012\%$ ($\pm 2\sigma$), largely overlapping with the mantle values, while shales younger than 2.2 Ga, yield an average $\Delta'^{17}O = -0.118 \pm 0.024\%$. This difference in $\Delta'^{17}O$ between the two age groups cannot be explained by different temperatures of equilibration or by mixing in different proportions of variably weathered detrital materials. The shale record spans the $\delta^{\prime 18}O-\Delta^{\prime 17}O$ trends defined by these processes (Fig. 11), and thus requiring different initial δ'^{18} O meteoric waters. Taking clues from the modern world, where meteoric water shows variable $\delta^{18}O$ – $\Delta'^{17}O$ compositions, the simplest explanation for some of the oxygen isotopic variations is that they were partly inherited from the waters involved in rock alteration on the continents. Starting roughly at the Archean-Proterozoic transition, this emerged crust interacted with waters that had more variable and on average more negative $\delta'^{18}O_{w}$ and more positive $\Delta'^{17}O_w$ values than before the GOE, with $\Delta'^{17}O_w$ shifted by approximately +0.1%.

The $\delta'^{18}O_W$ and $\Delta'^{17}O_W$ of precipitation in the modern world depends on the cumulative history of water loss from an air parcel traveling inland away from the coasts, to higher latitude, and higher altitude, resulting in lower $\delta'^{18}O_W$, higher $\Delta'^{17}O_W$, and more diverse compositions overall, as in Figures 1 and 11. This combined effect that I call "continentality"

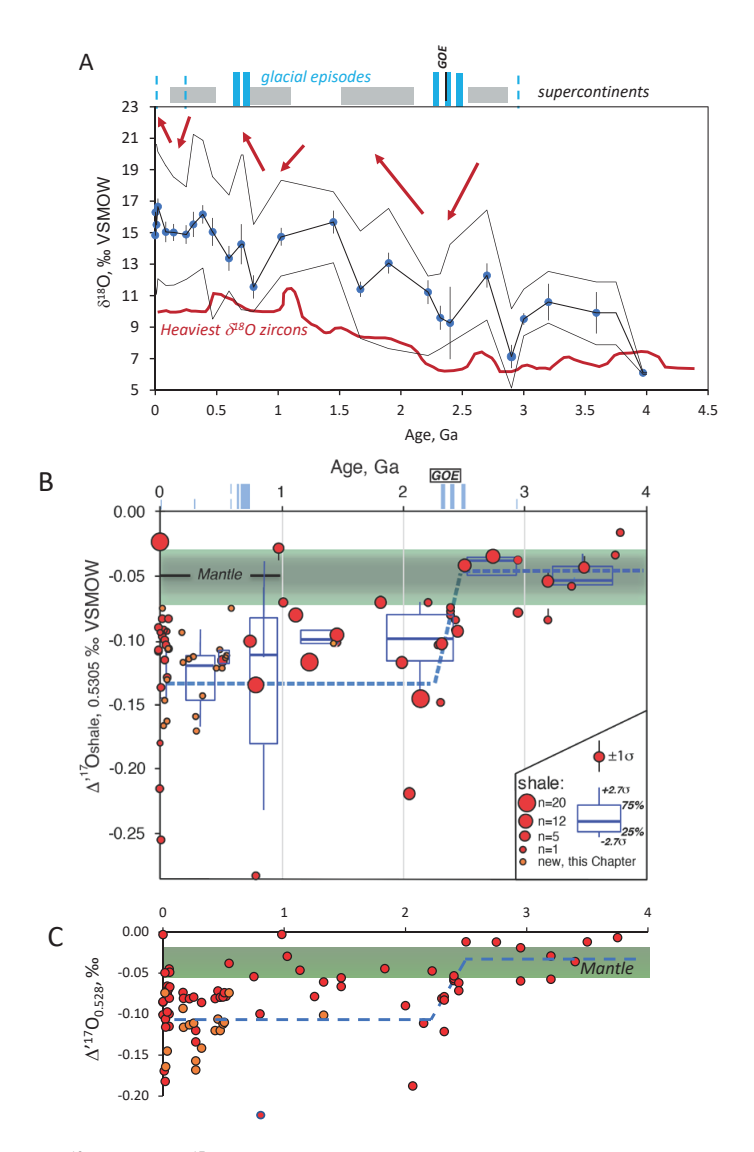


Figure 10. The δ^{18} O (**A**) and Δ'^{17} O (**B, C**) of average shales through time (data from Bindeman et al. 2016; 2018 with added data points for the last 1.2Ga, smaller circles, Table 2). **A**) average values and bounds, the highest δ^{18} O values (upper 10%) for each time interval are exceeding the 90th percentile, closely approaching the weathering product and thus the full extent of chemical weathering. The record is correlated to the supercontinent cycle and glaciations; the GOE is Great Oxidation Event which occurred broadly at 2.32 Ga, after the first Paleoproterozoic glaciation (Zakharov et al. 2017). The igneous zircon δ^{18} O record is shown (yellow line, Valley at al. 2005) demonstrating the coeval maturation of the crust resulting from increases in heavy in δ^{18} O sedimentary component. **B**) Notice step-wise Δ'^{17} O change at ~2.4–2.2 Ga, explained by the appearance of diverse, and similar to modern hydrologic and weathering cycle upon emergence of subaerial crust after the Archean, see Fig 11 and 5 for explanation of effects of diverse in δ^{18} O waters and temperatures. **C**) Same data as in B but plotted vs. a reference slope of 0.528, and demonstrating similar relationships. [Fig 10B is used by permission and with modification from Nature, from Bindeman et al. (2018), Nature, Vol. 557, p. 545–548, Fig. 2a].

Table 2. New triple oxygen isotope analyses of shales, computed.

								١								
	Spec number	O_{81} \otimes	O ₈₁ ,8	O ₂₁ ,8	δ^{17} O	$\nabla^{\prime 17}$	$\Phi^{\prime 17}$	u	O_{L1}	$\delta^{18}O_{\rm WP}$	$\delta^{17}O_{\rm WP}$	$\delta^{'18}O_{WP}$	$\delta'^{17}O_{\rm WP}$	$T^{\circ}C$	$\delta^{18}O_{\mathrm{MW}}$	$\Delta^{\prime 17} O_{MW}$
	F118066*	9.833	9.785	5.117	5.13	-0.074	0.01	7	-0.0495	8.166	4.284	8.133	4.275	74	-10.253	0.059
165	F114833	7.8	77.7	4.029	4.037	-0.093	900.0	5	-0.0736	4.1	2.098	4.092	2.096	27	-23.141	0.091
169	F108499	14.199	14.099	7.364	7.391	-0.116	0.004	9	-0.0808	16.898	8.806	16.757	8.767	19	-12.59	0.063
218	F106537	12.81	12.729	6.64	6.662	-0.113	0.01	5	-0.0812	14.12	7.348	14.021	7.321	20	-15.009	0.07
253	F112216	12.797	12.716	6.635	6.657	-0.111	900.0	2	-0.0792	14.094	7.338	13.996	7.311	19	-15.292	0.071
270	F108479	14.945	14.834	7.713	7.742	-0.157	0.009	5	-0.1199	18.39	9.509	18.223	9.464		no solution	
318	F110201A	22.512	22.262	11.669	11.737	-0.141	0.012	9	-0.0858	33.524	17.498	32.974	17.347	48	3.464	0.024
430	F110412	15.719	15.597	8.154	8.187	-0.12	0.007	5	-0.081	19.938	10.399	19.742	10.345	25	-10.45	0.059
453	F106636B	13.807	13.713	7.169	7.194	-0.106	0.009	5	-0.0717	16.114	8.413	15.986	8.378	37	-11.515	0.062
472	F112980	16.39	16.257	8.505	8.541	-0.12	0.003	9	-0.0794	21.281	11.106	21.057	11.045	36	-11.6	0.062
495	F109879	13.248	13.161	6.87	6.894	-0.112	0.007	2	-0.0791	14.996	7.811	14.885	7.781	56	-15.202	0.071
909	F108173	14.569	14.464	7.563	7.592	-0.11	0.012	5	-0.0738	17.638	9.208	17.484	9.166	34	-10.58	0.059
545	F123797A	14.48	14.376	7.553	7.581	-0.074	0.007	5	-0.0381	17.46	9.187	17.309	9.145		no solution	
1325	F115996A	16.318	16.186	8.485	8.522	-0.101	0.015	5	-0.0608	21.136	11.067	20.915	11.007	09	-1.834	0.037

Note: *Sample numbers, WR chemistry and description are from Retallack et al. (2019); WP – computed weathering product, T° C, MW computed values of temperature and meteoric water values solved based on triple oxygen isotopic values. Weathering product, temperature and meteoric water values.

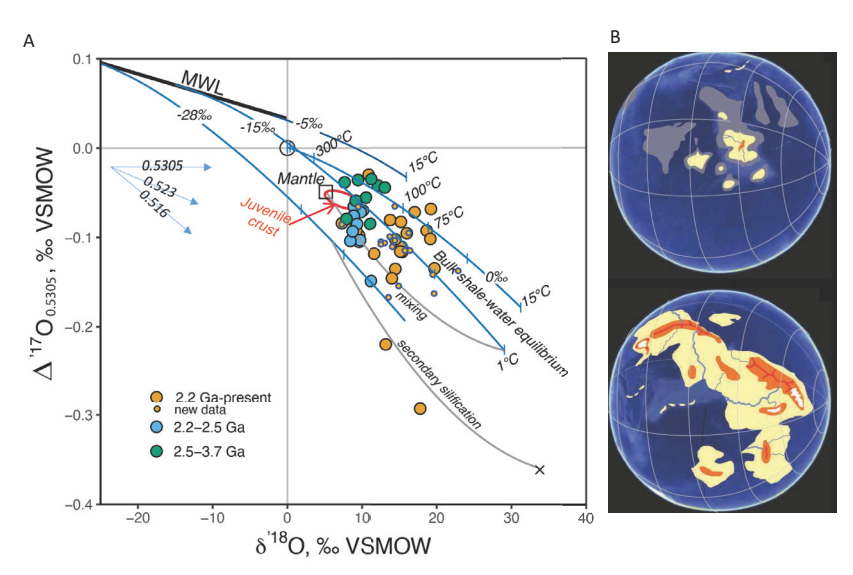


Figure 11. a) Triple-oxygen isotopes in shales of different age; (Bindeman et al. 2018 with added data for the last 1.2 Ga, smaller circles). See Figure 6 for explanations and Figure 5 for modern world values. Notice that Archean shales tend to be lower in δ^{18} O, and higher in Δ'^{17} O, with scatter around higher temperatures. b) Hypsometry maps for the Archean (top) and post-Archean (post) world hypsometry, showing their pronounced difference. This explains that the limited hydrologic cycle in the Archean is due to the small continental size. [Fig 11 is used by permission and with modification from Nature, from Bindeman et al. (2018), Nature, Vol. 557, p. 545–548, Figs. 1a and 3].

is invoked to explain the shale record, showing a stepwise change that coincides with the Archean-Proterozoic boundary (Fig. 10). Most likely, the observed changes in the shale triple-oxygen isotope record reflect the appearance of larger continents (Fig. 10) and higher elevations starting in the Proterozoic, which is broadly contemporaneous with final stages in the assembly of the first documented supercontinent, Kenorland (Mertanen and Pesonen 2012; Condie 2013) or alternatively, several supercratons occurring immediately before the GOE (Bleeker 2003). Supercontinent assembly and orogenic events result in high-mountain ranges and plateaus, e.g., the Himalayas and Tibet. Mountains even in relatively low to mid latitudes yield precipitation with very light $\delta^{\prime 18}$ O values correlated with elevation, about 2–3% drop per 1 km increase in altitude (Rowley et al. 2001). To illustrate "continentality", we here compiled $\delta^{18}O_W$ values for the modern world, from the Waterisotopes.org website (Fig. 12); future analyses should permit similar efforts with $\Delta'^{17}O_W$, and these would also account for the evaporation effects. Large continents such as Asia extended latitudes and with mountain ranges show significantly larger variations in $\delta^{18}O_W$, as compared to smaller land masses such as Madagascar or Malaysia for example. These effects are indeed expected to be much more dramatic in a supercontinent-type environment (Fig. 13).

Supporting our interpretations of triple oxygen variations in shales is the Sr isotope record of marine carbonates, that suggests the area of emerged continental crust increased significantly and irreversibly at around the Archean–Proterozoic boundary (Flament et al. 2008). From a geodynamic perspective, models of a cooling Earth call for a thickening of the lithosphere and the establishment of a higher continental freeboard by ca. 2.5 Ga due to increased mantle viscosity (Vlaar 2000; Condie 2013; Korenaga et al. 2017). Emergence of large landmasses (Fig. 10b) would also have led to a larger weathering sink for CO_2 that occurred in greater concentrations in the Archean, resulting in a transition to moderate surface temperatures after the GOE. This set of large-scale tectonic and near-surface changes may best explain the observed shift in the $\delta'^{18}O-\Delta'^{17}O$ composition of shales between 2.5 to 2.2 Ga (Fig. 10).

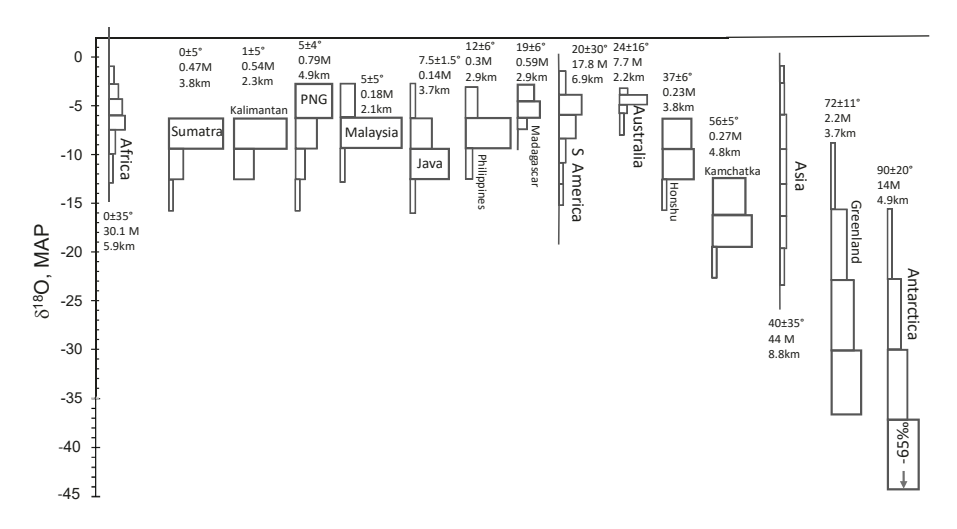


Figure 12. A compilation and summary of δ^{18} O values of mean annual precipitation (MAP) for the major modern terrestrial land mass of different size and hypsometry, scaled proportionally within each land mass area. Shown for each land mass is its latitude ranging from equatorial to polar, its surface area in square kilometers, and its highest elevation in km. Data for plotting is retrieved from waterisotopes.org.

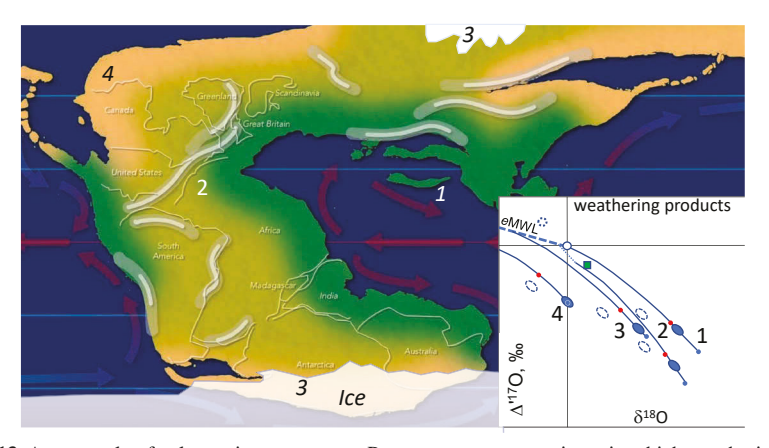


Figure 13. An example of paleoenvironments on a Pangea-type supercontinent in which weathering products (shales) or chemogenic sediments (e.g., carbonates and opals) form. **1)** tropical island, hot and high- δ^{18} O waters; **2)** wet interior of the continent; **3)** glaciated region;, **4)** dry interior of the continent, warm and cold currents and mountain ranges are shown. Inset is showing triple oxygen isotope the effect of temperature on the isotope fractionations (**concave down curves**) and effects of meteoric waters. Inset shows weathering environments shown. Weathering product is shown by **ovals** on fractionation curves (See Fig 6 for further explanations). Temperature of interaction (formation) is indicated by **dot** (**blue**—cold 1–10 °C MAT, **red**—hot, 25–35 °C MAT). eMWL is evaporated MWL, with a zero offset *Y* in Δ'¹⁷O as in Figure 9. Dashed circle indicate the hypothetical pre-early Phanerozoic low-δ¹⁸O seawater, **dashed ovals** denote their corresponding continental weathering products, assuming the slope of meteoric water line stays the same at 0.528. The base image credit is from the AtlasPro project on YouTube (https://www.youtube.com/watch?v=VKq0pr4rbRs&t=37s).

The observed shift in the triple-oxygen isotope composition of shales further requires lower post-GOE surface temperatures (Fig. 10) if modern meteoric water is used. Higher apparent temperature in the Archean oceans may also be related to a greater contribution of hydrothermal clays, or to Archean shales that would result in less positive $\delta'^{18}O$ and less negative $\Delta'^{17}O$ values. This is broadly consistent with previous studies of $\delta'^{18}O$ in cherts using the same duality of temperature vs. $\delta'^{18}O$ of the ocean. The herein inferred rapid increase in Earth's subaerial surface and overall hypsometry after ~2.5 Ga (Fig. 9) would have also increased Earth's albedo, the flux of nutrients to the oceans from the continents undergoing subaerial weathering, and the extent of continental margins, resulting in a higher burial rate of organic carbon and diminishing CO_2 concentration in the air. In combination, these changes could have contributed to global cooling, the Snowball Earth glaciations of the early Paleoproterozoic, and the following GOE, highlighting how Earth's interior could have influenced surface redox conditions and chemistry. The most dramatic change in Earth's history was marked by a transition from generally hot and largely anoxic surface conditions to an oxygenated atmosphere with moderate surface temperatures.

The Phanerozoic shale record

The Phanerozoic is a period of Earth's history when plate configuration, orogenies, and exposed continental areas are known, offering further information on the sequence of events. The Phanerozoic also includes the last complete supercontinent cycle involving destruction of Rodinia at 750-650 Ma, accretion of Pangea by ~330 Ma (Fig. 11), followed by its destruction starting in Late Triassic, ~220-190 Ma and advent on plant life on continents. Hypothetical climate and weathering conditions on Pangea are presented in Figure 11 which shows the anticipated triple oxygen effects. Early Permian glaciation and a colder climate at ~280 Ma was likely accompanied by a global decrease in temperatures, and thus the δ^{18} O value of precipitation (cf Eqn. 7). Therefore, weathering products should have lower δ^{18} O and higher Δ'^{17} O values, which should characterize mid-Pangean history. Triple oxygen isotopes in shales can assist in resolving the details of Pangean climate (Fig. 13) for the four environments shown. Tropical islands and tropical near coastal type environment 1 will exhibit higher $\delta^{18}O$ and $\Delta'^{17}O$ values. Intracontinental type environment 2 will display lower δ^{18} O but comparable Δ'^{17} O due to lower T of weathering. Polar environment 3 will exhibit the lowest $\delta^{18}O$ and $\Delta'^{17}O$. Finally, environments with dry, deeply intra-supercontinental conditions will yield waters so highly evaporated that they belong to a different "strongly evaporated water line" (aka modern arid Africa; Passey and Ji 2019), showing the lowest Δ'^{17} O and high- δ^{18} O values. As arid intracontinental conditions are perhaps well represented in the modern world (Fig. 1) by dry African environments, there is a great potential to discover even lower Δ'^{17} O values in African Permian–Triassic shales, lacustrine diatoms, and biogenic carbonates. Targeted investigation of geologic formations with known depositional environment and climate should test this hypothesis.

Figure 14 shows that the $\delta^{18}O$ and to a lesser extent the $\Delta'^{17}O$ values for the shales exhibit U- or W-shaped trends throughout the Phanerozoic (previously published and new data from Tables 1 and 2). Sr isotopic values in coeval carbonates, are also plotted for comparison, and it shows a similar U- shaped trend with a minimum near the Paleozoic–Mesozoic boundary. Since Sr and O isotopes in supracrustal rocks commonly correlate, we will explain these observed trends together. Figure 14 also shows estimated surface area of exposed continental crust in latitudes between 30° N and 30° S based on Lawver et al. (2011). The rationale for this estimation is that the majority of silicate chemical weathering occurs in the tropics, e.g., 2/3 of modern global Earth's sediment flux is from SE Asia (Milliman and Farnsworth 2011). We observe that the area of the Earth's surface in the tropics also exhibits W-shaped (or smile face) pattern, coeval with O and Sr isotopic trends. We present the following hypotheses that are in accordance with the Phanerozoic supercontinent cycle of Pangean assembly and disassembly, with associated orogenies and rifting events:

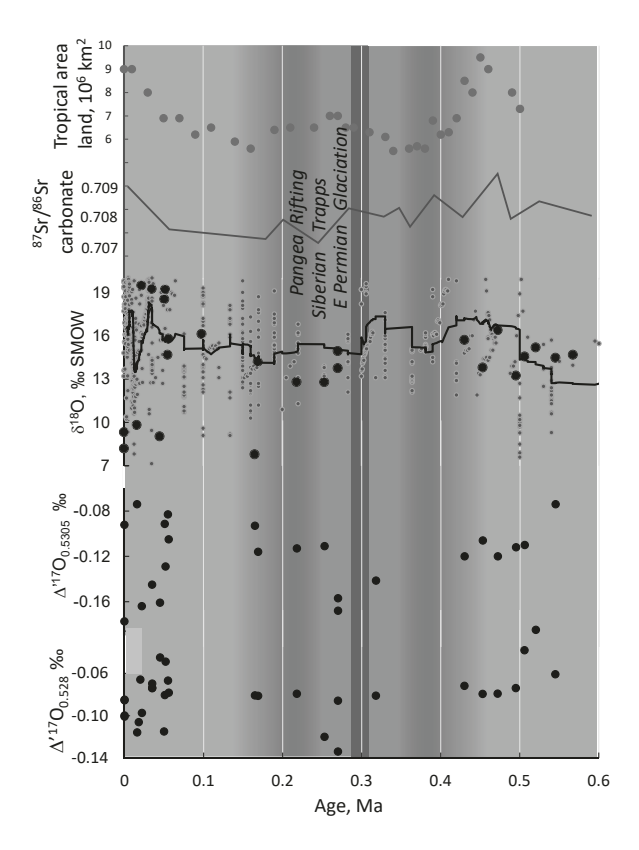


Figure 14. The correlation of the subaerial land masses between 30° N and S (derived from Atlas of Plate Reconstruction Project, Lawver et al. 2011) with δ^{18} O and Δ'^{17} O values of shales, and Sr isotopic values of coeval carbonates. Data from Bindeman et al. (2016, 2018) with added data points for the last 1.2 Ga, Table 2.

- (i) Orogeny during supercontinent assembly in the Devonian is accompanied by uplift, exposure and rapid erosion of fresh, unweathered igneous and metamorphic rocks with lower $\delta^{18}O$. The detrital contribution of these rocks to shales (since average shale is a mixture of weathering products and detrital components, the latter can also be previously weathered sedimentary rocks) drives the bulk of the shale $\delta^{18}O$ values down.
- (ii) Since orogenesis and erosion occurred in central Pangea and at higher altitudes during the Caledonian collisions, waters involved in weathering are depleted in $\delta^{18}O$ and enriched in $\Delta'^{17}O$; their interaction with rocks imprints these signatures on shales (cf. Fig. 5).

Secondary effects are related to the glacial episode in the Early Permian at ~280 Ma, causing further $\delta^{18}O$ depletion of meteoric water worldwide. Glaciation additionally produces fine-grained tillite, which upon interaction with synglacial and intracontinental low- $\delta^{18}O$ waters transfer these signatures to shales. It is thus instructive to investigate Early Permian formations for these effects. As an example, synglacially altered rocks formed during Snowball Earth episodes at 2.4–2.2 Ga (Herwartz et al. 2015; Zakharov et al. 2017, 2019), generated the lowest $\delta^{18}O$ rocks yet measured, formed in exchange with –45% $\delta^{18}O$ meteoric waters. The Pliocene Antarctic clay also records <28% $\delta^{18}O$ waters (Fig. 5).

The episode of supercontinent splitting and intracontinental rifting that has dominated the world since ~200 Ma results in opposite isotope effects:

- i) Lack of major orogenies, except the most prominent India-Asia collision after ~50 Ma, leads to peneplain development and formation of eroded mountain belts such as the Appalachian and Ural Mountains. This in turn leads to formation of more sedimentary rock, and thus higher δ¹⁸O values in shales. The ongoing chemical weathering and attendant repeated and more thorough isotope exchange of exposed sedimentary rocks in flood plains should further increase δ¹⁸O values of newlyformed shales.
- ii) Since the breakup of Pangea leads to continents that are smaller in size, especially in tropical latitudes, the δ^{18} O value of meteoric water involved in tropical weathering is globally higher, and Δ'^{17} O is lower (cf. environment 1 in Fig. 13). For example, the δ^{18} O in sediment-flux-weighted river water in the modern world is only -7.5%o, and these signatures are thus passed to shales.

Likewise, the Sr isotopic record (Fig. 14) in coeval carbonates also indicates competition between the erosional supply of high- 87 Sr/ 86 Sr $_{\rm initial}$ from eroding continents (including carbonates), and the supply of mantle-derived low- 87 Sr/ 86 Sr $_{\rm initial}$ Sr at mid-ocean ridges during rifting. As erosional flux reflects mountain denudation rates especially when they occur in the tropics, the Sr isotopic curve reflects that. To the first order, the Neoproterozoic shales have the highest δ^{18} O and Sr isotopic values, reflecting simply the weathering of a large proportion of continental crust and mountains after accretion of a Rodinia supercontinent at tropical latitudes at that time. The lowest 87 Sr/ 86 Sr and δ^{18} O values are coeval with the lowest amount of continental surface area exposed in tropical areas, combined with initiation of Pangea rifting at 210 Ma, and preceded by large quantities of erosion at the Siberian Traps, which erupted at 250 Ma.

PART III: THE TRIPLE OXYGEN ISOTOPE ANALYSIS OF GRANITES IN COMPARISON WITH SHALES RECORD: INSIGHT INTO THE EVOLUTION OF THE CONTINENTAL CRUST AND WEATHERING

This work presents triple oxygen isotope analyses of granites across geologic history (100 new triple oxygen analyses and >200 compiled δ^{18} O, Fig. 15, Table 3) with emphasis on orogenic and S-type granites available for post-Archean history, and a broader suite of granites in the Archean and Early Proterozoic, including orogenic, TTGs, and synmetamorphic (anatectic, migmatitic) types for which geodynamic classification is more difficult to unambiguously establish. For example, our oldest granites and TTGs from the Kaapvaal craton are interpreted to be partial melts of silicified metabasalts and metasediments based on silicon isotopes and bulk chemical compositions (André et al., 2019). In our sample selection and compilation of literature data for $\delta^{18}O$ in granites we exercised criteria of "maximum crustal origin" and minimized the use of I-type granites and A-type, intracontinental rift-related granites (e.g., Anderson and Morrison 2005) that commonly have a significant mantle-derived component. For example, voluminous orogenic granites that form batholiths typically represent large scale remelting of metamorphic supracrustal protoliths that span large areas/volumes of crust (e.g., Sylvester 1998; Schaltegger et al. 2019), and these large magma bodies provides a broad view of crustal evolution on giga-year timescales. Orogenic granites studied were commonly referred to as S-type, i.e., sedimentary-derived, many with peraluminous characteristics (e.g., Chappell and White 1974). Bucholz and Spencer (2019 and references therein) recommended replacing the term S-type with the expression "strongly peraluminous" granites. We further compiled published δ^{18} O values in well-studied orogenic granites (see Reference list) and utilized the recent dataset of Bucholz and Spencer (2019) for strongly peraluminous Precambrian granites with excess of Al₂O₃ and SiO₂ and are thus mostly of anatectic origin.

Table 3. Oxygen Isotope analyses of quartz and other minerals in granites and metaigneous rocks of different ages.

Sample	Type	Age Ga	Δ' ¹⁷ O Qz _{0.5305} , % ₀ VSMOW	•±∆′¹7O	$\Delta^{\prime 17} O_{0.528}$	δ ¹⁸ Ο Quartz	\doldright\r	δ ¹⁸ O Other Minerals	$\Delta^{\prime17}\mathrm{O}_{0.5305}$	Country/ US State	Collector	Reference/locality
ID3-85	sm	3.8	-0.059	0.003	-0.036	9.152	4.786			Greenland	A. Kays	Isua, Kays et al. (1972)
IC3-85	sw	3.8	-0.079	0.010	-0.056	9.412	4.902			=	=	Ashvall (1986)
2.8ma-2, vein	sm	3.8	-0.067	0.011	-0.057	4.334				=	=	=
2.8Ma-2	sm	3.8	-0.047	0.012	-0.036	4.214*		1.464	-0.041 ± 0.011 , Grt	=	=	=
2.8 M-1-85	ms	3.8	-0.070	0.010	-0.055	6.017		3.267	-0.064 ± 0.011 , Grt		=	=
IC3-85 qz-1	sm	3.8	-0.063	0.012	-0.040	9.436	4.931			=	=	=
IF-3 quartzite	sm	3.8	-0.077	0.014	-0.046	12.644	6.610			=	=	=
IF-1-85	ms	3.8	-0.113	0.010	-0.082	12.308	6.400			=	=	=
2.8MI-85	ms	3.8	-0.059	0.011	-0.050	3.261				=	=	=
Acasta gneiss		4	-0.061	0.010	-0.045	6.559		6.81, 6.77, Qz		Canada	UO collection	N Canada
Chinese Granite		3.8	-0.086	0.013	-0.071	6.131	3.167			N China	=	Bindeman et al. (2018)
Morton gneiss-1	. <u>Ē</u>	3.5	-0.103	0.008	-0.079	9.826	5.097			WIN	T. Vislova	Town of Morton MN
Morton gneiss-2	. <u>E</u>	3.5				8.220				=	:	=
MN23-16	. <u>Ē</u>	3.5	-0.085	0.013	-0.062	9.258	4.815			:	D. Blackwell	granitic gneiss, Montevideo, MN
LS-13	Ф	3.3	-0.094	0.008	-0.072	8.748	4.537			MI	UO collection	grey gneiss, Republic Mine Marquette MI (1)
LS-13	р	3.31				8.250				=	UO collection	=
OO-605	ď	3.2				7.950				Scotland	UO collection	Grey granite, S.E. Bushveld (2)
	р	3.46				8.270				S Africa	A. Hoffman	Andre et al. (2019)
	р	3.26				9.100				=	=	-
	р	3.24	-0.080	0.005	-0.058	8.857	4.608	5.092	-0.054 ± 0.006 , Zrc	=	=	-
	р	3.23	-0.074	900.0	-0.051	9.125	4.756			=	=	-
Bar-10	d	3.2	-0.089	0.015	-0.070	7.854		5.354	-0.083 ± 0.015 , Zrc	=	=	Ξ

BBL-14 p 312 -0.055 0.016 -0.036 1.024 5.357 9.372 9.373 9	Type	oe Age Ga	e A ⁷¹⁷ O Qz _{0.5305} , a %c VSMOW	O ⁷¹⁷ ∆±	$\Delta^{\prime 17}$ O _{0.528}	δ ¹⁸ Ο Quartz	O ₁₁ O	δ ¹⁸ Ο Other Minerals	Δ^{17} O _{0.5305}	Country/ US State	Collector	Reference/locality
3.12 -0.066 0.021 -0.044 9.781 5.112	D	3.1		0.016	-0.030	10.038	5.257			=	=	=
3.11 -0.068 0.024 9.392 4.967 <	р			0.021	-0.041	9.781	5.112			=	=	=
311 — 6077 6012 — 6084 9392 4 908 — 8730 — 8740 — 8740 — 8730 — 8740	р			0.012	-0.048	8.336	4.357			=	=	Ξ
3.11 6.136 4.725 3.8 4.725 3.8 4.725 3.8 4.725 3.8 4.725 3.8 4.725 3.8 4.725 3.8 4.725 4.725 4.725 4.725 4.725 4.725 4.725 4.725 4.725 4.725 4.725 4.725 4.725 4.725 4.746 4.725 4.725 4.746 4.726 4.746 4.726 4.746	ď			0.012	-0.054	9.392	4.905			=	=	Ξ
3.11 -0.109 0.014 -0.086 9.133 4.725 Scotland 1. Bindenana 2.74 -0.099 0.016 -0.074 10.71 5.284 SAfrica A. Hoffman 2.73 -0.099 0.016 -0.076 9.196 4.768 MN D. Blackwell 2.68 -0.069 0.010 -0.038 8.900 5.667 -0.067±0.006, Zrc Canada I. Vialley 2.68 -0.043 0.006 -0.053 8.140 5.667 -0.067±0.006, Zrc Canada I. Vialley 2.68 -0.043 8.706 8.140 5.667 -0.067±0.006, Zrc Canada I. Vialley 2.69 -0.043 8.706 8.139 4.294 7.299 -0.067±0.006, Zrc WY D. Biackwell 2.58 -0.067 -0.067 -0.067 -0.061 0.001 -0.043 8.790 7.299 -0.061 0.001 -0.044 7.910 -0.061	р		1			8.730				=	:	=
3 -0.099 0.016 -0.074 10.171 5.284 A. Hoffman I. Bindenand A. Hoffman 2.79 -0.082 0.036 0.038 9.996 4.768 A. 768 A. Hoffman A. Hoffman 2.69 -0.060 0.014 0.007 0.038 8.900 A. 766 A. Hoffman A. Hoffman 2.69 -0.067 0.009 0.038 8.900 A. 266 A. Hoffman A. Hoffman 2.60 -0.067 0.009 0.038 8.140 A. 294 A. 294 A. 1904 A. Hoffman 2.50 -0.047 0.007 0.006 A. 294 A. 294 A. 294 A. 294 A. A 494	b			0.014	-0.086	9.133	4.725			=	=	Ξ
2.74 — 6.082 0.020 — 0.058 9.595 4.997 — M.M. S. Africa A. Hoffman 2.75 — 0.099 0.014 — 0.076 9.196 4.768 — 0.067 ± 0.006, Zrc SAfrica A. Hoffman 2.69 — 0.069 0.010 — 0.038 8.906 — 0.067 ± 0.006, Zrc Canada J. Hoffman 2.68 — 0.067 — 0.038 8.167 — 8.407 — 0.067 ± 0.006, Zrc Canada J. Hoffman 2.62 — 1.106 — 1.116 — 1.1	m			0.016	-0.074	10.171	5.284			Scotland	I. Bindeman	Scouri
2.7 -0.099 0.014 -0.076 9.196 4.768 A.768 A.768 A.768 A.768 A.768 A.768 A.768 A.767 A.768 A.7760	b			0.020	-0.058	9.595	4.997			S Africa	A. Hoffman	Andre et al. (2019)
2.68 -0.060 0.010 -0.038 8.900 -0.067 ± 0.006, Zrc SAfrica A.Hoffman 2.68 -0.073 8.167 5.667 -0.067 ± 0.006, Zrc Canada 1. Valley 2.62 8.140 8.140 2.62 8.140 4.294 2.64 6.047 0.007 -0.043 9.799 4.294 <td>Ь</td> <td></td> <td></td> <td>0.014</td> <td>-0.076</td> <td>9.196</td> <td>4.768</td> <td></td> <td></td> <td>MN</td> <td>D. Blackwell</td> <td>granitic gneiss, Ojakanngas (2009) (3)</td>	Ь			0.014	-0.076	9.196	4.768			MN	D. Blackwell	granitic gneiss, Ojakanngas (2009) (3)
2.68 -0.073 8.167 5.667 -0.067 ± 0.006, Zrc Canada 1. Valley 2.62 8.140 9.140 <td>р</td> <td></td> <td></td> <td>0.010</td> <td>-0.038</td> <td>8.900</td> <td></td> <td></td> <td></td> <td>S Africa</td> <td>A. Hoffman</td> <td></td>	р			0.010	-0.038	8.900				S Africa	A. Hoffman	
2.65 -0.047 0.007 -0.026 8.140 -0.061 + 0.009, Zrc WY D. Blackwell 2.6 -0.047 0.009 -0.043 8.199 4.294 -0.061 ± 0.009, Zrc WY D. Blackwell 2.594 -0.067 0.009 -0.043 9.799 -0.061 ± 0.009, Zrc China John Valley 2.588 -1.588 -1.590 -1.599 -0.061 ± 0.009, Zrc China John Valley 2.54 -1.56 -1.599 -0.061 ± 0.009, Zrc China John Valley 2.58 -1.58 -1.590 -1.599 -0.061 ± 0.009, Zrc China John Valley 2.55 -1.58 -1.590 -1.599 -0.061 ± 0.009, Zrc China John Valley 2.56 -1.58 -1.590 -1.599 -1.599 -1.590	d			0.006	-0.053	8.167		2.667	-0.067 ± 0.006 , Zrc	Canada	J. Valley	Superior province Valley et al. (2005)
2.6 8.140 8.140 4.294 4.294 WY D. Blackwell 2.6 -0.047 0.007 -0.026 8.199 4.294 WY D. Blackwell 2.59 -0.067 0.009 -0.043 9.799 7.299 -0.061 ± 0.009, Zrc China UO collection 2.58 -0.067 0.010 -0.043 9.700 -0.061 ± 0.009, Zrc China John Valley 2.58 -0.067 0.010 -0.047 7.910	ď		5			7.130				India	UO collection	West Bengal
2.6 -0.047 0.007 -0.026 8.199 4.294 A.294 A.294 <th< td=""><td>р</td><td></td><td>2</td><td></td><td></td><td>8.140</td><td></td><td></td><td></td><td>=</td><td>=</td><td>Dharwar craton, Kamataka</td></th<>	р		2			8.140				=	=	Dharwar craton, Kamataka
2.64 7.760 7.760 7.299 7.299 4.0061 ± 0.009, Zrc India UO collection 2.584 -0.067 0.009 -0.043 9.799 7.299 -0.061 ± 0.009, Zrc China John Valley 2.585 2.56 2.57 2.700 2.70	р			0.007	-0.026	8.199	4.294			WY	D. Blackwell	Big Horn granite, Shell Falls
2.584 -0.067 0.009 -0.043 9.799 7.299 -0.061 ± 0.009, Zrc China John Valley 2.588 2.58 8.790 7.910 A.000	Ъ		5			7.760				India	UO collection	Pudukottai Town, Tamil Nadu
2.588 8.790 Bave Blackwell 2.55 -0.067 -0.047 7.910 -0.640, Grt -0.040 Grt -0.040 Grt -0.067 -0.068 Grt	р			0.009	-0.043	9.799		7.299	-0.061 ± 0.009 , Zrc	China	John Valley	Valley et al. (2005)
2.55 -0.067 0.010 -0.047 7.910 " Greg Retallack 2.156 -0.134 0.010 -0.107 10.691 9.640, Grt Brazil UO collection 2 10.690 10.690 " " " 2 9.380 " " "	m		88			8.790				SD	Dave Blackwell	granite, Milbank, Gries (1996)
2.156 -0.067 0.010 -0.047 7.910 " Greg Retallack 2 -0.134 0.010 -0.107 10.691 9.640, Grt Brazil UO collection 2 10.690 " " 2 9.380 " "	р		S			9.700				India	UO collection	Closepet Granite, Dharwar Craton
2 -0.134 0.010 -0.107 10.691 9.640, Grt Brazil UO collection 2 10.690 " "	р			0.010	-0.047	7.910				=	Greg Retallack	granite Ramakona, Madhya Pradesh (3)
2 10.690 2 9.380	B			0.010	-0.107	10.691		9.640, Grt		Brazil	UO collection	migmatite of 1.9 Ga orogeny of mid-Archean gneiss
2 9.380	m					10.690				=	=	
	m					9.380				=	=	

ocality	1972)	=	batholith	'olynsky	rea 1972)			Wollaston, Hearne craton	rea 1972)	1 Qtz 2001)	s Granite, . (2009)		ı Qtz pegmatite	=	ranite, 2004)		=	ovince
Reference/locality	Kays et al. (1972)		Cumberland batholith	Volodarsk-Volynsky Intrusion	Lake Hara area Kays et al. (1972)			Wollaston, I	Lake Hara area Kays et al. (1972)	Vernal Mesa Qtz Monzonite, Scott et al. (2001)	Harney Peak Granite, Lufken et al. (2009)		Vernal Mesa Qtz Monzonite, pegmatite		Grenville Granite, Peck et al. (2004)			quartzite. Grenville Province
Collector	Allan Kays	=	Dana Johnston	UO Collection	A. Kays	=	=	=	:	D. Blackwell	:	=	:	=	W. Peck		=	J. Valley
Country/ US State	SW Finland	=	N Baffin Land	Ukraine	NE Saskatchewan	=	=	=	:	00	SD	=	:	=	NY	=	=	:
$\Delta^{\prime 17} O_{0.5305}$																		
δ ¹⁸ O Other Minerals				6.760, Grt														
0''8	6.405		5.270		5.318		5.761		5.544		<i>911.7</i>	7.890	5.530	6.072	5.383	7.673	7.218	998:9
δ ¹⁸ Ο Quartz	12.172	12.090	10.169	7.360	10.272	9.200	11.021	9.850	10.675	12.540	14.970	15.169	10.583	11.628	10.405	14.770	13.860	12.234
$\Delta^{\prime 17} O_{0.528}$	-0.055		980.0-		-0.088		-0.049		-0.078		960'0-	-0.090	-0.044	-0.051	960.0-	860.0-	-0.076	-0.074
O′¹′∆±	0.01		0.01		0.011		0.008		0.004		0.011	0.012	0.013	0.013	0.013	0.022	0.01	0.008
Δ' ¹⁷ O Qz _{0.5305} , % ₀ VSMOW	-0.085		-0.111		-0.114		-0.076		-0.105		-0.134	-0.127	-0.070	-0.080	-0.122	-0.135	-0.110	-0.105
Age Ga	1.85	1.85	1.82	1.78	1.75	1.75	1.75	1.75	1.75	1.741	1.697	1.697	1.48	1.48	1.15	1.15	1.15	1.1
Туре	р	р	р	d	d	р	р	р	III	ď	р	р	d	d	р	р	р	ms
Sample	FN35-72	FN35-72	DJ-1	Volga Blue	K263-70	K332-70	K247-70	K247-70	K388-70	CoNM 6-08	SD14-15	SD1-10	BCNGP-2-Q8	BCNGP-1-08	MR-85	PR-21	BP-16	IPQ-1

gneissic granite. Nadol, Rajasthan (4)

G. Retallack

India

12.790

-0.092

-0.124

0.967

р

R5856 IPQ-1

E.	Type	Age Ga	Δ′17 O Qz _{0.5305} , % _c VSMOW	$ \sqrt{17}$ O	$\Delta^{\prime 17} \mathbf{O}_{0.528}$	δ ¹⁸ Ο Quartz	O ₁₁ δ	§¹8O Other Minerals	$\Delta^{\prime 17} O_{0.5305}$	Country/ US State	Collector	Reference/locality
	ь	9.0				12.000		9.260, Grt		Brazil Espirito Santo	UO collection	Ribeira Belt, Macluf, Buchwaldt (2001)
	d	0.65	-0.106	0.01	-0.074	12.990		10.080, Grt		Ξ	Ξ	Pedrosa-Soares et al. (1999), Mendes et al. (2000)
	р	19.0				13.230				=	=	
	р	89.0				12.240				=	=	
	р	69.0				091.6		6.410, Grt		=	=	
	Ь	0.56				13.530				=	=	
	р	0.56				10.330				=	=	
	р	0.55				12.410		10.000, Grt		Brazil, Aguia Branca	:	
	Ь	0.44	-0.129	0.007	-0.095	13.841	7.189			Buryatia, Russia	B. Litvinovsky	Angaro-Vitim batholith, Wickham et al. (1996)
	р	0.429	-0.064	0.005	-0.036	11.083	5.800			SW Australia	UO collection	Australian S type Granites, Berrydale batholith
	b	0.414	-0.078	0.010	-0.047	12.432	6.498			=	=	Chappell and White (1974)
	р	0.41	-0.081	0.005	-0.047	13.580	7.100			=	=	-
	р	0.389				090'6	4.778			=	=	-
	Ь	0.35				7.330		6.730, Plag		Norway, larrvakite	UO collection	Jayananda et al. (2000), Moyen et al. (2001)
	Ь	0.35	-0.068	0.005	-0.038	12.060	6.309	10.32, Plag		Central France	M. Dungan	Dent de Cheval, Caudjol
	Ь	0.101	-0.084	0.014	-0.057	11.002		8.502	-0.078 ± 0.014 , Zrc	CA	J.S. Lackey	Sierra Nevada, Valley et al. (2005)
	Ь	0.05				11.550		11.3		OR	UO collection	Ashland, OR
-	ď	0.04	-0.133	0.016	-0.106	10.699	4.081	7.949	-0.127, Amph	N Italy	U. Schaltegger	Adamello batholith, Schaltegger et al. (2019)

 -0.059 ± 0.02 , Zrc

5.659

8.159

-0.045

0.020

-0.065

0.04

VAL zrc powder

Sample	Type	Age Ga	Δ' ¹⁷ O Qz _{0.5305} , %c VSMOW	$O_{LL}\nabla$ =	$\Delta^{\prime 17} \mathbf{O}_{0.528}$	δ ¹⁸ Ο Quartz	O ₂₁ 8	δ ¹⁸ Ο Other Minerals	$\Delta'^{17}\mathbf{O}_{0.5305}$	Country/ US State	Collector	ReferenceAocality
							Ignimbrites	brites				
BFCQ Fish Canyon	>	0.028	-0.108	900.0	-0.089	7.470	2.270	4.477	-0.102 ± 0.006 , Sphene	00	O. Bachmann	Fish Canyon tuff
TM-10 Zrc	>	0.0012	-0.055	0.008	-0.032	9.178		6.677	-0.049 ± 0.008 , Zrc	NV	I. Bindeman	Timber Mt
Cheg-9	>	0.003	-0.085	900.0	-0.065	8.090	4.198			Caucasus, Russia	I. Bindeman	Chegem Tuff
CG-141	>	0.003	-0.122	0.012	-0.098	699.6	4.995			Bolivia	UO Collection	Cerro Galan Tuff
HRT-1	>	0.002	-0.082	90000	-0.062	7.717	4.005			WY	I. Bindeman	Huckleberry Ridge
HRT-1 Zrc	>	0.002	-0.079	0.009	-0.059	8.110		5.610	-0.073 ± 0.009 , Zrc	=	I. Bindeman	tuff, Yellowstone
HRT-3a qz	>	0.002	-0.062	0.007	-0.043	7.517	3.992			=	I. Bindeman	=
Krakatoa Px	>	0	-0.062	0.003	-0.045	7.009		4.509	-0.056 ± 0.003 , Cpx	Indonesia	A. Belousov	Krakatoa 1883 AD
Bishop tuff Late	>		-0.098	0.013	-0.078	8.123				CA	I. Bindeman	Bishop tuff
Toba	>	0.0007	-0.084	0.016	-0.061	9.135	4.751			Indonesia	C. Chesner	Toba tuff
LBT-4a	>	0.0001	-0.059	0.013	-0.040	7.731	4.035			NM	I. Bindeman	Lower Bandelier Tuff
Note: p: plutonic igneous; ms-meusedimentary; mi-rr quartz equivalent (typically for quartz-undersaturated corresponding APO along the close of 528-713. Aithic	eous; ms- ically for	metasedim r quartz-un	entary; mi-metaigneou dersaturated rocks) ca	1s, v-volcanic	. 8 ¹⁸ O analyses w g mineral analyz	vithout $\Delta^{17}O_{c}$ zed and corre	data were don cted to quart:	te by CO ₂ -methor z values by add onites from Gr	Note: p: plutonic igneous; ms-metasedimentary; mi-metaigneous, v-volcanic, $\delta^{18}O$ analyses without $\Delta^{19}O$ data were done by CO_2 -method for $\delta^{18}O$ only; Ages in italics are approximate, based on geologic relations. *Offset italics represent quartz equivalent (typically for quartz-undersaturated rocks) calculated using mineral analyzed and corrected to quartz values by adding (Qz-min) fractionation increment using high-T fractionation factors of Chiba et al. (1989) and corrected to quartz equivalent (Application of the Arman	are approximate, b: ement using high-	ased on geologic rel T fractionation fact	utions. *Offset italics represent ors of Chiba et al. (1989) and remitic Complex Objectments
collesponding a co	Hong the	Stope v.24	o, (1) zymerin, m	illey et al. (2)	UU4) GIIGISS LOUI	IIC DOON, 5.4-	3.0 Ua, (2) 2	Ullines mon. C.	100el suai vii 10au to Divirancia.	spilit, o.e. Duany	olu, (e) veriminon v	nannic Compies Gjaranngas,

2009, p.90, (3) India. From roadcut 10 km north of Ramakona on National Route 268, The granite is a 15 cm thick dike in schist; (4) India. From quarry dump 5 km east of Nadol on National Route 67, quarry

The $\delta^{18}O$ of quartz and other minerals in granites analyzed in this study is increasing with time (Fig. 15), comparable to the record for shales (Fig. 3, 10) and zircons (Valley et al. 2005; Dhuime et al. 2015; Hawkesworth et al. 2017, Fig. 10). A novel observation of this work is that I observe a step-wise change of $\Delta'^{17}O$ from -0.072 to -0.115% occurring at 2.1-2.4 Ga, broadly coinciding with the change in shale at Archean–Proterozoic transition (Fig. 10b). This step-wise change of $\Delta'^{17}O$ is somewhat less-well pronounced for granites than for shales (Fig. 15, 10b). The $\delta^{18}O$ of granites also increased by 3-4% from 7.8% to 10.5% across the Arc hean/Proterozoic boundary, although in a more gradual fashion. The lower $\delta^{18}O$, and higher- $\Delta'^{17}O$ range of granites of any age group indicate greater contribution by mantle derived magma differentiates or their remelts, and these values stay relatively constant across geologic history. For example rift-related and some anorogenic magmas (some Proterozoic rapakivi granites), are close in $\delta^{18}O$ to the mantle values. It is the upper $\delta^{18}O$, lower- $\Delta'^{17}O$ values that are characteristic of the crustal isotopic values. Spencer et al. (2019) used the zircon $\delta^{18}O$ record, also emphasized a step-wise change at ~2.3Ga.

However, we observe a clear difference in $\Delta'^{17}O$ between Archean shales and granites: shales are significantly shifted and overlap with the mantle -0.05% value, while granites are noticeably more negative than the mantle. Pure igneous differentiation of mantle-derived compositions (and a complementary processes of partial melting of basalts) leads to <1% increase in $\delta^{18}O$ (Eiler 2001) and thus should correspond to a very minute -0.01-0.015 decrease in $\Delta'^{17}O$ along any high-T slopes between 0.528 and 0.5305. This is insufficient to explain stronger negative $\Delta'^{17}O$ values.

The second observation is that Mid-Late Proterozoic granites in our dataset have the highest $\delta^{18}O$ and lowest $\Delta'^{17}O$ values as compared to Phanerozoic granites. Similar relations occur in the record of shales (Figs. 3, 10). Overall the shale record has wider range of $\delta^{18}O$ and $\Delta'^{17}O$ variations than that of granites, and this is expected. Isotopically, granites range from being mantle-like, represented by partial melts of basalts and their differentiates, to S-type, derived from diverse sedimentary protoliths in anatectic environments.

Comparing coeval record of Archean granites and shales

We explore $\delta^{18}O$ and $\Delta'^{17}O$ variations in granites and shales in Figure 16, which indicates potential trajectories of assimilation of a mantle-derived magma with crustal protoliths represented by shales, cherts, and hydrothermally altered rocks. Archean granites would require overall a narrower range of assimilants, ranging from marine-derived, higher- Δ'^{17} O cherts, to moderately low- Δ'^{17} O shales. Post-Archean granites clearly require a predominant high- δ^{18} O shale source. Granites on the lower part of the figure show low $\delta^{18}O$ but strongly negative $\Delta^{\prime 17}$ O, including early the Archean Acasta orthogneisses studied by Rumble et al. (2013) and us, are too low in Δ'^{17} O to be explained by any realistic igneous assimilation of these crustal sources. It is possible however that the Acasta orthogneisses with their oldest whole rock age of 4.02 Ga (Reimink et al. 2016) are produced by wholesale anatectic remelting of sedimentary or low-T hydrothermal protoliths without addition of mantle-like material, inheriting low- Δ'^{17} O signatures. As examples, the Acasta, Jack Hills and the Singhbhum craton zircons have the lowest ε_{Hf} value of -5 among its EoArchean peers (Bauer et al. 2017, 2020). Reimink et al. (2016, 2020) advocate for shallow processes including hydrothermal alteration for the earliest 4.02 Ga Acasta complex, consistent with an oceanic plateau setting, followed by deeper anataxis 3.6 Ga. Alteration by early Archean low- Δ'^{17} O and δ^{18} O waters remain as a topological possibility in Figure 16 (labeled "Low- Δ'^{17} O assimilant"). Involvement of evaporated low Δ'^{17} O waters, similar to those occurring in dry and lacustrine regions of Africa today (Passey and Ji 2019), can also shift protolithic Δ'^{17} O values downward. Addition of silica via protolith silicification (e.g., Fig. 11) by either globally low- δ^{18} O, or evaporated waters, is another possibility. Note that hydrothermal alteration by recent 0% ocean or predominant $\delta^{18}O = -7.5\%$ meteoric water will increase rather than decrease Δ'^{17} O values, and thus measured values cannot be a

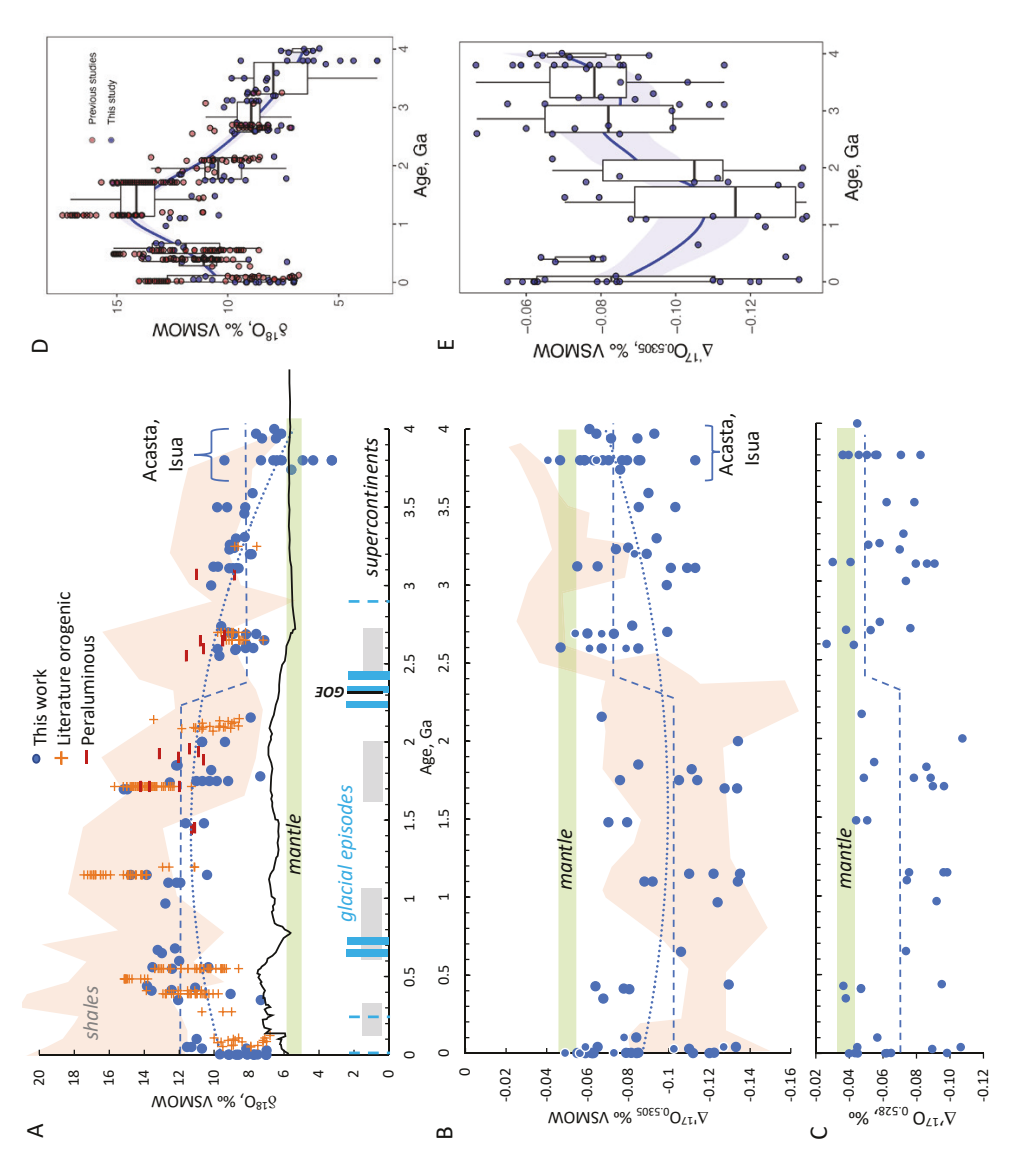


Figure 15. Triple oxygen isotopic values in quartz and other minerals in granites through time (Table 3) showing increase in $\delta^{18}O$ (**A**) and decrease in $\Delta^{\prime 17}O$ (**B**) after ~2.2 Ga. Panel C plots the dataset in B vs. 0.528 reference line and shows similar relations as in **B**. The shale record is superimposed in the background showing coeval relationship with granites. In particular, both shales and granites exhibit the highest- $\delta^{18}O$ values in 1.1–1.4 Ga than anywhere else in the geologic history. The + **markers** represent compiled data for selected well-studied orogenic granitic batholiths from the literature that indicate that Grenvillian orogeny (1.1–1.2 Ga) generated highest $\delta^{18}O$ (data from Peck et al. 2004), and coincident with the highest $\delta^{18}O$ values in shales. Strongly peraluminous granites (data compiled by Bucholz and Spencer, 2019) largely follow the orogenic granite trend. **Thin jagged black line** represents running average of $\delta^{18}O$ values of 9000 detrital zircons from Spencer et al. (2017). Notice comparable relations to the present dataset. A step-function describes $\Delta^{\prime 17}O$ data with change at 2.2–2.4 Ga, results are statistically significant using *t*-test, *p* values are 0.0003 (**B**) and 0.009 (**C**). Parabolic fits are also presented. Notice that Archean granites have lower $\Delta^{\prime 17}O$ values as compared to shales. The oldest samples from Acasta and Isua have metaigneous and metasedimentary origin. Panels **D** and **E** plot the same dataset using whiskers plot and interquartile statistics as for coeval shales in Fig. 10b.

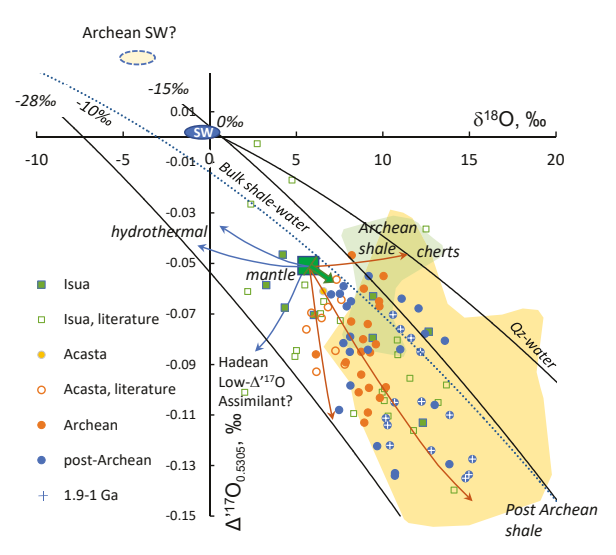


Figure 16. Triple oxygen isotopic variations in granites based on quartz (or quartz equivalents based on other minerals, Table 3) as compared to and early metasedimentary crust and shales (**colored fields**). Quartz–water fractionation curves (from Sharp et al. 2016) emanating from 0%c, -15 and -28%c waters on bulk shale–water fractionations emanating from -10%c water are shown for reference. Maximum extent of igneous differentiation of deep, wet amphibole- and pyroxene-bearing assemblages (e.g., Bucholz et al. 2017) is shown to reach δ^{18} O value of \sim 7.2%c with a hypothetical slope of 0.528. Like in Figure 14, Archean granites occupy smaller range of δ^{18} O and δ^{17} O values, while 1.9–1.1 Ga granites are the highest in δ^{18} O and lowest in δ^{47} O. The 3.8–4.0Ga Isua and Acasta gneisses and metasedimentary rocks (this work and literature data mostly from Rumble et al. 2013), are calibrated relative to San Carlos olivine of -0.051%c, equivalently to this Chapter and as in Miller and Pack (2021, this volume) and Sharp and Wostbrock (2021, this volume). **Brown arrows** denote mixing (assimilation) trajectories between mantle materials and shales and cherts on respective fractionation lines to explain the spread in the datapoints, **blue lines** denote high-*T* hydrothermal trends explaining the spread of the early Archean Isua data, requiring hydrothermal alteration and a mysterious low- $\Delta^{\prime 17}$ O assimilant. Literature data for Isua scatters likely due to greater analytical errors in these earlier studies.

result of recent exchange with water. Additionally, the low- $\Delta'^{17}O$ signature is also measured by us in Archean zircons and other minerals (Table 3) and thus secondary alteration of quartz in petrographically intact granites and TTGs is unlikely. If the earliest, Hadean "low- $\Delta'^{17}O$ assimilant" was indeed present, it likely has been reworked, similar to ϵ_{Hf} and ^{142}Nd record for the earliest crust (e.g., Bauer et al. 2017, 2020; Carlson et al. 2019 and references therein). See below our later speculation on the origin of this "low- $\Delta'^{17}O$ " component via cometary delivery.

Notice that if the entire hydrosphere including oceans were lower in $\delta^{18}O$ (e.g., Perry et al. 1978; Knauth and Lowe 2003), and thus all fractionation lines were shifted upward and to the left on Figure 16, this will assist in explaining the low- $\Delta'^{17}O$ data points. A hypothetical scenario wherein the Archean hydrosphere was both low- $\delta^{18}O$, and also relatively low- $\Delta'^{17}O$, e.g., shifted left and retained at its current $\Delta'^{17}O$, will explain these low- $\Delta'^{17}O$ granites, and also Archean cherts (Sengupta and Pack 2018; Hayles et al. 2019; Liljestrand et al. 2020; Zakharov et al. 2021, this volume), and shales. This brings us back to the above proposed testable hypothesis on testing the Early Earth, primordial low- $\Delta'^{17}O$ crustal values.

Figure 17 proposes a cartoon depicting an Archean greenstone belt with shallow submarine rifting, and partially flooded low elevation continents barely emerged from seawater, filled by evaporating lakes with hydrothermal activity. Diagenesis also proceeds with participation of such fluids, similar to evaporated African Lakes (Passey and Levin 2021, this volume).

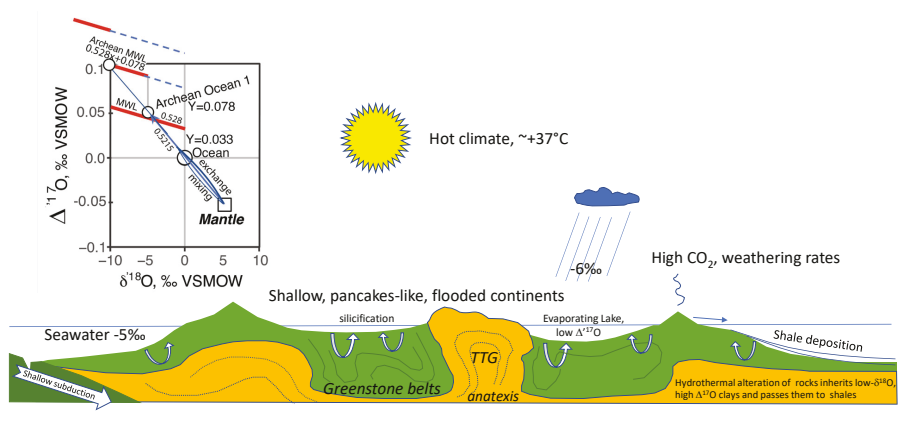


Figure 17. A cartoon cross section illustrating Archean continents with a relatively warm (ca. $+37\,^{\circ}$ C) average climate, yielding high weathering and silicification rates on continents, aided by intracontinental rifting and hydrothermal alteration. Inset shows proposed trajectory of hydrospheric changes moving along a straight line connecting the mantle and modern ocean water. Each circle represents ocean isotopic values and MWL maintains the modern slope of 0.528 but is shifted upward by the amount *Y*, which we use in resolving the isotopic value of meteoric water and the ocean (Eqn. 8) if assumption about temperature are made. See also Figure 6b and text for discussion.

This would support climate in the Archean that is comparable to the modern tropics at 35–37 °C. The origin of secondary silicification in the Archean rocks is a subject of discussion extending far beyond the field of triple oxygen isotopes (Condie 2013; Trail et al. 2018; André et al. 2019). Secondary silicification may result from strongly evaporated waters on land, and from extreme weathering on barely emerged land in a CO₂-rich atmosphere.

In summary, it appears that the shale and granite record for the Archean is both coeval and dichotomous at the same time. Shales will predominantly form in greenstone belts and rift zones, will contain significant proportion of higher-T hydrothermal clays, and are isotopically shifted toward seawater and perhaps near coastal, low altitude higher δ^{18} O waters. This reflects the small size of Archean continents and Archean continental surface areas and thus the narrow compositional range of meteoric waters available on such small continents or island arcs (Fig. 10b). Note that if Archean seawater were -5-15% lower in δ^{18} O as is shown on Figure 16, the argument still holds, requiring lower temperature of clay formation (dashed circles on Figs. 13 and 16). Granites and TTGs would form in adjacent thickened crust of protocontinents (Fig. 17). A hot Archean climate would favor evaporation and silicification, aided by perhaps shallow hydrothermal processes involving meteoric and shallow marine waters. Granites would inherit a greater proportion of silicified material and this additional silica may contribute to making granites themselves (André et al. 2019; Borisova et al. 2020).

Post-Archean granites and shales

The overlapping post-Archean granites, when compared to coeval shales are easier to explain using uniformitarian principles of derivation from and assimilation of coeval and preexisting shales (Fig. 16). Granites inherit the low- Δ'^{17} O, and high- δ^{18} O signatures from shales, siliciclastic sediments, and their metamorphic equivalents during anatexis (e.g., Fig. 4). The rock cycle takes tens to hundreds million years so one would expect the low Δ'^{17} O granites to "lag behind" low- Δ'^{17} O and high- δ^{18} O values of shales. Figure 15 hints at a lag of perhaps of up to 0.2 Ga or less. Chapman et al. (2013) observe minimal (a few million years) time lag between subducting sediments and magmatism in Sierra Nevada, based on δ^{18} O analyses of zircons and their rims.

More research involving geochronology and rock cycle transitions at particular locales with well-studied and dated sedimentary to metamorphic to igneous transitions, is needed to address this question.

Figure 15 compares three coeval records: shales, quartz in granites (this work), and detrital and igneous zircons (Spencer et al. 2017). To the first order, on ~0.5 billion year timescales, peaks and troughs coincide (within ~0.2 Ga) in the geologic record, which is an important observation. Supercontinents and panglobal glacial episodes are also shown and exhibit some connection to the record. In particular, the lowest δ^{18} O shales troughs coincide with Neo and Paleoproterozoic and early Permian glaciations, supporting conclusions in Bindeman et al. (2016) on the involvement of ultra-low-δ¹⁸O meteoric and diagenetic waters during glacial episodes (e.g., Bindeman and Lee 2018), Indeed, the lowest- δ^{18} O rocks with δ^{18} O values of -27% SMOW are dated to two Paleoproterozoic glacial episodes at 2.4 and 2.3 Ga (Zakharov et al. 2019). Low- δ^{18} O shales also coincide with the end of the supercontinent and increased rifting, supplying juvenile +5-6% mantle oxygen to the record. There is a general lack of granites during Huronian and Neoproterozoic panglobal ice ages, and is known as the magmatic shutdown (Condie 2013). In this case the δ^{18} O (and Δ'^{17} O!) in dated detrital zircons should help fill the gap. Zircons also show the low values in the Neoproterzoic, but the minimum appears to slightly predate the earliest Sturtian glaciation. More research is needed to identify coeval (subglacial) granites and zircons with ultra-low- δ^{18} O values of this age and also Paleoproterozoic age. The existing dataset of Spencer et al. (2019) with 9000 δ^{18} O analyses should be further split into detrital and igneous subsets to get better resolution of the above possibilities of glacial influence, supercontinent assembly, and granite-shale time lag questions. For example, the issue of the time lag is described in Bucholz and Spencer (2019) as future directions of research.

Alternative testable hypotheses of Archean–Proterozoic Δ'¹⁷O transition

The argument here then, is that granite and shales record exhibit a step-wise change of $\Delta'^{17}O$ at the Archean–Proterozoic boundary. A question in opposition: what if low- $\Delta'^{17}O$ granites appeared first, and shales simply inherited this signature via their weathering? As studied low- $\Delta'^{17}O$ granites are metasedimentary derived, this brings the question back to older sediments. Even with the addition of mantle material via direct mixing with mantle–magma differentiates, to direct derivation by melting of metabasaltic (rather than siliciclastic) protoliths, the question is redirected to simultaneous $\Delta'^{17}O$ change in the mantle-derived magmas.

The record is further explained if, for some reason, the upper mantle $\Delta'^{17}O$ value changed step-wise at the Archean–Proterozoic boundary. Consider a scenario where the Archean upper mantle is providing magmas that generated Archean crust and sediments, and was lower in $\Delta'^{17}O$ by up to -0.05%. This does not require that the $\Delta'^{17}O = -0.05\%$ difference is representative of the *entire* convecting mantle, past or present, but may reflect its upper portion, perhaps a stagnant lid of sublithospheric mantle formed from the magma after the giant impact at ~4.44 Ga. This early "low- $\Delta'^{17}O$ " component would have since been largely dissolved in the mantle and disappeared since 2.4Ga, due to for example intensification of plate tectonics. The ancient Archean continental keels, made of buoyant harzburgite and dunite, while not participating in mantle convection may still preserve, if originally present, this $\Delta'^{17}O$ depleted material. This hypothesis can be tested using xenoliths of Archean age from kimberlites. In order to create a -0.05% upper mantle, the Giant Impact itself can be called as an explanation. The impactor in this case would have been HED-meteorite like planetary body with $\Delta'^{17}O = -0.3\%$. A cometary material of "Late Veneer" Bombardment can also be called as an additional source of added material.

Current discussion on the difference between the Earth and the Moon in triple oxygen space (Herwartz et al. 2014; Young et al. 2016; Greenwood et al. 2018; Cano et al. 2020) should be tested against the earliest rocks presently available. These authors argue in favor of a much smaller Δ'^{17} O range not exceeding 0.1%, likely <0.04%, and thus we consider "primordial" Δ'^{17} O of the early crust testable, but a less likely hypothesis than continental emergence at the Archean–Proterozoic boundary.

PART IV. SEDIMENTARY PROXIES SHOWING TEMPORAL δ^{18} O INCREASE

Several paleoclimatic archives such as carbonates, cherts, and shales, show a δ^{18} O increase throughout geologic time (Fig. 3). At face value, these provide independent lines of support for a temporal increase in δ^{18} O of the hydrosphere, by as much as 10-15%c, and strongly negative (-10 to -20%) Precambrian oceans (Veizer et al. 1999; Veizer and Prokoph 2015). Alternatively, this record assuming constant δ^{18} O ocean similar to modern (e.g., Muehlenbachs and Clayton 1976) indicates greater temperatures in the past and thus smaller mineral-water fractionations per Equations (2) and (3) (Fig. 3). Although diagenetic transformation and secondary alteration processes involving meteoric waters were undoubtedly involved and important (see discussion above), I believe that these three records still carry at least a portion of primary depositional signatures, reflecting surface conditions. I argued above that shales do. One should also note that an increase in three proxies on Figure 3 appears convincing of global change of δ^{18} O_{seawater} or T, each of these proxies record somewhat different reservoirs and processes, and exhibit a different pattern and magnitude of increase. Cherts represent biotically and abiotically precipitated amorphous silica that matures and commonly become lighter in δ^{18} O during diagenesis (Marine-Carbonne et al. 2010; Cammack et al. 2018). The origin ranges from low-T cold seawater diatoms or chemical precipitate, to vent fluid-dominated (thus mostly basaltic origin). Carbonates represent organic (shells, foraminifera, stromatolites), or inorganic precipitates from carbonate oversaturated seawater or lake water. Both carbonates and cherts are also subject to alteration, and reset after formation when exposed to the low- δ^{18} O hydrosphere (Ryb et al. 2018; Liljestrand et al. 2020). Shales represent the products of weathering by diverse in δ^{18} O meteoric waters, shifted down on weighted average by -7.5% in the dominant modern sediment formed in the tropics to mid-latitudes (Bindeman et al. 2019).

The long debate about constant vs. increasing $\delta^{18}O$ of oceans and hence hydrosphere is related to debate about paleotemperature on early earth and especially in the Archean. Given mineral proxy—water isotope fractionations as function of temperature, one solution is zero permil $\delta^{18}O$ oceans and high temperatures of 45 to 85 °C (reaching clearly unrealistic 130 °C! for some cherts, Perry et al. 1978). This is viewed as unsustainable for any life except extreme theromphilic, and violating long term "wet-bulb" sea-land hydrological climate feedback not allowing the warmest temperature to exceed globally averaged 37 °C (Pierrehumbert 1994; Huber 2012; Buzan and Huber 2020). Hydrothermal alteration products in ophiolites and altered oceanic crust on the other hand demonstrate relative ($\pm 2\%$) constancy of $\delta^{18}O$ of seawater through time (Muehlenbachs and Clayton 1976; Gregory et al. 1991; Holmden and Muehlenbachs 1993; Muehlenbachs et al. 2003; Sengupta and Pack 2018; Zakharov and Bindeman 2019). A common critique of these record is that they do not fully reflect seawater, but isotopically shifted seawater that has interacted with basalts and mantle rocks upstream.

The isotopically negative oceans and modern range of temperatures is also not an easily acceptable solution. The steady state $\delta^{18}O$ value of seawater is fundamentally a balance of high temperature processes: seafloor hydrothermal alteration that increases $\delta^{18}O$ water (about 70–80% of all fluxes), and low-temperature processes such as weathering and low-T benthic alteration (about 15–20% of all fluxes), which decreases $\delta^{18}O$ values. Other processes play a minor role, and thus it is a balance and relative importance of spreading vs. weathering. Given a large oxygen reservoir in the hydrosphere at 1.25×10^{24} g, and small fluxes measuring in 10^{15} g %/yr, $\sim 10^{8}$ yr are required to change $\delta^{18}O$ of oceans by more than 1% (Muehlenbachs and Clayton 1976; Walker and Lohmann 1989).

Application of triple oxygen isotopes are called upon to solve these problems by providing an additional equation to the oxygen isotopic system, potentially permitting resolving $\delta^{18}O_w$ and temperature differences, along the line similar to Figure 6. However, largely because the MWL and the fractionation and mixing equation lines are nearly parallel for any sedimentary proxies (e.g., Fig. 6), the error of such resolution for carbonates, cherts, and shales is large. If one assumes a modern MWL, then Archean temperatures are high, +25 to 100 °C, based on the shale record (Fig. 18).

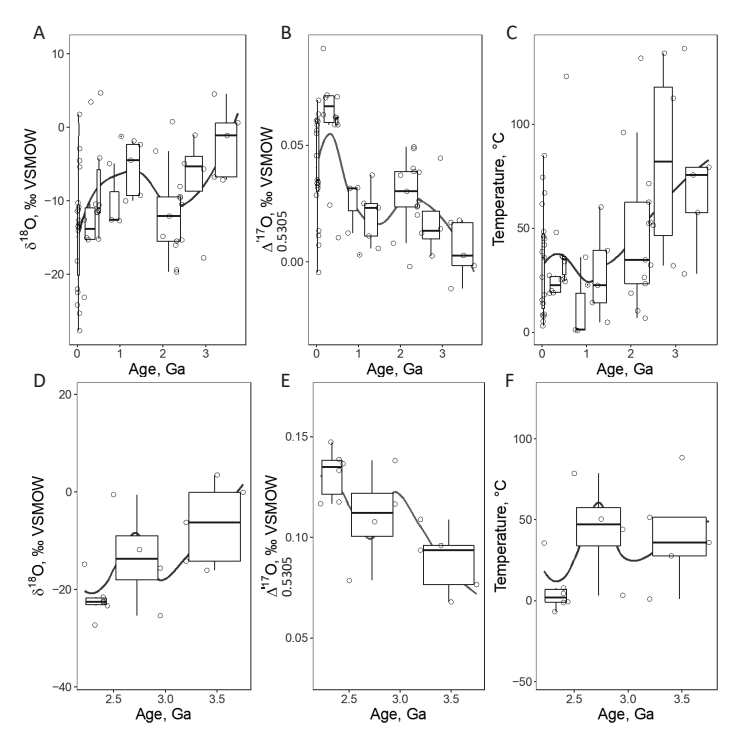


Figure 18. Calculated environmental parameters on Earth: T (a), $\Delta'^{17}\rm{O}_{MW}$ (b) and $\delta^{18}\rm{O}_{MW}$ (c) vs. age based on the solution of three equations with three input parameters: $\delta'^{18}\rm{O}_{shale}$, $\delta'^{17}\rm{O}_{shale}$, Modern meteoric water line (Eqn. 4), and CIA, as explained in Figure 6. Note that T and $\delta'^{18}\rm{O}_{water}$ solve within realistic bounds using assumptions and isotopic fractionations as in Equations (5) and (6). Furthermore, the lowest $\delta'^{18}\rm{O}_{water}$ values are for the 5 Ma-old clay samples from Antarctica and the 2.5–2.2 Ga synglacial Paleoproterozoic shales, confirming the participation of low- $\delta'^{18}\rm{O}_{w}$ synglacial waters in diagenesis (cf. Bindeman et al. 2016). The highest recent T and $\delta'^{18}\rm{O}_{water}$ values are for 55.5 Ma Paleocene–Eocene thermal maximum shales (Freiling et al. 2014). **d–f** represent the same solution for rocks greater than 2 Ga but by assuming ocean of -5% and corresponding MWL equation: $\delta'^{17}\rm{O} = 0.528 \cdot \delta'^{18}\rm{O} + 0.078$ as is explained on Figures 6 and 17. Note more realistic surface temperatures in the Archean, low T and low- $\delta'^{18}\rm{O}_{MW}$ during 2.2–2.4 Ga Paleoproterozoic glaciations in both a and c panels.

The other sedimentary archives, i.e., carbonates and cherts, suffer from syn- and post-diagenetic shifts, along the concave up curves connecting the rock with low- $\delta^{18}O$ and high- $\Delta'^{17}O$ waters, comparable to mixing curves in Figure 6. Using triple oxygen isotopes Liljestrand et al. (2020) considered the diagenetic effects upon carbonates and cherts respectively; these effects will shift $\Delta'^{17}O$ downward and along the concave down mixing lines. Thus the inferred high temperatures were interpreted to reflect diagenesis. In contrast, our insight into diagenetic transformation (Fig. 9) does not return the same result for Texas shales that rather indicate that weathering conditions are preserved.

I consider a compromised solution, globally elevated temperatures in the Archean, (perhaps MAT=37 °C) and slightly isotopically negative oceans, perhaps -4 to -5‰. Such values can reconcile the balance between low- and high temperature geochemical fluxes within currently accepted limits, with some modifications as indicated below (Fig. 18). A simple solution for -5‰ seawater shifted away and linearly from the mantle with a slope of 0.5215 would generate an "Archean MWL" also shifted up (Fig. 17). Sengupta and Pack (2018) proposed even steeper shift along the slope of ~0.51 by taking into account estimated triple oxygen isotopic values of typical end-member products (deep sea clays, altered MORB and others) and mass balances that

were based on the original Muehlenbachs (1998) work. As these balances are likely to change (see above), we here adopted even a simple solution of hydrothermal water–rock interaction globally following the linear path away from the mantle and toward seawater, and weathering/diagentic processes also nearly linearly connecting crustal rocks with parental weathering waters on meteoric water line. Linearity is explained by combination of concave down fractionation and concave up mixing during diagenesis (Figs. 6, 9). The justification for this slope includes consideration of lines for each of the high and low-T processes involved: 0.5212 of hydrothermal alteration of MORB ($\delta^{18}O=5.7\%c$, $\Delta'^{17}O=-0.051\%c$) with seawater (0,0%c); weathering 0.522 (+14.8%c, -0.164%c sediment) and (-7.3%c, +0.02%c) weathering water (average values in Bindeman et al. 2019). At a combination of these slopes, any mass balance puts the line away from the mantle or crustal rocks very close to the modern seawater as is shown on Figure 17. This effort is by no mean final and should be refined further when balances of low and high-T fluxes are revised (e.g. Kanzaki 2020a,b). This way we generate hypothetical "Archean meteoric water lines" estimates with *excess* of $\Delta^{17}O$, the main subject of this Chapter.

The new, "Archean MWL" equation at $-5\%e \delta^{18}O_{sw}$ becomes:

$$\delta'^{17}O = 0.528 \,\delta'^{18}O + 0.078 \tag{9}$$

and it was used in hydrologic modeling similar to the one performed above (Fig. 6) to resolve T and δ^{18} O and Δ'^{17} O of meteoric waters parental to shales. Results are shown on Figure 18 and demonstrate that global temperatures stay largely below 50°±10°C, if meteoric waters parental to shales were initially derived from -5% ocean. Further tuning of Archean MWL and global temperatures are possible with specialized and perhaps multi-proxies studies, but this exercise here shows that using shales to reconstruct global ocean values works. Proposed moderately high temperatures in the Archean and the Precambrian most likely also carry preservation and sampling bias. For analogy with the modern world (Fig. 1), where most weathering and shale production occurs in tropical environments of SE Asia, most commonly sampled Precambrian shales likely sample the most common shales and thus record tropical environments. Paleotemperatures of 50±10°C are no surprise, as daytime temperatures in modern deserts routinely reach 50 °C, and ground temperature where some weathering reactions take place can exceed 90 °C. Furthermore, temperatures during the Paleocene-Eocene Thermal Maximum (55.6 Ma ago) were higher than the modern, semi-glacial world, by at least 5–8 °C (Bowen et al. 2015). Therefore, the Archean temperatures perhaps need not exceed modern by a conceivable 20 °C to explain the triple oxygen isotopic record of shales.

To justify moderately depleted -5% ocean, mass balance of fluxes into the hydrosphere would need to be adjusted to balance the proportion of low and high-temperature alteration of the oceanic crust to enable meaningful δ^{18} O changes on 10^7-10^8 yr timescales, as exchange in mid-ocean ridge hydrothermal systems constitute the main flux of exchanging ocean. I also think we need to be thinking outside the uniformitarian principles where modern environments are transferred to the Archean. Walker and Lohmann (1989) suggested that low-T hydrothermal alteration dominated the Archean, and the temporal evolution of increasing δ^{18} O is a result of temporally increasing proportion of submarine high-T water-rock interaction. Kasting et al. (2006) suggested that the box models of strong coupling between hydrosphere and ocean crust (Muehlenbachs and Clayton 1972, 1976) and Holland (1984) could have varied with time, and the relative role of low and high-T interaction at ocean floor. I point out new developments to better understand both the magnitude of each flux, their relative ratio, and the values of the endmembers. More importantly, it is important to think outside the box and move away from "box models" which always have a prescribed solution of balancing fluxes, and move toward real world dynamics of these fluxes. Kanzaki (2020a) demonstrated through 2D numerical hydrothermal simulations that the degree of MORB alteration is non-linear with depth and in earlier employed box models (Muehlenbachs and Clayton 1976; Muehlenbachs 1998). Kanzaki (2020b) performed further 2D numerical simulations of water rock interaction with spreading to argue that due to incomplete exchange, there is a strong decoupling of δ^{18} O values of rocks

and seawater. Although not explicitly stated therein, this means that oceanic crust is subducted while largely unaltered on 10^{7} – 10^{8} yr timescales, corresponding to range of ages of oceanic crust in the present world. Thus the overall high-T hydrothermal contribution at MOR, and the flux of oxygen from the mantle to the hydrosphere, making it higher in δ^{18} O, is significantly smaller than previously assumed. If so, the relative roles of continental chemical weathering and shale production become more important in driving change in δ^{18} O of the hydrosphere on long timescales, which are governed in part by variations in exposed landmass (Fig. 11). The trends observed on Figure 3 call for greater and more intense weathering in the past, perhaps due to a greater CO₂ concentration, greater temperatures, and perhaps due to greater exposure of fresh igneous and metamorphic rocks on the surface. With time the sedimentary cover shields these fresh low- δ^{18} O rocks from weathering. Further modulations are possible due to the advent of plant life on land. Ibarra et al. (2020) and D'Antonio et al. (2020) demonstrated that the advent of vascular plants in the Devonian decreased overall weathering rates by a factor of two due to increased carbon burial effects on CO₂ weathering balance. Furthermore, plants and increased sedimentary rock and soil cover may act to slow the process for δ^{18} O on a longer term, by shielding fresh rocks from weathering (cf. Drever 1994).

I, here, further draw attention to the possibility of temporal accumulation of heavy $\delta^{18}O$ in the crust and shales via progressive accumulation of weathering products since 4.4 Ga, and especially temporal increase in the value of the *surface* $\delta^{18}O$. This should lead to an overall decrease in weathering $\delta^{18}O$ flux with time. For the continental weathering flux, not only the exposed area of the crust subjected to weathering is important, but also the proportion of preexisting sedimentary cover upon it. Sedimentary rocks not only physically blanket crystalline igneous and metamorphic rocks available to the heavy oxygen from the hydrosphere via shale production as is argued above, but greater proportion of sedimentary cover may additionally produce very small overall $\delta^{18}O$ flux to the ocean since sedimentary rocks are already weathered and high- $\delta^{18}O$, thus in equilibrium with hydrosphere. Periods of orogenesis generate increased exposure of crystalline rocks and thus greater weathering flux leading to a lower $\delta^{18}O$ hydrosphere, as compared to periods lacking mountain building which would agree with the Phanerozoic trends on Figure 14.

Future triple O work should target well-studied Phanerozoic formations to resolve these effects. In particular, continental breakup leads to continental flooding (young and shallow oceans basins, warmer climate, greater ocean) and also sediment cover, diminishing the role of fresh-rock weathering, increasing hydrosphere δ^{18} O.

This combined with an increased role of seafloor spreading during continental breakup, leads to higher $\delta^{18}O$ value of the hydrosphere. There may be a time lag between realization of the above torques on oxygen isotopic value of world oceans, perhaps by many tens of Myr, due to the enormous size of reservoir. It would be interesting to compare the temporal evolution of triple-O isotopes with the evolution of crustal residence times inferred from Nd isotopes (cf. Michard et al. 1985). Assembly and breakup of Pangea is the most recent example of possible realization of these torques and thus Late Proterozoic–Phanerozoic record of shales should provide insight into this (Fig. 14).

We observe that mid Phanerozoic is accompanied by low- $\delta^{18}O$ value of shales, while more recent and especially late Neoproterozoic, have the highest $\delta^{18}O$ shales and contemporaneous granites. The magnitude of the change of 5–6% $\delta^{18}O$ could potentially be in agreement with similar change in $\delta^{18}O$ of seawater (Wallmann 2001, 2004). Other factors that can influence this is: colder temperatures in the mid Permian would promote greater fractionations, large continents in mid Phanerozoic longer vapor transport and low- $\delta^{18}O$ values, also promoting low- $\delta^{18}O$ shale values (Fig. 14).

Temporal increase in $\delta^{18}O$ of the ocean may also reflect time accumulated loss of low- $\delta^{18}O$ interior of slabs (e.g., Bindeman et al. 2019), or progressively decreasing loss earliest low- $\delta^{18}O$ crust, formed at high-T by interaction with hydrosphere. Added water will rehydrate the mantle but produce minimal isotopic shift on it. Steady supply of low- $\delta^{18}O$ water to the

mantle with subducting slabs should also lead to sea level change (Wallmann 2001, 2004; Korenaga et al. 2017). Continental emergence which happened at ~2.4 Ga (Fig. 11) may have a component of sea level drop due to rehydration of the mantle by plate tectonic forces.

We further speculate that *if* the early high- Δ'^{17} O, low- δ'^{18} O water that define the earlier hydrosphere was due to Late Veneer cometary delivery (potentially having very different Δ'^{17} O and δ'^{18} O signatures, e.g., low- Δ'^{17} O Isua data, pending verification), this is a testable hypothesis as such water should be reflected in sediments precipitating from it, and then propagated into the earliest crust before dissolving in the younger record. These processes of a loss of the originally birthmarked and lingering low- δ^{18} O crust and hydrosphere can be tested by using Δ'^{17} O in shales and other earliest proxies.

SUMMARY: DEFINING THE Δ'^{17} O CRUSTAL ARRAY

This Chapter presented new and compiled data for $\Delta'^{17}O$ values in siliciclastic sediments and granites across the geologic history. Figure 19 presents the summary of these data plotted against 0.528 and 0.5305 reference slopes for comparison with other materials presented in this volume. A noticeable feature is that a slope of the trend is best reconciled with $\lambda = 0.523$. A combined fitted linear trend through shales and granites passes in the close vicinity of the mantle. A forced fit through the mantle (assuming that crust contains many mantle-derived rocks such as basalts and gabbros, their remelts and differentiates such as A and I type granites), yields a line with a slope of 0.523 that passes slightly below the SMOW value at $\Delta'^{17}O = -0.01\%$. When dataset is further split between Archean and post-Archean shales and granites, the trends overlap within error. Modern river clays sampling the most diverse climates (temperatures and $\Delta'^{18}O_{MW}$ values, data from Bindeman et al. 2019) provide the glimpse into ranges of weathering conditions applicable to the past environments. Overall, modern river clays are overlapping and conjoining with the ancient shale fields. When all 170 data points for granites, shales, and modern river clays are lumped together, these represent silicate crust. Such "crustal $\Delta'^{17}O-\delta'^{18}O$ array" has the fitted line with a slope of $\lambda=0.5235$ and Δ'^{17} O intercept of -0.021%; when forced through the mantle it becomes fitted $\lambda = 0.5228$ and $\Delta'^{17}O$ intercept of -0.01%, similar to fit through granites alone. Figure 19b and c provide density plots for Δ'^{17} O crustal array with utilities for other studies and Chapters in this volume.

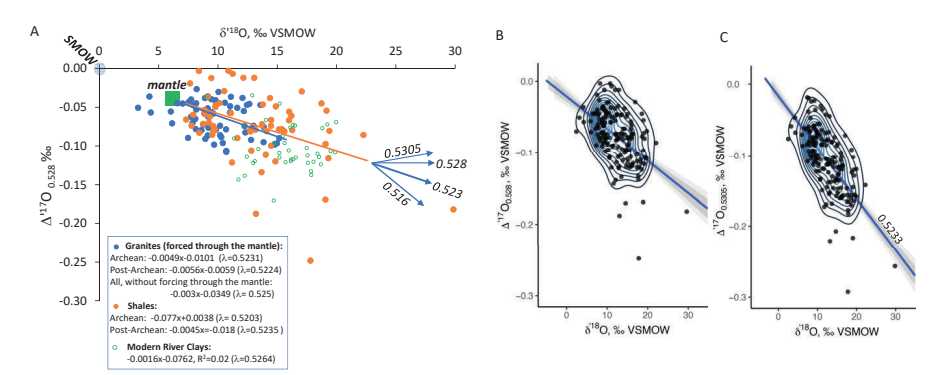


Figure 19. (a) Triple oxygen isotopic composition of the crustal rocks (granites, shales, and modern river sediments) of all ages relative to the 0.528 reference slope. Various fit lines for split datasets are shown (see inset and main text). Notice that the dataset clusters around the slope λ =0.523, and intercept is slightly less that SMOW by 0.01 to 0.008‰, broadly characterizing the silicate terrestrial crust. **b–c**) "crustal arrays": density plots for all data in (a) relative to $\Delta'^{17}O = 0.528$ and $\Delta'^{17}O = 0.5305$ reference slopes.

ACKNOWLEDGEMENTS

This paper is benefited from sample donation by Greg Retallack, William Peck, Jade Star Lackey, John Valley, Dave Blackwell, Axel Hofmann, Allan Keys, Shirley Dutton and Texas drillcore facility supervisors. I thank Jim Palandri, Mike Hudak for lab assistance, David Zakharov for help with statistical treatment, Oleg Melnik for help with equation solving. I am also very grateful to Germain Bayon, David Zakharov and Jim Palandri for prior collaboration and internal comments on this Chapter, external reviews by Claire Bucholz and Sukanya Sengupta and further comments by Greg Retallack, Ann Bauer, and William Peck are acknowledged with warm gratitude. Andreas Pack is thanked for his careful editorial handling. Partly supported by NSF grant EAR 1833420.

REFERENCES

- Anderson LJ, Morrison J (2005) Ilmenite, magnetite, and peraluminous Mesoproterozoic anorogenic granites of Laurentia and Baltica. Lithos 80:45–60
- André, L, Abraham K, Hofmann A, Monin L, Kleinhanns IC, Foley S (2019) Early continental crust generated by reworking of basalts variably silicified by seawater. Nature Geoscience 12:769–773
- Bao H, Cao X, Hayles JA (2016) Triple oxygen isotopes: fundamental relationships and applications. Annu Rev Earth Planet Sci 44:463–492
- Bauer K, Vennemann T (2014) Analytical methods for the measurement of hydrogen isotope composition and water content in clay minerals by TC/EA. Chem Geol 363:229–240
- Bauer AM, Fisher CF, Vervoort JD, Bowring SA (2017) Coupled zircon Lu-Hf and U-Pb isotopic analyses of the oldest terrestrial crust, the >4.03 Ga Acasta Gneiss Complex. Earth Planet Sci Lett 458:37–48
- Bauer AM, Reimink JR, Chacko T, Foley BJ, Shirey SB, Pearson DG (2020) Hafnium isotopes in zircons document the gradual onset of mobile-lid tectonics Geochem Persp Lett 14:1–6
- Bekker A, Holland HD (2012) Oxygen overshoot and recovery during the early Paleoproterozoic. Earth Planet Sci Lett 317–318:295–304
- Bayon G, Delvigne C, Ponzevera E, Borges AV, Darchambeau F, De Deckker P, Lambert T, Monin L, Toucanne S, André L (2018) The silicon isotopic composition of fine-grained river sediments and its relation to climate and lithology. Geochim Cosmochim Acta 229:147–161
- Bayon G, Skonieczny C, Delvigne C, Toucanne S, Bermell S, Ponzevera E, André L (2016) Environmental Hf–Nd isotopic decoupling in World river clays. Earth Planet Sci Lett 438:25–36
- Bayon G, Freslon N, Germain Y et al. (2020) A global survey of radiogenic strontium isotopes in river sediments. Chem Geol subm
- Bindeman IN (2008) Oxygen isotopes in mantle and crustal magmas as revealed by single crystal analysis Rev Mineral Geochem 69:445–478
- Bindeman IN, Lee JE (2018) The possibility of obtaining ultra-low-8¹⁸O signature of precipitation near equatorial latitudes during the Snowball Earth glaciation episodes. Precambrian Res 319:211–219
- Bindeman IN, Bekker A, Zakharov DO (2016) Oxygen isotope perspective on crustal evolutionon early Earth: A record of Precambrian shales with emphasis on Paleoproterozoic glaciations and Great Oxygenation Event. Earth Planet Sci Lett 437:101–113
- Bindeman IN, Zakharov DO, Palandri J, Greber ND, Dauphas N, Retallack GJ, Hofmann A, Lackey JS, Bekker A (2018) Rapid emergence of subaerial landmasses and onset of a modern hydrologic cycle 25 billion years ago. Nature 557:545–548
- Bindeman IN, Bayon G, Palandri J (2019) Triple oxygen isotope investigation of fine-grained sediments from major world's rivers: insights into weathering processes and global fluxes into the hydrosphere Earth Planet Sci Lett 528:115851
- Bleeker W (2003) The late Archean record: a puzzle in ca 35 pieces. Lithos 71:99-134
- Borisova AY, Zagrtdenov NR, Toplis MJ, Bohrson WA, Nedelec A, Safonov OG, Pokrovski GS, Ceuleneer G, Bindeman IN, Melnik OE, Jochum KP (2020) Planetary felsic crust formation at shallow depth. arXiv:200301508
- Bowen GJ (2019) The Online Isotopes in Precipitation calculator, version 31, http://waterisoutahedu/waterisotopes/pages/data_access/oipchtml)
- Bowen GJ, Maibauer BJ, Kraus MJ, Röhl U, Westerhold T, Steimke A, Gingerich PD, Wing SL, Clyde WC (2015) Two massive, rapid releases of carbon during the onset of the Palaeocene–Eocene thermal maximum. Nat Geosci 8:44–47
- Brenner AR, Fu RR, Evans DAD, Smirnov AV, Trubko R, Rose IR (2020) Paleomagnetic evidence for modern-like plate motion velocities at 3.2Ga. Sci Adv 6:eaaz8670
- Bucholz C, Spencer CJ (2019) Strongly peraluminous granites across the Archean–Proterozoic transition. J Petrol 60:1299–1348

Bucholz CE, Jagoutz O, VanTongeren JA, Setera J, Wang Z (2017) Oxygen isotope trajectories of crystallizing melts: Insights from modeling and the plutonic record. Geochim Cosmochim Acta 207:154–184

Bucholz ČE, Stolper EM, Eiler JM, Breaks FW (2018) A comparison of oxygen fugacities of strongly peraluminous granites across the Archean–Proterozoic boundary. J Petrol 59:2123–2156

Buick R, Rasmussen B, Krapez B (1998) Archean oil: evidence from extensive hydrocarbon generation and migration 2.5–3.5 Ga. Am Ass Petrol Geol Bull 82:50–69

Buzan JR, Huber M (2020) Moist heat stress on a hotter Earth. Annu Rev Earth Planet Sci 48:23.1–23.33

Cammack JN, Spicuzza M, Cavosie A, et al. (2018) SIMS microanalysis of the Strelley Pool Formation cherts and the T implications for the secular-temporal oxygen-isotope trend of cherts. Precambrian Res 304:125–139

Cao X, Liu Y (2011) Equilibrium mass-dependent fractionation relationships for triple oxygen isotopes Geochim Cosmochim Acta 75:7435–7445

Capuano RM (1992) The temperature dependence of hydrogen isotope fractionation between clay minerals and water: Evidence from a geopressured system. Geochim Cosmochim Acta 56:2547–2554

Chapman AD, Saleeby JB, Eiler J (2013) Slab flattening trigger for isotopic disturbance and magmatic flare-up in the southernmost Sierra Nevada batholith, California. Geology 41:1007–1010

Chappell BW, White AJR (1974) Two contrasting granite types. Pac Geol 8:173-4

Carlson RW, Garçon M, O'Neil J, Reimink J, Rizo H (2019) The nature of Earth's first crust. Chem Geol 530:119321 Cavosie AJ, Valley JW, Wilde SA (2018) The oldest terrestrial mineral record: Thirty years of research on Hadean zircon from Jack Hills. Western Australia. *In:* Earth's Oldest Rocks. Elsevier

Churchman GJ, Clayton RN, Sridhar K, Jackson ML (1976) Oxygen isotopic composition of aerosol size quartz in shales. J Geophys Res 81:381–386

Clayton RN, Mayeda TK (2009) Kinetic isotope effects in oxygen in the laboratory dehydration of magnesian minerals. J Phys Chem A 113:2212–2217

Colón DP, Bindeman IN, Gerya TV (2019) Understanding the isotopic and chemical evolution of Yellowstone hot spot magmatism using magmatic-thermomechanical modeling. J Volcanol Geotherm Res 370:13–30

Condie KC (2013) Plate Tectonics & Crustal Evolution, Pergamon Press, 3rd Edition

Criss RE (1999) Principles of Stable Isotope Distribution. Oxford U Press

Dansgaard W (1964) Stable isotopes in precipitation. Tellus 16:436–468

D'Antonio MP, Ibarra DE ; C Kevin Boyce CK (2020) Land plant evolution decreased, rather than increased, weathering rates. Geology 48:29–33

Delgado A, Reyes E (1996) Oxygen and hydrogen isotope compositions in clay minerals: a potential single-mineral geothermometer. Geochim Cosmochim Acta 60:4285–4289

Dellinger M, Bouchez J, Gaillardet J, Faure L, Moureau J (2017) Tracing weathering regimes using the lithium isotope composition of detrital sediments. Geology 45:411–414

Dhuime B, Wuestefeld B, Hawkesworth CJ (2015) Emergence of modern continental crust about 3 billion years ago. Nat Geosci 8:552–555

Drever JI (1994) The effect of land plants on weathering rates of silicate minerals. Geochim Cosmochim Acta 58:2325–2332

Ducea MN, Chapman AD (2018) Sub-magmatic arc underplating by trench and forearc materials in shallow subduction systems; A geologic perspective and implications. Earth Sci Rev 185:763–779

Dutton SP, Loucks RG, Ambrose WA (2015) Factors controlling permeability variation in onshore, deep Paleogene Wilcox Sandstones in the northern Gulf of Mexico Basin: Targeting high-quality reservoirs. GCAGS J 4:1–14

Eberl DD (1993) Three zones for illite formation during burial diagenesis and metamorphism. Clays Clay Mineral 41:26–37 Eiler JM (2001) Oxygen isotope variations of basaltic lavas and upper mantle rocks. Rev Mineral Geochem 43:319–364

Eslinger, E V, Savin, S M (1976) Mineralogy and ¹⁸0/¹⁶0 ratios of fine-grained quartz and clay from site 323: Initial Reports of the Deep Sea Drilling Project 35, CD Hollister, C Craddock et al. (eds), US Gov Printing Office, Washington, DC, 489-496

Flament N, Coltice N, Rey PF (2008) A case for late-Archaean continental emergence from thermal evolution models and hypsometry. Earth Planet Sci Lett 275:326–336

Friedman I, Lipman PW, Obradovich JD, Gleason JD, Christiansen RL (1974) Meteoric water in magmas. Science 184:1069–1072

Galloway WE, Whiteaker TL, Ganey-Curry P (2011) History of Cenozoic North American drainage basin evolution, sediment yield, and accumulation in the Gulf of Mexico basin. Geosphere 7:938–973

Gaschnig RM, Rudnick RL, McDonough WF, Kaufman AJ, Valley J, Hu Z-C, Gao, S (2016) Compositional evolution of the upper continental crust through time, as constrained by ancient glacial diamictites. Geochim Cosmochim Acta 186:316–343

Gilg HA, Girard J-P, Sheppard SMF (2004) Conventional and less conventional techniques for hydrogen, oxygen isotope analysis of clays, associated minerals and pore waters in sediments and soils. *In:* Handbook of Stable Isotope Analytical techniques, Volume 1, PA de Groot, Elsevier BV, p 38–61

Goldschmidt VM (1933) Grundlagen der quantativen Geochemie. Fortschr Mineral 17:112–156

Goldstein SJ, Jacobsen SB (1988) Nd and Sr isotopic systematics of river water suspended material: implications for crustal evolution. Earth Planet Sci Lett 87:249–265

- Greber ND, Dauphas N, Bekker A, Ptáček MP, Bindeman IN, Hofmann A (2017) Titanium isotopic evidence for felsic crust and plate tectonics 35 billion years ago Science 357:1271–1274
- Gregory RT (1991) Oxygen isotope history of seawater revisited: Timescales for boundary event changes in the oxygen isotope composition of seawater *In*: Stable Isotope Geochemistry: A Tribute to Samuel Epstein, HP Taylor, JR O'Neil, IR Kaplan (eds) Geochemical Society, p 65–76
- Greenwood RC, Barrat J-A, Miller MF, Anand M, Dauphas N, Franchi IA, Sillard P, Starkey NA (2018) Oxygen isotopic evidence for accretion of Earth's water before a high-energy Moon-forming giant impact. Sci Adv 4:eaao5928
- Hacker BR, Kelemen PB, Behn MD (2011) Differentiation of the continental crust by relamination. Earth Planet Sci Lett 307:501–516
- Hamza MS, Epstein S (1980) Oxygen isotopic fractionation between oxygen of different sites in hydroxyl-bearing silicate minerals Geochim Cosmochim Acta 44:173–182
- Harris C, Faure K, Roger E, Diamond RE, Scheepers R (1997) Oxygen, hydrogen isotope geochemistry of S- and I-type granitoids: the Cape Granite suite, South Africa. Chemical Geology 143:95–114. (Cape Granites S Africa 551 Ma)
- Hartmann J, Moosdorf N (2012) The new global lithological map database GLiM: a representation of rock properties at the Earth surface. Geochem Geophys Geosyst 13:Q12004
- Hawkesworth C.J. Cawood P.A. Dhuime B, Kemp AIS (2017) Earth's continental lithosphere through time. Annu Rev Earth Planet Sci 45:169–198
- Hayes JM, Strauss H, Kaufman AJ (1999) The abundance of ¹³C in marine organic matter and isotopic fractionation in the global biogeochemical cycle of carbon during the past 800 Ma. Chem Geol 161:103–125
- Hayles JA, Cao X, Bao H (2016) The statistical mechanical basis of the triple isotope fractionation relationship. Geochem Perspect Lett 3:1–11
- Hayles J, Gao C, Cao X, Liu Y, Bao H (2018) Theoretical calibration of the triple-oxygen isotope thermometer. Geochim Cosmochim Acta 235:237–245
- Herwartz D (2021) Triple oxygen isotope variations in Earth's crust. Rev Mineral Geochem 86:291–322
- Herwartz D, Pack A, Friedrichs B, Bischoff A (2014) Identification of the giant impactor Theia in lunar rocks. Science 344:1146–1150
- Herwartz D, Pack A, Krylov D, Xiao Y, Muehlenbachs K, Sengupta S, Di Rocco T (2015) Revealing the climate of snowball Earth from Δ¹⁷O systematics of hydrothermal rocks. PNAS 112:5337–5341
- Hoffman PF (2013) The Great Oxidation and a Siderian snowball Earth: MIFS based correlation of Paleoproterozoic glacial epochs. Chem Geol 362:143–156
- Holeman JN (1968) The sediment yield of major rivers of the world. Water Resour Res 4:737-747
- Holland HD (1984) The chemical evolution of the atmosphere and oceans. Princeton University Press
- Holmden C, Muehlenbachs K (1993) The ¹⁸O/¹⁶O ratio of 2-billion-year-old seawater inferred from ancient oceanic crust. Science 259:1733–1736
- Hopkinson TN, Harris NB, Warren CJ, Spencer CJ, Roberts NM, Horstwood MS, Parrish RR (2017) The identification and significance of pure sediment-derived granites. Earth Planet Sci Lett 467:57–63
- Hower J, Eslinger EV, Hower ME, Perry EA (1976) Mechanism of burial metamorphism of argillaceous sediment: 1 Mineralogical and chemical evidence. GSA Bull 87:725–737
- Hsieh JCC, Chadwick OA, Kelly EF, Savin SM (1998) Oxygen isotopic composition of soil water: Quantifying evaporation and transpiration. Geoderma 82:269–293
- Huber M (2012) Progress in greenhouse climate modeling. Paleontol Soc Pap 18:213–262
- Ibarra DE, Rugenstein JKC, Bachan A, Baresch A, Lau KV, Thomas DL (2019) Modeling the consequences of land plant evolution on silicate weathering Am J Sci 319:1–43
- Jung S, Mezger K, Hoernes S (2001) Trace element, isotopic (Sr, Nd, Pb, O) arguments for a mid-crustal origin of Pan-African garnet-bearing S-type granites from the Damara orogen (Namibia) Precambrian Research 110:325—355
- Kanzaki Y (2020a) Interpretation of oxygen isotopes in Phanerozoic ophiolites and sedimentary rocks. Geochem Geophys Geosystems 21:e2020GC009000
- Kanzaki Y (2020b) Quantifying the buffering of oceanic oxygen isotopes at ancient midocean ridges, Solid Earth Discuss 11:1475–1488
- Kasting JF, Howard MT, Wallmann K, Veizer J, Shields G, Jaffres J (2006) Paleoclimates, ocean depth, and oxygen isotopic composition of seawater. Earth Planet Sci Lett 252:82–93
- King EM, Valley JW, Davis DW, Edwards GR (1998) Oxygen isotope ratios of Archean plutonic zircons fromgranite greenstone belts of the Superior Province: indicator of magmatic source. Precambrian Res 92:365–38
- Knauth LP, Lowe DR (2003) High Archean climatic temperature inferred from oxygen isotope geochemistry of cherts in the 35 Ga Swaziland Supergroup, South Africa. Bull Geol Soc Am 115:566–580
- Korenaga, J, Planavsky NJ, Evans, DAD (2017) Global water cycle and the coevolution of the Earth's interior and surface environment. Phil Trans R Soc A 375:20150393
- Kump LR (2014) Hypothesized link between Neoproterozoic greening of the land surface and the establishment of an oxygen-rich atmosphere. PNAS 111:14062–14065

- Lackey JS, Valley JW, Chen JH, Stockli DF (2008) Dynamic magma systems, crustal recycling, alteration in the central Sierra Nevada batholith: The oxygen isotope record. J Petrol 49:1397–1426
- Lackey JS, Cecil MR, Windham CJ, Frazer RE, Bindeman IN, Gehrels GE (2012) The Fine Gold Intrusive Suite: The roles of basement terranes, magma source development in the Early Cretaceous Sierra Nevada batholith. Geosphere 8:292–313
- Land LS (1992) Saline formation waters in sedimentary basins: Connate or diagenetic? Proceedings of the 7th International Symposium on Water–Rock Interaction, A. A. Balkema, Rotterdam, p 865–868
- Land LS, Lynch FL (1996) δ¹⁸O values of mudrocks: More evidence for an ¹⁸O-buffered ocean. Geochim Cosmochim Acta 60:3347–3352
- Land LS, Milliken KL, Mack LE, Lynch FL (1997) Burial metamorphism of argillaceous sediment: A re-examination. Bull Geol Soc America 109:2–15
- Lawrence JR, Taylor HP, Jr (1972) Hydrogen and oxygen isotope systematics in weathering profiles. Geochim Cosmochim Acta 36:1377–1393
- Lawver LA, Dalziel IWD, Norton IO, Gahagan LM (2011) The Plates 2011. Atlas of Plate Reconstructions (500 Ma to Present Day), Plates Progress Report No 345–0811, University of Texas Technical Report No 198:189 pp
- Levin NE, Raub TD, Dauphas N, Eiler JM (2014) Triple oxygen isotope variations in sedimentary rocks Geochim Cosmochim Acta 139:173–189
- Li S, Gaschnig RM, Rudnick RL (2016) Insights into chemical weathering of the upper continental crust from the geochemistry of ancient glacial diamictites Geochim Cosmochim Acta 176:96–117
- Liljestrand FL, Knoll AH, Tosca NJ, Phoebe ACohen PA, Macdonald FA, Peng Y, Johnston DT (2020) The triple oxygen isotope composition of Precambrian chert. Earth Planet Sci Lett 537:116167
- Lohmann KC, Walker JCG (1989) The δ^{18} O record of Phanerozoic abiotic marine calcite cements. Geophys Res Lett 16:319–322
- Longstaffe FJ (1983) Stable isotope studies of diagenesis of clastic rocks. Geosci Canada 10:47-58
- Longstaffe FJ, Schwarcz HP (1977) ¹⁸O/¹⁶O of Archean clastic metasedimentary rocks: a petrogenetic indicator for Archean gneisses? Geochim Cosmochim Acta 41:1303–1312
- Luz B, Barkan E (2010) Variations of ¹⁷O/l⁶O and ¹⁸O/l⁶O in meteoric waters. Geochim Cosmochim Acta 74:6276–6286 Lynch FL (1997) Frio shale mineralogy and the stoichiometry of the smectite-to-illite reaction: The most important reaction in clastic sedimentary diagenesis. Clays Clay Miner 45:618–631
- Lynch FL, Mack LE, Land LS (1997) Burial diagenesis of illite/smectite in shales and the origins of authigenic quartz and secondary porosity in sandstones. Geochim Cosmochim Acta 61:1995–2006
- McLennan SM, Hemming, S, McDaniel, DK, Hanson GN (1993) Geochemical approaches to sedimentation, provenance, tectonics *In:* MJ Johnsson and A Basu (Eds) Processes controlling the composition of clastic sediments Geol Soc Am Spec Pap 284:21–40
- Mackenzie FT (editor) (2005) Sediments, Diagenesis, and Sedimentary Rocks. 1st Edition. Treatise on Geochemistry, Second Edition, Volume 7, Elsevier
- Marin-Carbonne J, Chaussidon M, Robert F (2010) The silicon and oxygen isotope compositions of Precambrian cherts: A record of oceanic paleo-temperatures? Precambrian Res 247:223–234
- Mertanen S, Pesonen LJ (2012) Paleo–Mesoproterozoic assemblages of continents: paleomagnetic evidence for near equatorial supercontinents. *In*: From the Earth's Core to Outer Space. Lecture Notes in Earth System Sciences 137, I Haapala (ed) Springer-Verlag Berlin Heidelberg, p 11–35
- Michard A, Gurriet P, Soudant M, Albarede F (1985). Nd isotopes in French Phanerozoic shales: external vs. internal aspects of crustal evolution. Geochim Cosmochim Acta 49:601–610
- Miller MF (2002) Isotopic fractionation and the quantification of ¹⁷O anomalies in the oxygen three-isotope system: an appraisal and geochemical significance. Geochim Cosmochim Acta 66:1881–1889
- Miller MF, Pack A (2021) Why measure ¹⁷O? Historical perspective, triple-isotope systematics and selected applications. Rev Mineral Geochem 86:1–34
- Miller MF, Pack A, Bindeman IN, Greenwood RC (2020) Standardizing the reporting of Δ'¹⁷O data from high precision oxygen triple-isotope ratio measurements of silicate rocks and minerals Chem Geol 532:119332
- Milliken KL, Land LS, Loucks RG (1981) History of burial diagenesis, Frio Formation, Brazoria County, Texas Bull Am Assoc Petrol Geol 65:1397–1413
- Milliman JD, Farnsworth KL (2011) River Discharge to the Coastal Ocean: A Global Synthesis. Cambridge University Press. Cambridge
- Mix H, Chamberlain CP (2014) Stable isotope records of hydrologic change and paleotemperature from smectite in Cenozoic western North America. Geochim Cosmochim Acta 141:532–546
- Morton RA, Land LS (1987) Regional variations in formation water chemistry, Frio Formation (Oligocene), Texas Gulf Coast. Bull Am Assoc Petrol Geol 72:191–206
- Muehlenbachs K (1998) The oxygen isotopic composition of the oceans, sediments and the seafloor. Chem Geol 145:263–273
- Muehlenbachs K, Clayton RN (1976) Oxygen isotopic composition of oceanic crust and its bearing on seawater. J Geophys Res 81:4365–4369

- Muehlenbachs K, Furnes H, Fonneland HC, Hellevang B (2003) Ophiolites as faithful records of the oxygen isotope ratio of ancient seawater: The Solund-Stavfjord Ophiolite Complex as a Late Ordovician example. Geol Soc, London, Spec Publ 218:401–414
- Mulch A, Sarna-Wojcicki AM, Perkins ME, Chamberlain CP (2008) A Miocene to Pleistocene climate, elevation record of the Sierra Nevada (California). PNAS 105:6819–6824
- Nabelek PI, Russ-Nabelek C, Denison JR (1992) The generation and crystallization conditions of the Proterozoic Harney Peak Leucogranite, Black Hills, South Dakota, USA: Petrologic and geochemical constraints. Contrib Mineral Petrol 110:173–191
- Nesbitt HW, Young GM (1982) Early Proterozoic climates and plate motions inferred from major element chemistry of lutites. Nature 299:715–717
- Newman ACD (1987) Chemistry of clays and clay minerals Mineralogical society monograph series No 6, Mineralogical society, Longman
- O'Neil JR, Chappell BW (1977) Oxygen, hydrogen isotope relations in the Berridale batholith. J Geol Soc Lond 33: 559–571
- O'Neil JR, Shaw SE, Flood RH (1977) Oxygen, Hydrogen Isotope Compositions as Indicators of Granite Genesis in the New England Batholith, Australia. Contrib Mineral Petrol 62:313–328
- O'Neil J, Boyet M, Carlson RW, Paquette J-L (2013) Half a billion years of reworking of Hadean mafic crust to produce the Nuvvuagittuq Eoarchean felsic crust. Earth Planet Sci Lett 379:13–25
- Pack A (2021) Isotopic fingerprints of atmospheric molecular O_2 in rocks, minerals, and melts. Rev Mineral Geochem 86:217–240
- Pack A, Herwartz D (2014) The triple oxygen isotope composition of the Earth mantle and understanding Δ17O variations in terrestrial rocks and minerals. Earth Planet Sci Lett 390:138–145
- Pack A, Tanaka R, Hering M, Sengupta S, Peters S, Nakamura E (2016) The oxygen isotopecomposition of San Carlos olivine on the VSMOW2-SLAP2 scale. Rapid Commun Mass Spectrom 30:1495–1504
- Parra-Avila LA, Belousova E, Fiorentini ML, Eglingerd A, Blocke S, Millera J (2018) Zircon Hf and O-isotope constraints on the evolution of the Paleoproterozoic Baoulé-Mossi domain of the southern West African Craton. Precambrian Res 306:174–188
- Passey BH, Ji H (2019) Triple-oxygen isotope signatures of evaporation in lake waters and carbonates: A case study from the western United States. Earth Planet Sci Lett 518:1–12
- Passey BH, Levin NE (2021) Triple oxygen isotopes in meteoric waters, carbonates, and biological apatites: implications for continental paleoclimate reconstruction. Rev Mineral Geochem 86:429-462
- Payne JL, Hand M, Pearson NJ et al. (2015) Crustal thickening and clay: Controls on O isotope variation in global magmatism and siliciclastic sedimentary rocks. Earth Planet Sci Lett 412:70–76
- Peck WH (2016) Protolith carbon isotope ratios in cordierite from metamorphic and igneous rocks. American Mineralogist 101:2279–2287
- Peck WH, Valley JW, Corriveau L, Davidson A, McLelland J, Farber DA (2004) Oxygen-isotope constraints on terrane boundaries and origin of 1.18–1.13 Ga granitoids in the southern Grenville Province. Geol Soc Am Memoir 197:163–182
- Perry EC, Jr, Ahmad SN, Swulius TM (1978) The oxygen isotope composition of 3,800 my old metamorphosed chert and iron formation from Isukasia, West Greenland. J Geol 86:223–239
- Pettijohn FJ (1957) Sedimentary Rocks, second edition, Harper, New York
- Peucat JJ, Capdevila R, Drareni A, Choukroune P, Fanning CM, Bernard-Griffiths J, Fourcade S (1996) Major, trace element geochemistry and isotope (Sr, Nd, Pb, O) systematics of an Archaean basement involved in a 2.0Ga very high-temperature (1000°C) metamorphic event in Ouzzal Massif, Hoggar, Algeria. J Metamorph Geol 14:667–692
- Pierrehumbert RT (1994) Thermostats, radiator fins, and the local runaway greenhouse. J Atmos Sci 52:1784–1806 Pollington AD, Kozdon R, Valley JW (2011) Evolution of quartz cementation during burial of the Cambrian Mt Simon Sandstone, Illinois Basin: In situ microanalysis of ¹⁸O. Geology 39:1119–1122
- Pope EC, Bird DK, Rosing MT (2012) Isotope composition and volume of Earths early oceans. PNAS 109:4371–4376
 Ptáček MP, Dauphas N, Greber ND (2020) Chemical evolution of the continental crust from a data-driven inversion of terrigenous sediment compositions. Earth Planet Sci Lett 539:116090
- Reimink JR, Chacko T, Stern RA, Heaman LM (2016) The birth of a cratonic nucleus: Lithogeochemical evolution of the 4.02–2.94 Ga Acasta Gneiss Complex. Precambrian Res:281:453–472
- Reimink JR, Davies JH, Bauer AM, Chacko T (2020) A comparison between zircons from the Acasta Gneiss Complex and the Jack Hills region. Earth Planet Sci Lett 531:115975
- Retallack GJ (2001) Soils of the past an Introduction to Pedology, Blackwell Science, Oxford, 2nd edition
- Retallack GJ (2007) Cenozoic paleoclimate on land in North America. J Geol 115:271-294
- Robert F, Chaussidon M (2006) A palaeotemperature curve for the Precambrian oceans based on silicon isotopes in cherts. Nature 443:969–72
- Ronov AB, Yaroshevsky AA (1969) Chemical composition of the Earth's crust, in the Earth's crust and upper mantle, ed PJ Hart, American Geophysical Union, Washington, DC

- Rowley DB, Pierrehumbert R, Currie B (2001) A new approach to stable isotope-based paleoaltimetry: implications for paleoaltimetry and paleohypsometry of the High Himalaya since the Late Miocene. Earth Planet Sci Lett 188:253–268
- Rozanski R, Araguás-Araguás L, Gonfiantini R (1993) Isotopic patterns in modern global precipitation In: PK Swart, KC Lohmann, J Mckenzie, S Savin (Eds) Climate Change in Continental Isotopic Records, Geophysical Monograph 78, p 1–36
- Rozel A, Golabek G, Jain C, Tackley PJ, Gerya TV(2017) Continental crust formation on early Earth controlled by intrusive magmatism. Nature 545:332–335
- Rumble D, Miller MF, Franchi IA, Greenwood RC (2007) Oxygen three-isotope fractionation lines in terrestrial silicate minerals: an inter-laboratory comparison of hydrothermal quartz and eclogitic garnet. Geochim Cosmochim Acta 71:3592–3600
- Rumble D, Bowring S, Iizuka T, Komiya T, Lepland A, Rosing MT, Ueno Y (2013) The oxygen isotope composition of Earth's oldest rocks and evidence of a terrestrial magma ocean. Geochem Geophys Geosystems 14:1929–1939
- Rudnick RL, Gao S (2003) Composition of the continental crust. *In:* Treatise on Geochemistry, Volume 3. RL Rudnick HD Holland, KK Turekian (eds) Elsevier, pp 1–64
- Ryb U, Eiler JM (2018) Oxygen isotope composition of the Phanerozoic ocean and a possible solution to the dolomite problem. PNAS 115:6602–6607
- Sageman BB, Lyons TW (2004) Geochemistry of fine-grained sediments, sedimentary rocks. In: Sediments, diagenesis, and sedimentary rocks. FT Mackenzies(Ed) Vol 7 Treatise in Geochemistry, Elsevier, Oxford, p. 115–158
- Savin S, Epstein S (1970a) The oxygen and hydrogen isotope geochemistry of clay minerals. Geochim Cosmochim Acta 34:25–42
- Savin S, Epstein S (1970b) The oxygen and hydrogen isotope geochemistry of ocean sediments and shales. Geochim Cosmochim Acta 34:43–63
- Savin SM, Hsieh JCC (1998) The hydrogen and oxygen isotope geochemistry of pedogenic clay minerals: principles and theoretical background. Geoderma 82:227–253
- Savin SM, Lee ML (1988) Isotopic studies of phyllosilicates. Rev Mineral Geochem 19:189–223
- Schoenemann SW, Schauer AJ, Steig EJ (2013) Measurement of SLAP2 and GISP δ¹⁷O and proposed VSMOW– SLAP normalization for δ¹⁷O and ¹⁷O excess. Rapid Commun Mass Spectrom 27:582–590
- Schoenemann SW, Steig EJ, Ding Q, Markle BR, Schauer AJ (2014) Triple water-isotopologue record from WAIS Divide, Antarctica: controls on glacial-interglacial changes in ¹⁷O excess of precipitation. J Geophys Res Atmos 119:8741–8763
- Sengupta S, Pack A (2018) Triple oxygen isotope mass balance for the Earth's oceans with application to Archean cherts. Chem Geol 495:18–26
- Shackleton NJ, Kennett JP (1975) Paleotemperature history of the Cenozoic and the initiation of Antarctic glaciation; oxygen and carbon isotope analyses in DSDP sites 277:279 and 281. Initial Rep Deep Sea Drill Proj 29:743–755
- Schaltegger U, Nowak A, Ulianov A, Fisher CM, Gerdes A, Spikings R, Whitehouse MJ, Bindeman I, Hanchar JM, Duff J, Vervoort (2019) Zircon petrochronology and 40Ar/39Ar thermochronology of the Adamello Intrusive Suite, N Italy: Monitoring the growth and decay of an incrementally assembled magmatic system. J Petrol 60:701–722 Sharp ZD (2017) Principles of Stable Isotope Geochemistry, 2nd Edition
- Sharp ZD, Gibbons JA, Maltsev O, Atudorej V, Pack A, Sengupta S, Shock EL, Knauth LP (2016) A calibration of the triple-isotope fractionation in the SiO₂–H₂O system and applications to natural samples. Geochim Cosmochim Acta 186:105–119
- Shaw DB, Weather CE (1965) The mineralogical composition of shales. J Sed Petrol 35:213–222
- Sheppard SMF, Gilg HA (1996) Stable isotope geochemistry of clay minerals. Clay Minerals 31:1-24
- Silverman SR (1951) The isotope geology of oxygen. Geochim Cosmochim Acta 39:5669–584
- Simon L, Lécuyer C (2005) Continental recycling: The oxygen isotope point of view. Geochem Geophys Geosystems 6:Q08004
- Sobolev SV, Brown M (2019) Surface erosion events controlled the evolution of plate tectonics on Earth. Nature 570:52–57
- Spencer CJ, Roberts NMW Santosh M (2017) Growth, destruction, and preservation of Earth's continental crust Earth Sci Rev172:87–106
- Spencer CJ, Partin CA, Kirkland CL, Raub TD, Liebmann J, Stern RA (2019) Paleoproterozoic increase in zircon δ¹⁸O driven by rapid emergence of continental crust. Geochim Cosmochim Acta 257:16–25
- Suchecki R K, Land L S (1983) Isotopic geochemistry of burial-metamorphosed volcanogenic sediments, Great Valley sequence, northern California. Geochim Cosmochim Acta 47:1487–1499
- Surma J, Assonov S, Staubwasser M (2021) Triple oxygen isotope systematics in the hydrologic cycle. Rev Mineral Geochem 86:401–428
- Sylvester PJ (1998) Post-collisional strongly peraluminous granites. Lithos 45:29–44
- Taylor SR, McLennan SM (1995) The geochemical evolution of the continental crust. Rev Geophys 33:241–265
- Taylor HP, Epstein S (1962) Relationship between ¹⁸O/¹⁶O ratios in coexisting minerals of igneous and metamorphic rocks, part 1, principles and experimental results. Geol Soc Am Bull 73:461–480

- Trail D, Boehnke P, Savage PS, Liu MC, Miller ML, Bindeman I (2018) Origin, significance of Si and O isotope heterogeneities in Phanerozoic, Archean, and Hadean zircon. PNAS 115:10287–10292
- Turner S, Tonarini S, Bindeman I, Leeman WP, Schaefer BF (2007) Boron and oxygen isotope evidence for recycling of subducted components over the past 2.5 Gyr. Nature 447:702–705
- Uemura R, Barkan E, Abe O, Luz B (2010) Triple-isotope composition of oxygen in atmospheric water vapor. Geophys Res Lett 37:L04402
- Valley JW (1986) Stable isotope geochemistry of metamorphic rocks. Rev Mineral 16:445–489
- Valley JW, Peck WH, King EM, Wilde SA (2002) Cool early Earth. Geology 30:351–354
- Valley JW, Lackey J S, Cavosie AJ, CC Clechenko, MJ Spicuzza, MAS Basei, IN Bindeman, VP Ferreira, AN Sial, E M King, W H Peck, A K Sinha, C S Wei (2005) 44 Billion years of crustal maturation: Oxygen isotope ratios of magmatic zircon. Contrib Mineral Petrol 150:561–580
- Veizer J, Prokoph A (2015) Temperatures and oxygen isotopic composition of Phanerozoic oceans Earth Sci Rev 146:92–104Veizer J, Ala D, Azmy K, Bruckschen P, Buhl D, Bruhn F, Strauss, H (1999) ⁸⁷Sr/⁸⁶Sr, δ¹³C and δ¹⁸O evolution of Phanerozoic seawater. Chem Geol 161:59–88
- Vlaar NJ (2000) Continental emergence and growth on a cooling earth Tectonophysics 322:191–202
- Wallmann K (2001) The geological water cycle and the evolution of marine $\delta^{18}O$ values. Geochim Cosmochim Acta 65:2469–2485
- Wallmann K (2004) Impact of atmospheric CO_2 and galactic cosmic radiation on Phanerozoic climate change and the marine $\delta^{18}O$ record. G-cubed 5:Q06004
- Walker JCG, Lohmann KC (1989) Why the oxygen isotopic composition of sea water changes with time. Geophys Res Lett 16:323–326
- Watts KE, Bindeman IN, Schmitt AK (2011) Large-volume rhyolite genesis in caldera complexes of the Snake River Plain: Insights from the Kilgore tuff of the Heise volcanic field, Idaho, with comparison to Yellowstone and Bruneau-Jarbidge Rhyolites. J Petrol 52:857–890
- Wedepohl KH (1995) The composition of the continental crust. Geochim Cosmochim Acta 59:1217–1239
- Wetmore PH, Mihai N Ducea MN (2011) Geochemical evidence of a near-surface history for source rocks of the central Coast Mountains Batholith, British Columbia. Int Geol Rev 53:230–260
- Wilde SA, Valley JW, Peck WH, Graham CM (2001) Evidence from detrital zircons for the existence of continental crust and oceans on the Earth 4.4 Gyr ago. Nature 409:175–178
- Wilkinson M, Crowley SF, Marshall JD (1992) Model for the evolution of oxygen isotope ratios in the pore fluids of mudrocks during burial. Mar Petrol Geology 9:98–105
- Wostbrock JAG, Sharp ZD (2021) Triple oxygen isotopes in silica–water and carbonate–water systems. Rev Mineral Geochem 86:367–400
- Wostbrock JAG, Cano E, Sharp ZD (2020) An internally consistent triple oxygen isotope calibration of standards for silicates, carbonates and air relative to VSMOW2 and SLAP2. Chem Geol 533:119432
- Yeh H-W, Epstein S (1978) Hydrogen isotope exchange between clay minerals and seawater. Geochim Cosmochim Acta 42:140–143
- Yeh H-W, Eslinger E (1986) Oxygen isotopes and the extent of diagenesis of clay minerals during sedimentation and burial in the sea. Clays Clay Miner 34:403–406
- Yeh H-W, Savin SM (1976) The extent of oxygen isotope exchange between clay minerals and sea water. Geochim Cosmochim Acta 40:743–748
- Yeh H-W, Savin SM (1977) Mechanism of burial metamorphism of argillaceous sediments: 3 Oxygen isotopic evidence. Geol Soc Am Bull 88:1321–1330
- Young ED, Galy A, Nagahara H (2002) Kinetic and equilibrium mass-dependent isotope fractionation laws in nature and their geochemical and cosmochemical significance Geochim Cosmochim Acta 66:1095–1104
- Young ED, Yeung LY, Kohl IE (2014) On the Δ^{17} O budget of atmospheric O₂. Geochim Cosmochim Acta 135:102–125 Young ED, Kohl IE, Warren PH, Rubie DC, Jacobson SA, Morbidelli A (2016) Oxygen isotopic evidence for vigorous mixing during the Moon-forming giant impact Science 351:493–496
- Zakharov DO, Bindeman IN, Slabunov AI, Ovtcharova M, Coble MA, Serebryakov NS, Schaltegger U (2017) Dating the Paleoproterozoic snowball Earth glaciations using contemporaneous subglacial hydrothermal systems. Geology 45:667–670
- Zakharov DO, Bindeman IN, Serebryakov NS, Prave AR, Azimov PYa, Babarina II (2019) Low δ¹⁸O rocks in the Belomorian belt, NW Russia, and Scourie dikes, NW Scotland: a record of ancient meteoric water captured by the early Paleoproterozoic global mafic magmatism. Precambrian Res 333:105431
- Zakharov DO, Marin-Carbonne J, Alleon J, Bindeman IN (2021) Temporal triple oxygen isotope trend recorded by Precambrian cherts: A perspective from combined bulk and in situ secondary ion probe measurements. Rev Mineral Geochem 86:323–365
- Zanazzi A, Judd E, Fletcher A, Bryant H, Kohn M (2015) Eocene–Oligocene latitudinal climate gradients in North America inferred from stable isotope ratios in Perissodactyl tooth enamel. Palaeogeogr Palaeoclimatol Palaeoecol 417:561–568